FROM FERMI ACCELERATION TO COLLISIONLESS DISCHARGE HEATING

by

M. A. Lieberman and V. A. Godyak

Memorandum No. UCB/ERL M97/65

15 September 1997

FROM FERMI ACCELERATION TO COLLISIONLESS DISCHARGE HEATING

by

M. A. Lieberman and V. A. Godyak

Memorandum No. UCB/ERL M97/65

15 September 1997

ELECTRONICS RESEARCH LABORATORY

College of Engineering
University of California, Berkeley
94720

FROM FERMI ACCELERATION TO COLLISIONLESS DISCHARGE HEATING

M.A. Lieberman[1] and V.A. Godyak[2]

[1]Department of Electrical Engineering and Computer Sciences
and the Electronics Research Laboratory
University of California
Berkeley, CA 94720

[2]OSRAM SYLVANIA Products, Inc.
71 Cherry Hill Drive
Beverly, MA 01915

ABSTRACT

The heating of electrons by time-varying fields is fundamental to the operation of radio frequency (rf) and microwave discharges. Ohmic heating, in which the phase of the electron oscillation motion in the field is randomized locally by interparticle collisions, can dominate at high pressures. Phase randomization can also occur due to electron thermal motion in spatially inhomogeneous rf fields, even in the absence of collisions, leading to *collisionless* or *stochastic* heating, which can dominate at low pressures. Generally, electrons are heated collisionlessly by repeated interaction with fields that are localized within a sheath, skin depth layer, or resonance layer inside the discharge. This suggests the simple heating model of a ball bouncing elastically back and forth between a fixed and an oscillating wall. Such a model was proposed originally by Fermi to explain the origin of cosmic rays.

In this review, Fermi acceleration is used as a paradigm to describe collisionless heating and phase randomization in capacitive, inductive, and electron cyclotron resonance (ECR) discharges. Mapping models for Fermi acceleration are introduced, and the Fokker-Planck description of the heating and the effects of phase correlations are described. The collisionless heating rates are determined in capacitive and inductive discharges and compared with self-consistent (kinetic) calculations where available. Experimental measurements and computer simulations are reviewed and compared to theoretical calculations. Recent measurements and calculations of nonlocal heating effects, such as negative electron power absorption, are described. Incomplete phase randomization and adiabatic barriers are shown to reduce the heating in low pressure ECR discharges.

"...a dispersive medium is also an absorbing medium." (Landau and Lifshitz, 1960)

I. INTRODUCTION

The heating of electrons by time-varying fields is fundamental to the operation of radio frequency (rf) and microwave plasma discharges. In a *uniform* oscillating electric field $\mathbf{E}(t) = \mathrm{Re}\,\mathbf{E}_0\, e^{j\omega t}$, a single electron has a coherent velocity of motion that lags the phase of the electric field force $-e\mathbf{E}$ by 90°. Hence the time-average power transfered from the field to the electron is zero. Electron collisions with other particles destroy the phase coherence of the motion, leading to a net transfer of power. For an ensemble of n electrons per unit volume, it is usual to introduce the macroscopic current density $\mathbf{J} = en\mathbf{u}$, with $\mathbf{u}$ the macroscopic electron velocity, and to relate the amplitudes of $\mathbf{J}$ and $\mathbf{E}$ through a local conductivity: $\mathbf{J}_0 = \sigma_p \mathbf{E}_0$, where $\sigma_p = e^2 n/m(\nu_m + j\omega)$ is the plasma conductivity and ν_m is the electron collision frequency for momentum transfer. In this "fluid" approach, the average electron velocity $\mathbf{u}$ still oscillates coherently but lags the electric field by less than 90°, leading to an ohmic power transfer per unit volume:

$$p_{\mathrm{ohm}} = \frac{1}{2}\mathrm{Re}\,\mathbf{J}_0 \cdot \mathbf{E}_0^* = \frac{1}{2}|\mathbf{E}_0|^2\,\mathrm{Re}\,(\sigma_p) = \frac{1}{2}|\mathbf{J}_0|^2\,\mathrm{Re}\,(\sigma_p^{-1}).$$

Although the average velocity is coherent with the field, the fundamental mechanism that converts electric field energy to thermal energy is the breaking of the phase-coherent motion of individual electrons by collisions: the total force (electric field force plus that due to collisions) acting on an individual electron becomes spatially non-uniform and non-periodic in time.

These observations suggest that a spatially *non-uniform* electric field by itself might lead to electron heating, even in the absence of interparticle collisions, provided that the electrons have thermal velocities sufficient to sample the field inhomogeneity. This phenomenon of *collisionless* or *stochastic* heating has been well-known in plasma physics since Landau (1946) demonstrated the collisionless damping of an electrostatic wave in a warm plasma. Since that time, collisionless dissipation has been studied extensively in fusion and space plasma physics. However, within the last decade and with the increased emphasis on industrial applications of low pressure gas discharges, it has become evident that collisionless dissipation phenomena are fundamental to rf and microwave discharges.

As will be seen in the following review, stochastic collisionless interactions leading to electron heating can be a basic feature of warm plasmas having space dispersion. The electron response ($\mathbf{J}$) at some point in the plasma is defined not only by the field ($\mathbf{E}$) at that point, but by an integrated effect over the neighboring space. Due to the spatial variation, the time-varying field seen by an individual "thermal" electron is non-periodic. The electron can lose phase coherence with the field (which is strictly periodic), resulting in stochastic interaction with the field and collisionless heating. Two fundamental issues arise: (1) what is the

rate of energy transfer to electrons assuming that phase coherence is lost; and (2) what are the conditions for loss of phase coherence? These issues form the principal topic of our review.

In almost all discharges, the spatial variation of the time-varying field is strongly non-uniform, with a low field in the bulk of the plasma and one or more highly localized field regions (rf sheath, skin depth layer, etc), usually near the plasma boundaries. An electron, being confined for hundreds to thousands of bounce times by the dc ambipolar and boundary sheath potential in the discharge, interacts repeatedly with the high field regions, but interacts only weakly during its drift through the plasma bulk. This suggests a dynamical model to investigate the energy transfer and loss of phase coherence: a ball bounces elastically back and forth between a fixed and an oscillating wall. This model was first introduced by Fermi (1949) to explain the origin of cosmic rays. The process in which the ball repeatedly interacts with the oscillating wall, resulting in phase randomization and stochastic heating, is known as *Fermi acceleration*. This process has been studied extensively as a paradigm in dynamics. In this review, we adapt the Fermi acceleration model as our fundamental approach for understanding collisionless heating in weakly ionized gas discharges.

In the usual model of Fermi acceleration, the wall oscillation motion is specified and the motion of the ball is then determined. From the structure of the motion in the velocity-position phase space of the ball, the conditions for phase randomization and the heating rates can be determined. However, the corresponding problem of collisionless electron heating in discharges has additional complexity, because the spatially non-uniform rf or microwave heating fields must be determined self-consistently with the electron motions. This self-consistent problem has been treated within conventional (warm plasma) kinetic theory for rf inductive discharges assuming that all electron phases are randomized. The issue of partial phase randomization and fully self-consistent treatments of other types of discharges is an active area of research.

In Section II we describe the model of Fermi acceleration. We motivate its introduction to explain the origin of cosmic rays, and introduce mapping models to describe the dynamics. We introduce a Fokker-Planck formalism to describe the collisionless heating in the presence of complete phase randomization, and we describe the effects of partial phase randomization. In Section III, we review collisionless heating in capacitive rf discharges. We describe the early studies and introduce a simple Fermi acceleration model for a homogeneous sheath to determine the collisionless heating rate. We describe modifications to the heating rate due to self-consistent sheath models and make comparisons to experiments and to fluid and particle-in-cell (PIC) simulations. We also describe other collisionless heating models, such as for magnetized capacitive discharges, and we introduce some other approaches to determine the collisionless heating. In Section IV we review collisionless heating in inductive rf discharges. We introduce the classical and anomalous skin effects and a Fermi acceleration model of the collisionless (anomalous) heating. We compare this to a self-consistent kinetic model and describe recent experiments that identify effects due to collisionless heating, such as the existence of regions of negative electron power absorption within the discharge bulk due to space dispersion caused by electron thermal motion. In Section V, we review briefly some features of collisionless heating in electron cyclotron resonance (ECR) discharges. We introduce a Fermi acceleration heating model and

show some comparisons to experiments. Both the model and the experiments suggest that incomplete phase randomization can reduce the heating rate and lead to an adiabatic barrier to the heating. In Section VI we summarize our conclusions and suggest some further issues that need to be resolved.

II. FERMI ACCELERATION

A. Cosmic Rays: Discovery and Properties

In the morning of August 7, 1912, Austrian physicist Viktor Hess ascended to over five kilometers in a balloon gondola as "an observer for atmospheric electricity" (Harwit, 1984; Friedlander, 1989). During the journey, he made careful measurements of the rate of discharging of three electroscopes, and he noted a several-fold increase in the rate of discharging as the balloon rose in altitude. In his publication in Physikalische Zeitschrift in November 1912, Hess suggested that the results of his observations were best explained "by a radiation of great penetrating power entering our atmosphere from above." Further flights confirmed these findings, and the American physicist Robert Millikan, although initially skeptical of the extraterrestrial origin, introduced the name *cosmic rays*.

It is now generally agreed that the majority of cosmic rays have a galactic origin. The cosmic ray flux is isotropic and of order 1 $\mathrm{cm}^{-2}\mathrm{s}^{-1}$, the energy density is approximately 1 $\mathrm{eV/cm}^3$, and the lifetime is approximately 10^7 years. Cosmic rays are mostly protons, but are rich in heavy nuclei compared to solar abundences. The particle energy ranges from $W \sim 10^8$–10^{20} eV, with a power law distribution $\mathcal{N}(W) \propto W^{-(2-2.5)}$.

Cosmic rays are believed to originate from supernovas such as the well-studied Crab nebula, which is the remnant of a supernova in 1054 A.D. With one galactic supernova every fifty years within a galactic disk volume of 10^{67} cm^3 creating 10^{43} J of fast particles, the energy balance is

$$\frac{10^{43}\ \mathrm{J}}{50\ \mathrm{yrs}} \approx \frac{e \times 1\ \mathrm{eV/cm}^3 \times 10^{67}\ \mathrm{cm}^3}{10^7\ \mathrm{yrs}}.$$

Measurements of radiation from supernova remnants clearly show the presence of synchrotron radiation, demonstrating the existence of high-energy ($> 10^{11}$ eV) electrons. Exactly how the fast particles are formed and accelerated is not well understood. Early theories emphasized acceleration across high voltages or by means of shock waves.

B. Fermi's Proposal

In 1949, Fermi put forth the idea that "cosmic rays are originated and accelerated primarily in the interstellar space of the galaxy by collisions against moving magnetic fields". He went on to assert the basic acceleration mechanism as follows:

> *It may happen that a region of high field intensity moves toward the cosmic-ray particle which collides against it. In this case, the particle will gain energy in the collision. Conversely, it may happen that the region of high field intensity moves away from the particle. Since the particle is much faster, it will overtake the irregularity of the field and be reflected backwards, in this case with*

loss of energy. The net result will be average gain, primarily for the reason that head-on collisions are more frequent than overtaking collisions because the relative velocity is larger in the former case.

Fermi noted that this idea naturally leads to a power law energy distribution, but that it fails to explain in a straightforward way the heavy nuclei observed in the primary cosmic radiation.

C. Fermi Maps and Dynamical Chaos

The Fermi problem of a particle bouncing between a fixed and an oscillating wall is illustrated in Fig. 1. This model of energy gain by repeated collisions of a particle with an oscillating wall was examined numerically by Ulam and associates (Ulam, 1961), who found that the particle motion appeared to be stochastic, but did not increase its energy on the average. Ulam's result was explained using a combination of analytical and numerical work by subsequent authors. The Fermi problem was treated using an exact area-preserving dynamical mapping for a sawtooth wall velocity by Zaslavskii and Chirikov (1965). Similar studies were performed by Brahic (1971). A "simplified" mapping, in which the oscillating wall imparts momentum to the particle but occupies a fixed position, was introduced by Lieberman and Lichtenberg (1972) and studied for arbitrary wall velocities (Lichtenberg et al, 1980; see also Lichtenberg and Lieberman, 1992, Sec. 3.4).

To find the exact mapping dynamics for this system, we introduce a fixed surface of section as some x = const. Defining $u_n = v_n/2\omega a$ to be the normalized velocity, $\theta_n = \omega t$ to be the phase of the moving wall at the nth collision with the fixed surface at $x = 0$, then a difference equation for the motion of the particle can be determined in terms of a wall motion $x_w(t) = aF(\psi)$, where F is an even periodic function of the phase $\psi = \omega t$, with period 2π and with $F_{\max} = -F_{\min} = 1$. We obtain, in implicit form the equations of motion

$$u_{n+1} = u_n + F'(\psi_c), \tag{2.1a}$$

$$\theta_{n+1} = \psi_c + \frac{[2\pi M - \frac{1}{2}F(\psi_c)]}{u_{n+1}}, \tag{2.1b}$$

$$\psi_c = \theta_n - \frac{1}{2}\frac{F(\psi_c)}{u_n}. \tag{2.1c}$$

Here ψ_c is the phase at the next collision with the moving wall, after the nth collision with the fixed surface $x = 0$, $M = l/2\pi a$, with l the distance between the walls, and $F' = dF/d\psi$ is the velocity impulse given to the ball. In this form it is easy to see that measuring the distance from the fixed wall as x, conjugate to v, then the phase θ is a time-like variable conjugate to the energy-like variable $w = u^2$. That is, in the extended phase space $(v, x, -w, t)$, the choice of a surface $x = 0$ gives an area-preserving mapping for the remaining pair $(-w, t)$. As we show in Sec. IID, this implies that a stochastic orbit has a uniform invariant distribution over the accessible (w, θ) phase space. Hence, assuming all phases are accessible, the energy w has a uniform invariant distribution.

Because of its implicit form, (2.1) is not convenient for numerical or analytical study. Substituting $w = u^2$, assuming a sinusoidal wall motion in (2.1), and expanding to first order in F' (and F), we obtain

$$w_{n+1} = w_n + 2\sqrt{w_n}\,\sin\theta_n, \tag{2.2a}$$

$$\theta_{n+1} = \theta_n + \frac{2\pi M}{\sqrt{w_{n+1}}} + \frac{\cos\theta_n}{\sqrt{w_{n+1}}}. \tag{2.2b}$$

A still simpler form can be constructed if the sinusoidally oscillating wall imparts momentum to the ball, according to the wall velocity, without the wall changing its position in space. The problem defined in this manner has many of the features of the more physical problem. In this simplified form the mapping is

$$u_{n+1} = |u_n + \sin\psi_n|, \tag{2.3a}$$

$$\psi_{n+1} = \psi_n + \frac{2\pi M}{u_{n+1}} \pmod{2\pi}. \tag{2.3b}$$

The mapping in (2.3) serves as an approximation (with suitably defined variables) to many physical systems in which the transit time between kicks is inversely proportional to a velocity. The absolute-value signs in (2.3) correspond to the velocity reversal, at low velocities $u < 1$, which appears in the exact equations (2.1). The absolute value has no effect on the region $u > 1$, which is the primary region of interest. For the simplified problem, a proper canonical set of variables are the ball velocity and phase just before the nth impact with the moving wall. The normalized velocity u then has a uniform invariant distribution, as will be seen in Sec. IID.

Transformations of the type (2.1)–(2.3) can be examined numerically for many thousands of iterations, thus allowing both detailed knowledge of the structural behavior and statistical properties of the dynamical system to be determined. Figure 2 shows the u–ψ surface for the simplified Fermi map (2.3) with $M = 100$ for 623,000 wall collisions of a single trajectory, with an initial condition at low velocity $u_0 \approx 1$. The surface has been divided into 200 × 200 cells, with a blank indicating no occupation of that cell. We find that the phase plane consists of three regions:

(1) a region for large u, $u > u_b = \sqrt{2\pi M}$, in which invariant adiabatic curves predominate and isolate narrow layers of stochasticity near the separatrices of the various resonances;

(2) an interconnected stochastic region for intermediate values of u, $u_s \approx \frac{1}{2}u_b < u < u_b$, in which adiabatic islands near linearly stable periodic solutions are embedded in a stochastic sea; and

(3) a predominantly stochastic region for small u, $u < u_s$, in which all primary periodic solutions appear to be unstable.

Both regions (2) and (3) exhibit *strong* or *global stochasticity* of the motion. In the latter region, although some correlation exists between successive iterations, over most of the region it is possible to approximate the dynamics by assuming a *random phase approximation* for the phase coordinate, thus describing the momentum coordinate by a diffusion equation. We explore this question more fully in the next subsection.

D. The Fokker-Planck Equation

In regions of the phase space that are stochastic or mostly stochastic with small isolated adiabatic islands, it may be possible to describe the evolution of the distribution function in action space (or velocity space) alone. This is, in fact, the problem of most practical interest. In the Fermi acceleration problem, for example, the motivation was to find a possible mechanism for heating of cosmic rays. The variations in the phases of the particles with respect to their accelerating fields are of little interest except as they are required for determining the heating rates and the final energy distribution.

Let us consider in what sense the evolution of the distribution function $f(u,n)$ can be described by a stochastic process in the action u alone. Clearly we must confine our attention to a globally stochastic region of the phase space in which adiabatic islands do not exist or occupy negligible phase space volume. In such a region, it may be possible to express the evolution of $f(u,n)$, the distribution in u alone, in terms of a Markov process in u (Wang and Uhlenbeck, 1945):

$$f(u,n+\Delta n)=\int f(u-\Delta u,n)W_t(u-\Delta u,n,\Delta u,\Delta n)\,d(\Delta u), \tag{2.4}$$

where $W_t(u,n,\Delta u,\Delta n)$, the transition probability, is the probability that an ensemble of phase points having an action u at a "time" n suffers an increment in action Δu after a "time" Δn. If we make the additional assumption that there exists an intermediate time scale $\Delta n \gg 1$ such that $\Delta u \ll (f^{-1}df/du)^{-1}$, then we can expand the first argument of the integrand fW_t in (2.4) to second order in Δu to obtain the Fokker-Planck equation

$$\frac{\partial f}{\partial n}=-\frac{\partial}{\partial u}(Bf)+\frac{1}{2}\frac{\partial^2}{\partial u^2}(Df). \tag{2.5}$$

For Hamiltonian systems, the friction coefficient B and the diffusion coefficient D are related (Landau, 1937) as

$$B=\frac{1}{2}\frac{dD}{du}, \tag{2.6}$$

allowing (2.5) to be written in the form of a diffusion equation

$$\frac{\partial f}{\partial n}=\frac{\partial}{\partial u}\left(\frac{D}{2}\frac{\partial f}{\partial u}\right). \tag{2.7}$$

Assuming that phase randomization occurs on the time scale Δn, then we can average Δu over a uniform distribution of phases to obtain the so-called *quasilinear diffusion coefficient*

$$D(u)=\frac{1}{2\pi}\int_0^{2\pi} d\psi[\Delta u(\psi)]^2. \tag{2.8}$$

$B(u)$ is then obtained directly from (2.6).

For the simplified Fermi map (2.3) with sinusoidal velocity, for which $\Delta u=\sin\psi$, we obtain $D=\frac{1}{2}$ and $B=0$. Hence the Fokker-Planck equation for the velocity distribution is

$$\frac{\partial f}{\partial n}=\frac{1}{4}\frac{\partial^2 f}{\partial u^2}. \tag{2.9}$$

Similarly, for the Fermi map (2.2), we obtain

$$\bar{D} = \frac{1}{2\pi}\int_0^{2\pi} 4w\cos^2\theta\, d\theta = 2w \tag{2.10}$$

and the Fokker-Planck equation for the energy distribution g is, from (2.7)

$$\frac{\partial g}{\partial n} = \frac{\partial}{\partial w}\left(w\frac{\partial g}{\partial w}\right). \tag{2.11}$$

To obtain a steady-state solution to the Fokker-Planck equation, we assume perfectly reflecting barriers at $u = 0$ and $u = u_b$. Setting $\partial/\partial n = 0$ in (2.9) and taking the net flux to be zero, we obtain a uniform invariant distribution in velocity $f(u) = \text{const}$ for the simplified map. For the map (2.2), we obtain similarly a uniform invariant distribution in energy $g(w) = \text{const}$. Introducing the velocity distribution $f(u)$ for (2.2) through

$$f(u)\,du = g(w)\,dw \tag{2.12}$$

and using $dw = u\,du$, we see that $f(u) = \text{const} \times u$ for (2.2). In Fig. 3 we compare the numerically calculated distributions for $M = 100$ and 5×10^6 interactions with these predictions. In the region below $u_s = (\pi M/2)^{1/2} \approx 12.5$, the predictions are verified. Above u_s, the distributions both fall off due to the presence of islands and higher-order correlations in the phase space, with the dips near the island centers.

We can also solve the transient Fokker-Planck equation. For the simplified Fermi mapping (2.3), with initial conditions of a δ-function at $u = 0^+$, we can solve (2.9) to obtain

$$f(u,n) = \frac{2}{(\pi n)^{1/2}}\exp\left(-\frac{u^2}{n}\right), \tag{2.13}$$

which yields the distribution function for the transient heating of he particles. This time development only holds, of course, until the particles begin to penetrate into the region with islands, $u > u_s$.

E. The Effects of Correlations

The complete dynamics, including the transition region with adiabatic islands embedded in a stochastic sea, is very complicated and can only be solved numerically. To gain some understanding of the diffusion in the phase space region where correlations are important, it is convenient to first transform the Fermi map to a local map near a resonance. Taking the simplified Fermi map of (2.3), we obtain the so-called *standard mapping* by linearization in action space near a given period-1 fixed point. These fixed points are located at

$$\frac{2\pi M}{u_1} = 2\pi m, \qquad m \text{ integer}. \tag{2.14}$$

Putting $u_n = u_1 + \Delta u_n$ and shifting the angle

$$\theta_n = \psi_n - \pi, \qquad -\pi < \theta_n < \pi,$$

then the mapping equations take the standard form

$$I_{n+1} = I_n + K \sin\theta_n, \tag{2.15a}$$

$$\theta_{n+1} = \theta_n + I_{n+1}, \tag{2.15b}$$

where

$$I_n = -\frac{2\pi M \Delta u_n}{u_1^2} \tag{2.16}$$

is the new action and

$$K = \frac{2\pi M}{u_1^2} \tag{2.17}$$

is the *stochasticity parameter.* We have thus related K to the old action u_1. The conversion from Fermi to standard mapping is illustrated in Fig. 4 for two different values of u_1, leading to two different values of K.

The dynamics of the standard mapping (2.15) can be considered to evolve on a two-torus, with both θ and I taken modulo 2π. The periodicity of the mapping in I gives rise to a special type of periodic orbit (period-1 fixed point) in which I advances by $\pm 2\pi$ every iteration of the mapping. The condition for these so-called *accelerator modes* is that $I_{1l} = 2\pi m$ and $K \sin\theta_{1l} = 2\pi l$, m and l integers, with $l \neq 0$. The accelerator modes are stable provided $|2 \pm K\cos\theta_{1l}| < 2$, which implies that stability windows for period-1 fixed points exist for successively higher values of K as I increases ($\cos\theta_{1l}$ decreases). Remnants of these accelerator modes, called *quasi-accelerator modes,* can exist in the Fermi mapping, leading to enhanced diffusion.

The quasilinear transport coefficients for the standard mapping (2.15) are $D_I = K^2/2$ and $B_I = 0$. Since this mapping locally approximates the Fermi mapping, we can relate D_I to D for the Fermi mapping. Using $\Delta I = -K\Delta u$, we find that the diffusion coefficients are related by

$$D(u) = \frac{D_I(K(u))}{K^2(u)} \tag{2.18}$$

The island structure embedded in the Fermi stochastic sea is exceeding complex, and, in fact, has fractal properties. We might expect this structure to lead to long time correlation of stochastic orbits in the neighborhood of adiabatic orbits, and this is in fact what happens. The quasilinear transport coefficients are determined using the random phase assumption applied to a single step jump in the action $\Delta u_1 = u_1 - u_0$. However, as pointed out in Sec. IID, the Fokker-Planck description of the motion is valid only in the limit $n \gg n_c$, where n_c is the number of steps for phase randomization to occur. We should therefore consider the jump $\Delta u_n = u_n - u_0$, where $n > n_c$. This was first done using Fourier techniques for the standard mapping in the limit of large K by Rechester and White (1980) and for any K by Rechester et al (1981). To order K^{-1}, the result is (Lichtenberg and Lieberman, 1992, Sec. 5.5a):

$$D_n = D_{QL}[1 - 2\mathrm{J}_2(K) - 2\mathrm{J}_1^2(K) + 2\mathrm{J}_2^2(K) + 2\mathrm{J}_3^2(K)], \tag{2.19}$$

where $D_{QL} \equiv D_I/2 = K^2/4$ and the J's are Bessel functions. A numerical calculation of D_{50} using 3000 particles is compared with (2.19) in Fig. 5 (Rechester and White, 1980). There is good agreement, except

near the first few peaks of D, which are due to the presence of *accelerator modes*. For K near but greater than the critical value $K_c \approx 0.9716$, one finds numerically that

$$D_\infty \approx 0.1(K - K_c)^3. \tag{2.20}$$

For $K < K_c$, an adiabatic (invariant) barrier exists and there is no long-time diffusion.

For the Fermi map in which the phase is randomized within a region of the velocity space for which the local approximation gives a near-constant stochasticity parameter K, it is possible to derive a local (in velocity) diffusion coefficient (Murray et al, 1985). In this regime, for which $(1/f)(\partial f/\partial u) \ll K(u)/2\pi$, the diffusion coefficient becomes, using (2.18),

$$D_\infty(u) = \frac{D_\infty(K(u))}{K^2(u)}. \tag{2.21}$$

Let us note that if we are interested in using the Fermi map to model a heating mechanism, then particles will generally start at low velocities, where the stable islands have negligibly small area. As the particles are heated they enter regions of phase space within which large islands exist. Without extrinsic stochasticity, the particles will not penetrate these islands. Hence, although the equilibrium distribution is uniform in the ergodic phase space surrounding the islands, the phase-averaged distribution $f(u, n)$ will not be uniform, as is seen in Fig. 3. To correct for this effect, one must divide $D_\infty(u)$ by the fraction of phase space occupied by stochastic orbits. The details of the calculation are described in Murray et al (1985); see also Lichtenberg and Lieberman (1992). The enhanced diffusion due to quasi-accelerator modes is treated in Lichtenberg et al (1987).

Deterministic Fermi acceleration mappings are useful tools for understanding the purely dynamical aspects of the phase randomization and heating of particles by periodic fields. However, let us note that for the heating of electrons in weakly ionized gas discharges, the *extrinsic stochasticity* associated with electron-electron, electron-ion, and electron-neutral collisions can play a critical, and in many cases dominating role. The interplay between the intrinsic dynamical chaos and the extrinsic chaos due to collisions has received much attention both in the dynamics community (see Lichtenberg and Lieberman, 1992, Sec. 5.6) and in the discharge heating community (Lieberman and Lichtenberg, 1994; Kaganovich et al, 1996; Kaganovich, 1997).

III. CAPACITIVE RF DISCHARGES

We begin with the application of Fermi acceleration to electron heating in capacitive discharges where collisionless dissipation of rf power has been intensively studied over the last few decades, due to the wide application of these discharges in plasma processing (Lieberman and Lichtenberg, 1994). A sandwich-like (sheath-plasma-sheath) structure of the capacitive rf discharge, first proposed by Schneider (1954) and now widely accepted in analyzing the basic properties, is shown in Fig. 6. A typical discharge consists of a vacuum chamber containing two planar electrodes separated by a spacing of order 2–10 cm and driven by an

rf power source. The substrates are placed on one electrode, feedstock gases are admitted to flow through the discharge, and effluent gases are removed by the vacuum pump. The typical rf driving voltage is V_{rf} = 100–1000 V, and for etching of thin films pressures are in the range 10–100 mTorr, power densities are 0.1–1 W/cm^2, and the driving frequency is usually 13.56 MHz. Plasma densities are relatively low, 10^9–10^{10} cm^{-3}, and electron temperatures are of order 3 V. For deposition of films, pressures tend to be higher, and frequencies can be lower than 13.56 MHz.

The operation of capacitively driven discharges is reasonably well understood. The mobile plasma electrons, responding to the instantaneous electric fields produced by the rf driving voltage, oscillate back-and-forth within the positive space charge cloud of the ions. The massive ions respond only to the time-averaged electric fields. Electron thermal motion and oscillation of the electron cloud create sheath regions near each electrode that contain net positive charge when averaged over an oscillation period; i.e., the positive charge exceeds the negative charge in the system, with the excess appearing within the sheaths. This excess produces a strong time-averaged electric field within each sheath directed from the plasma to the electrode. Ions flowing out of the bulk plasma near the center of the discharge can be accelerated by the sheath fields to energies of order of V_{rf} as they flow to the substrate, leading to energetic-ion enhanced processes. The positive ions continuously bombard the electrode over an rf cycle, whereas electrons are lost to the electrode only when the oscillating cloud closely approaches the electrode. During that time, the instantaneous sheath potential collapses to near-zero, allowing sufficient electrons to escape to balance the ion charge delivered to the electrode. Except for such brief moments, the instantaneous potential of the discharge must always be positive with respect to any large electrode or wall surface; otherwise the mobile electrons would quickly leak out. The sheath impedance is generally much larger than that of the plasma and plays the essential role in limiting the rf discharge current.

A. Early Work

Because the sheath width oscillates, electrons reflecting from the sheath are velocity dispersed. This idea was proposed by Gabor et al (1955) in their attempt to resolve the "Langmuir paradox" of a Maxwellian electron distribution in the positive column of a dc glow discharge having negligible electron-electron Coulomb collisions. They believed that the electron interaction with rf fluctuations (oscillations) in the sheath was without energy exchange and was maintained solely by the energy flux of low energy electrons, thus, generating a high energy tail of the distribution.

Later Pavkovich and Kino (1963) and Gould (1964), analyzing the sheath impedance at high frequency, showed that electron reflection in the oscillating sheath is accompanied by rf energy absorption, due to a type of transit time heating.

An explicit application of Fermi acceleration to electron heating in rf discharges was by Godyak (1971):

In an oscillating double sheath, the potential distribution, and thus the coordinate of the electron-reflection point depend on the time, and the electron reflection is analogous to that of solid particles

from a vibrating wall. On the average particles acquire energy in this case (the Fermi acceleration mechanism).

Godyak went on to determine the electron power deposition for a dc sheath with a small sinusoidally vibrating fluctuation, and put forward the idea that Fermi acceleration might be a major mechanism to sustain a capacitive discharge at low gas pressures. These ideas were further developed by Godyak (1976a,b) and by Akhiezer and Bakai (1976). The latter authors used a simplified Fermi model (2.3) to determine the heating rate, and noted that if there was a velocity barrier for heating, then the steady state distribution in velocity was uniform for velocities below the barrier, in agreement with the calculation in Section IID. Goedde et al (1988) later considered the case in which electrons are continuously injected into a capacitive discharge at low velocity and are lost by inelastic collisions or escape to the walls at higher velocity, and determined the steady state distribution, finding a power law electron energy distribution.

B. Homogeneous Discharge Model

Let us consider the collisionless power absorption in the simplest model of a capacitive discharge with a homogeneous ion background in the electrode gap and with a high rf sheath voltage. Such a simplified discharge model qualitatively describes the main features of capacitive discharges in practice.

Electrons reflecting from the large decelerating fields of a moving high voltage sheath can be approximated by assuming the reflected velocity is that which occurs in an elastic collision (in the moving reference frame) of a ball with a moving wall

$$u_r = -u + 2u_{es} \tag{3.1}$$

where u and u_r are the incident and reflected electron velocities parallel to the time varying electron sheath velocity u_{es}. If the parallel electron velocity distribution at the sheath edge is $f_{es}(u,t)$, then in a time interval dt and for a speed interval du, the number of electrons per unit area that collide with the sheath is given by $(u-u_{es})f_{es}(u,t)dudt$. This results in a power transfer per unit area,

$$dS_{\rm stoc} = \frac{1}{2}m(u_r^2 - u^2)(u-u_{es})f_{es}(u,t)\,du. \tag{3.2}$$

Using $u_r = -u + 2u_{es}$ and integrating over all incident velocities, we obtain

$$S_{\rm stoc} = -2m\int_{u_{es}}^{\infty} u_{es}(u-u_{es})^2 f_{es}(u,t)\,du. \tag{3.3}$$

In the physical problem f_{es} varies with time, as the sheath oscillates, and the problem becomes quite complicated. For the uniform density model we note that

$$\int_{-\infty}^{\infty} f_{es}(u,t)\,du = n_{es}(t) = n, \text{ a constant.} \tag{3.4}$$

Furthermore, for the purpose of understanding the heating mechanism we make the simplifying approximations that $f_{es}(u,t)$ can be approximated by a Maxwellian, ignoring the plasma drift, and that $u_{es} \ll \bar{v}_e = (8eT_e/\pi m)^{1/2}$, the mean electron speed. These approximations simplify the calculation. Consistent

with our approximation, we can set the lower limit in (3.3) to zero. Before performing the average over the distribution function, we substitute

$$u_{es} = u_0 \cos \omega t, \tag{3.5}$$

in (3.3) and average over time. Only the term in $\sin^2 \omega t$ survives giving

$$\bar{S}_{\text{stoc}} = 2mu_0^2 \int_0^\infty u f_{es}(u)\, du. \tag{3.6}$$

Now, consistent with our approximation that f_{es} is Maxwellian, we note that the integral gives the usual random flux $\Gamma_e = \frac{1}{4} n \bar{v}_e$, and (3.6) becomes

$$\bar{S}_{\text{stoc}} = \frac{1}{2} m u_0^2 n \bar{v}_e. \tag{3.7}$$

Inside the plasma the rf current I_1 is almost entirely conduction current, such that

$$I_1 = J_1 A = -enu_0 A, \tag{3.8}$$

where A is the cross-sectional area. Substituting (3.8) into (3.7) yields the stochastic electron power in terms of the (assumed) known current. Since we are calculating the power per unit area, we use the current density, to obtain, for a single sheath,

$$\bar{S}_{\text{stoc}} = \frac{1}{2} \frac{m \bar{v}_e}{e^2 n} J_1^2. \tag{3.9}$$

Within the homogeneous model, the time-average electron heating per unit area due to ohmic heating in the discharge bulk is

$$\bar{S}_{\text{ohm}} = \frac{1}{2} J_1^2 l \text{Re}\,(\sigma_p^{-1}), \tag{3.10}$$

where l is the length of the bulk region containing electrons and $\sigma_p = e^2 n / m(\nu + j\omega)$ is the plasma conductivity. Substituting σ_p into (3.10), we find

$$\bar{S}_{\text{ohm}} = \frac{1}{2} J_1^2 \frac{m \nu_m l}{e^2 n}, \tag{3.11}$$

where ν_m is the electron-neutral momentum transfer frequency.

Adding (3.9) (for two sheaths) and (3.11), the total time average electron power per unit area is

$$S_e = \frac{1}{2} \frac{m}{e^2 n} (\nu_m l + 2\bar{v}_e) J_1^2. \tag{3.12}$$

A useful interpretation of this result is to introduce an effective collision frequency

$$\nu_{\text{eff}} = \nu_m + \frac{2\bar{v}_e}{l}. \tag{3.13}$$

Then we can consider that the stochastic heating introduces an additional, gas pressure-independent collision frequency, the electron bounce frequency $2\bar{v}_e/l$, into the expression for ohmic heating of the discharge.

C. Self-Consistent Sheath

We describe now the stochastic heating for a collisionless high voltage rf sheath (Lieberman, 1988). The structure of the rf sheath is shown in Fig. 7. Ions crossing the ion sheath boundary at $x = 0$ accelerate within the sheath and strike the electrode at $x = s_m$ with high energies. The ion motion is collisionless. Since the ion flux $n_i u_i$ is conserved and u_i increases as ions transit the sheath, n_i drops. This is sketched as the heavy solid line in the figure. The electron sheath edge oscillates from $x = 0$ to $x = s_m$, as shown, where $s(t)$ is the distance from the ion sheath boundary at $x = 0$ to the electron sheath edge. Time averaging this motion over an rf cycle, we obtain $\bar{n}_e(x)$, the time-average electron density within the sheath, sketched as the dashed line in Fig. 7. The time-average electron space charge leads to a modified Child law for the dc ion current density,

$$\bar{J}_i = en_s u_B = K_i \epsilon_0 \left(\frac{2e}{M}\right)^{1/2} \frac{\bar{V}^{3/2}}{s_m^2} \tag{3.14}$$

where $\bar{V}$ is the dc (time-average) sheath potential and $K_i = 200/243 \approx 0.82$. This has the same scaling with $\bar{V}$ and dc sheath thickness s_m as the normal Child law without electron shielding, which has $K_i = 4/9 \approx 0.44$. For a fixed current density and sheath voltage, the self-consistent rf ion sheath thickness s_m is larger than the Child law sheath thickness by the factor $\sqrt{50/27} \approx 1.36$. This increase is produced by the reduction in space charge within the sheath due to the nonzero, time-average electron density.

The solution for the electron sheath motion is sketched in Fig. 8 (Lieberman and Lichtenberg, 1994, Section 11.2). The electron sheath motion is periodic but not sinusoidal. The sheath moves faster when it is near the electrode than when it is near the plasma because the ion density is smaller near the electrode. This, along with the increase in the sheath length over that for the homogeneous model, leads to an increase in the stochastic heating over that found for the homogeneous model. The power transferred to the electrons by the sheath is found from (3.3), but now f_{es} is not a fixed Maxwellian, but is a time varying function with a time varying density $n_{es}(t)$ at the electron sheath edge $s(t)$. To determine f_{es}, we first note that the sheath is oscillating because the electrons in the bulk plasma are oscillating in response to a time-varying electric field. If the velocity distribution function within the plasma at the ion sheath edge $x = 0$ in the absence of the electric field is a Maxwellian $f_m(u)$ having density n_s, then the distribution within the plasma at the ion sheath edge is $f_s(u,t) = f_m(u - u_s)$, where $u_s(t) = -u_0 \sin \omega t$ is the time-varying oscillation velocity of the plasma electrons. At the moving electron sheath edge, because $n_{es} < n_s$, not all electrons having $u > 0$ at $x = 0$ collide with the sheath at s. Many electrons are reflected within the region $0 < x < s$ where the ion density drops from n_s to n_{es}. This reflection is produced by an ambipolar electric field whose value maintains quasineutrality $n_e \approx n_i$ at all times. The transformation of f_s across this region to obtain f_{es} is complicated. However, the essential features to determine the stochastic heating are seen if we approximate

$$f_{es} = \frac{n_{es}}{n_s} f_m(u - u_s), \qquad u > 0. \tag{3.15}$$

Inserting (3.15) into (3.3) and transforming to a new variable $u' = u - u_0$, we obtain

$$S_{\rm stoc}(t) = -\frac{2m}{n_s}\int_{u_{es}-u_s}^{\infty} u_{es} n_{es}[u'^2 - 2u'(u_{es}-u_s) + (u_{es}-u_s)^2] f_m(u')\, du'. \tag{3.16}$$

Averaging over an oscillation period and integrating over f_m yields $\bar{S}_{\rm stoc}$.

If the assumption is made that the sheath motion is much slower than the electron thermal velocity, as for the homogeneous model calculation, then one obtains (Lieberman and Lichtenberg, 1994, Section 11.2) for $\bar{V} \gg T_e$ that

$$\bar{S}_{\rm stoc} = \frac{3\pi}{32} H m n_s \bar{v}_e u_0^2, \tag{3.17}$$

where

$$H = \frac{e}{\pi\epsilon_0 T_e \omega^2} n_s u_0^2 = \frac{4}{3\pi}\left(\frac{2\bar{V}}{T_e}\right)^{1/2}. \tag{3.18}$$

Using (3.18), we can compare (3.9) and (3.17) at the same driving voltage. Substituting the first equality in (3.18) into (3.9) and (3.17) yields

$$\bar{S}_{\rm stoc}(\text{homogeneous model}) = \frac{\pi\epsilon_0 m \bar{v}_e T_e}{2e}\omega^2 H \tag{3.19a}$$

$$\bar{S}_{\rm stoc}(\text{self-consistent model}) = \frac{\pi\epsilon_0 m \bar{v}_e T_e}{2e}\omega^2 \frac{3\pi}{16} H^2 \tag{3.19b}$$

We see that, at a fixed driving voltage, both models yield a stochastic heating proportional to ω^2; however, the stochastic heating for the self-consistent model is a factor of $3\pi H/16$ larger than for the homogeneous model. As an example, for $\bar{V} = 600$ V, $T_e = 3$ V, we find $3\pi H/16 \approx 8.5$. Results similar to this were also obtained for a collisional sheath (Lieberman, 1989).

D. Experimental Results

Early experiments to investigate stochastic heating are described in Godyak (1976a), Godyak et al (1976b), Godyak and Popov (1979), and Popov and Godyak (1985), and are summarized in Godyak's 1986 review. In these works electrical and plasma parameters were studied in a parallel-plate capacitive rf discharge symmetrically driven at 40–110 MHz in mercury vapor. The current-voltage characteristic, the rf power, the plasma density and the electron temperature were simultaneously measured in the mercury pressure range between 2×10^{-4} and 1×10^{-1} Torr.

The effective collision frequency $\nu_{\rm eff}$ versus pressure was evaluated from the shape of the measured discharge current-voltage characteristic (Godyak et al, 1976b; Godyak and Popov, 1979) and directly by measuring the rf power absorbed by the discharge (Popov and Godyak, 1985). In the last case $\nu_{\rm eff}$ was obtained from the relationship for the power absorbed per unit area

$$S_{\rm abs} = \frac{1}{2}\frac{|\tilde{J}_{\rm rf}|^2}{e^2 n} m \nu_{\rm eff} l, \tag{3.20}$$

where $|J_{\rm rf}|$ is the cross-section averaged discharge current density. The measurements were done at relatively low rf voltages, and the power absorption due to ion acceleration in the rf sheaths was neglected. The effective

collision frequency found from experiment as a function of mercury pressure is shown in Fig. 9. Both the asymptotic leveling off of ν_{eff} at low pressure p, characteristic of stochastic heating which is independent of p, and the linear increase of ν_{eff} with p at high p, characteristic of ohmic heating, are clearly visible. The good agreement of the measurements with ν_{eff} calculated from the stochastic heating formula is somewhat fortuitous, however, as a uniform sheath rather than a self-consistent sheath was used in the calculation, and the ion power loss S_i was neglected in determining ν_{eff} from the measurements.

In these early studies, it was shown that the presence of stochastic heating at the plasma boundaries reduces the rf electric field and electron oscillatory velocity in the plasma bulk (Godyak, 1976a; Popov and Godyak, 1986). This happens due to non-local electron energy balance in a low pressure rf discharge when rf power absorbed in the rf sheaths compensates the electron energy losses over the entire plasma volume, so that there is no need for a large bulk rf field to maintain the discharge.

A comprehensive experimental study of symmetric rf discharge characteristics in argon at 13.56 MHz has been performed by Godyak and Piejak (1990) and Godyak et al (1991, 1992). The discharge length and diameter were 6.7 cm and 14.3 cm, respectively, approximating a uniform plane parallel configuration. Measurements were made of rf voltage, rf current, total power absorbed, the central plasma density n_0, mean electron energy $\langle \mathcal{E}_e \rangle$, and electron energy distribution function (EEDF) f_e. The rf power was determined by averaging $V_{\text{rf}}(t) I_{\text{rf}}(t)$ over an rf cycle, and n_0, $\langle \mathcal{E}_e \rangle$ and f_e were determined using Langmuir probes. Also, the ion current to the rf electrodes and dc bias voltage in the rf sheath were measured to determine the ion power loss. Measurements were performed over a wide range of pressures from 3 mTorr to 3 Torr and for powers up to 100 W. The corresponding rf voltage amplitudes were up to 1500 V, and the rf current amplitudes were up to 2 A.

Having measured the discharge rf power, the discharge current, and the EEDF, the plasma density was found by integration over the EEDF, and the collisional power absorption P_{ohm} was then estimated using the plasma conductivity formula. This was compared to the total rf power P_e transferred to the plasma electrons. The latter was found as the difference between the total measured discharge power and that corresponding to the ion loss. The result is shown in Fig. 10. As is seen, at relatively high gas pressure ($p \geq 0.1$ Torr), the power absorption is entirely due to collisional dissipation, $P_e/P_{\text{ohm}} \approx 1$. At low pressure $P_e \gg P_{\text{ohm}}$, and the ratio P_e/P_{ohm} reaches three orders of magnitude at the lowest pressure of 3 mTorr. Such an enormous difference between P_e and P_{ohm} is due to the stochastic heating in the rf sheaths and a simultaneous sharp drop in collisional electron heating in the plasma because of electron cooling in the collisionless heating regime.

The electron cooling occurs during the heating mode transition when the discharge switches from a collisionally to a stochastically dominated mode (Godyak and Piejak, 1990). The heating mode transition

is shown in Fig. 11 in the evolution with gas pressure of the electron energy probability function (EEPF) $g_p(\mathcal{E})$. The EEPF is defined as

$$\int_0^\infty \mathcal{E}^{1/2} g_p(\mathcal{E})\, d\mathcal{E} = n_e, \tag{3.21}$$

where $\mathcal{E} = mv^2/2$ is the electron kinetic energy; the EEPF is defined such that a plot of $\ln g_p$ versus $\mathcal{E}$ is a straight line for a Maxwellian distribution. In Fig. 11 we see a transition from a Druyvesteyn-like distribution, $g_p \propto \exp(-\text{const} \times \mathcal{E}^2)$, which is typical for collisional electron heating at $\nu_m^2 \gg \omega^2$ at high argon pressure to a bi-Maxwellian distribution at low argon pressure when stochastic heating dominates. This transition is accompanied by a corresponding sharp change in plasma density and mean electron energy (Godyak and Piejak, 1990). In the stochastic heating regime the majority of electrons have a very low energy, and being trapped by the ambipolar dc field they are not able to reach the rf sheaths where stochastic heating takes place. Having their energy close to the Ramsauer minimum of the argon cross section, the low energy electrons have a very low electron-atom collision frequency and thus, they collisionlessly oscillate in a weak rf field unable to gain energy.

On the other hand, the high energy electrons easily overcome the ambipolar potential and effectively interact with the oscillating rf sheaths, bouncing between them. Phase randomization must occur for these electrons to be heated. The randomization can arise directly from the dynamics or can be induced by external stochastic forces. The condition for dynamical stochasticity is (see Section IIC)

$$u < u_s = (\pi M/2)^{1/2}. \tag{3.22}$$

Unnormalizing (3.22) using $u = v/2\omega a$ and $M = l/2\pi a$ yields for the electron velocity $v < \omega\sqrt{la}$. For typical experimental parameters $l = 6.7$ cm, $a \approx 0.5$ cm, and $\omega = 85.2 \times 10^6$ s^{-1}, we obtain $v < 1.6 \times 10^8$ cm/s, corresponding to a longitudinal energy of $\mathcal{E}_e < 7.3$ V. Since the flux-averaged longitudinal electron energy is $2\mathrm{T}_e \lesssim 6$ V, the condition for dynamical phase randomization is marginally satisfied for the majority of electrons. However, at lower driving frequencies and/or short electrode gaps, the condition for dynamical phase randomization is not met. In this case, high frequency plasma or sheath fluctuations can effectively randomize the electron phase even when the electron mean free path is larger than the plasma width l. This randomization mechanism may be responsible for the effective collisionless ($\lambda_e > l$) electron heating by rf sheaths in experiments where the condition of dynamical phase randomization is not satisfied. Phase randomization due to rare ($\lambda_e > l$) collisions of fast electrons with atoms can also introduce phase randomization, since the average lifetime of electrons ($\approx l/u_B$) is always much larger than the bounce time ($\approx l/\bar{v}_e$). Here $u_B = (e\mathrm{T}_e/M)^{1/2}$ is the Bohm (ion sound) velocity. Thus, over their lifetime, the bouncing electrons have enough chance to be randomized via electron-atom collisions. As was shown recently by Kaganovich et al (1996), there are many scenarios for electron phase randomization which depend on the relationship between the bounce frequency, the driving frequency, and the electron-neutral collision frequency. However, let us note in the low pressure regime where $\lambda_e \gg l$, that the fraction of electrons whose phase is randomized

in one transit due to collisions with gas atoms is of order $n_g \sigma_m l$, where σ_m is the electron-neutral momentum transfer frequency and n_g is the neutral atom density. Hence expression (3.9) must be multiplied by this factor, yielding $\bar{S}_{\rm stoc} \approx \bar{S}_{\rm ohm}$, with a pressure scaling $\bar{S}_{\rm stoc} \propto p$. Hence this phase randomization mechanism does not lead to an effective collision frequency independent of pressure.

Another kind of EEDF transition due to change in rf power was obtained by Godyak (1990) and was studied by Buddemeier et al (1995) through experiment and numerical simulation. In Fig. 12, we see evolution of the measured electron probability function with discharge current (and voltage) at a fixed low argon pressure, from a Druyvesteyn-like distribution at low discharge voltage to a two-temperature distribution at higher voltage. This transition is associated with the nonlinear nature of electron heating in the rf sheath. At small discharge voltage, the sheath heating is small or comparable to the bulk collisional electron heating. With increasing rf current, the stochastic heating begins to dominate with a corresponding restructuring of the electron energy distribution. These results are consistent with the scaling laws for sheath and bulk heating (e.g., see Lieberman and Lichtenberg, 1994, Sec. 11.2).

E. Fluid and Particle Simulations

Monte Carlo and particle-in-cell (PIC) simulations of capacitively coupled discharges at low pressure performed in the last decade have confirmed the existence of collisionless electron heating produced by oscillating electrode sheaths (Kushner, 1986; Surendra et al, 1990; Surendra and Graves, 1991; Vender and Boswell, 1992; Wendt and Hitchon (1992); Surendra and Vender, 1994; Buddemeier et al, 1995). Stochastic heating due to reflection from oscillating sheaths was observed by Kushner (1986) using a Monte Carlo calculation, and the subsequent PIC calculations also found EEPF's with high energy tails attributed to stochastic heating. Electron energy loss across the oscillating sheath was investigated in several of these works, and a number of authors also show the transition from weak to strong sheath heating.

Nitschke and Graves (1994) performed fluid simulations at low pressure using a helium-like model gas and compared these to particle-in-cell (PIC) simulations of the same system. The fluid simulations do not incorporate the physics of stochastic heating, while the PIC simulations do. Below 100 mTorr, disagreement in the electron heating predicted by each simulation leads to significant differences in the discharge properties. At the same applied frequency (12 MHz) and voltage (500 V), the PIC simulations at 50 mTorr and 120 mm gap spacing yield roughly twice the electron power deposition as the fluid simulations. From power balance, this yields twice the density for the PIC simulation compared with the fluid simulations. By adding into the fluid model the appropriate analytic expression for stochastic heating as an "additional" power source, the fluid and PIC simulations were brought into closer correspondence.

Comparisons were also made between the measurements of Godyak and Piejak (1990) and PIC simulations by Vahedi et al (1994). The comparisons are in argon for an electrode diameter of 14.3 cm, a discharge length of 2 cm, and an external current source of 2.56 mA/cm^2 at 13.56 MHz. The gas pressure was varied between 70 and 500 mTorr to observe the transition from stochastically to ohmically dominated electron

heating. Except for the normalization, the f_e's obtained from the simulations agree well with the measured f_e's, showing the transition from a two temperature distribution at 70 mTorr to a single temperature distribution at 500 mTorr.

Another simulation of discharge behavior (Wood, 1991; Wood et al, 1995; see also Lieberman and Lichtenberg, 1994, Section 11.4), was performed at $p = 3$ mTorr (argon) with a spacing of 10 cm between parallel plates, and over a range of rf voltages between 100 and 1000 volts. A two temperature distribution was found, as in the experiments, and the distribution varied in both space and time. It is clear that a deeper understanding of the discharge behavior involves the space and time variations of f_e. Figure 13 shows the one dimensional electron distribution function $f_e(x, v_x, t)$ versus v_x at 15 positions near the sheath region ($x = 0$–3 cm) and at eight different times during the rf cycle. Each plot covers 1/32 of a cycle temporally, and each line in a plot covers a 2 mm thick region spatially. The units on the vertical axis are proportional to f_e. At time 0/32, the sheath is fully expanded, and the two-temperature nature of the discharge near the sheath can be seen as the wide "base" and narrow "peak" of the distribution. As the rf cycle progresses to time 8/32, the distributions in the sheath region at each position display a drift toward the electrode (negative velocity) that is approximately equal to the sheath velocity. By time 12/32, fast electrons have arrived from the opposite electrode, moving at a velocity of about 4×10^6 m/s (small peak at extreme left of figure). At time 16/32, the sheath is fully collapsed, the drift in the sheath has disappeared, and the fast electron group moving toward the electrode shows a lower velocity as slower electrons arrive from the opposite electrode. As the sheath begins to expand, as shown here at times 18/32 and 20/32, the electrons in the sheath region are strongly heated, and the beginning of an electron beam produced by this expansion can be seen moving away at a positive velocity. As the sheath continues to expand, the drift of the distribution in the sheath away from the electrode can be seen to initially match the sheath velocity (time 22/32) but then decays (time 24/32) to a velocity much slower than when the sheath was collapsing. One consequence of the complicated f_e near the sheath edge is that the average electron velocity at the moving sheath edge does not correspond to the sheath velocity during the entire rf cycle, as predicted from the model equations.

The existence of more energetic electrons near the plasma edge due to stochastic heating increases the ionization there at higher pressures ($\lambda_e < l$), tending to flatten the plasma profile. Furthermore, the ionization is not constant, but follows the density variations in space and time of the more energetic electrons. This is shown for a PIC simulation by Vender and Boswell (1990) in the plot of Fig. 14, in which the darkness of each square is proportional to the number of ionizing collisions within that square of position and time intervals. Most of the ionization is seen to occur along a path of fastest electrons that are reflected off of the sheath at the phase at which it is most rapidly expanding. There is also somewhat more ionization near the sheaths, an effect that becomes more pronounced at higher pressures where the ionization mean-free-path is shorter, which has been observed in various experiments.

The spatial distribution of the electron power absorption has been examined in several PIC simulations. While the absorption is large and positive near and within the rf sheaths, it can become negative within

certain regions in the discharge bulk under conditions of strong stochastic heating (Vender, 1990; Surendra and Graves, 1991). This is particularly apparent in simulations at low pressures in a Ramsauer gas, where the ohmic dissipation (which is always positive) is small. Negative power absorption occurs where the phase of the electron current (transfered from the stochastic heating at the rf sheath edge by the electron thermal motion) differs from the phase of the local electric field by more than 90°. There have been no experimental measurements confirming the existence of negative power absorption in capacitive rf discharges, although some experimental results have hinted at the existence of this effect (e.g., see Sato and Lieberman, 1990, Fig. 7). Negative power absorption in inductive discharges is treated extensively in Section IV.

F. Other Collisionless Heating Models

The effect of a weak dc magnetic field on the stochastic electron heating by oscillating rf sheaths has been studied by Lieberman et al (1991), Okuno et al (1994), Hutchinson et al (1995), Turner et al (1996), and Park and Kang (1997). It was shown in the first work that there can be stochastic heating enhancement due to multiple correlated collisions of electrons with the moving sheath. A gyrating electron that collides once with the moving sheath collides again in a time interval of approximately half a gyroperiod. The electron trajectory can be coherent over many such sheath collisions, leading to large energy gains. An estimate of the time-average power per unit area delivered to the electrons by the oscillating sheath for a homogeneous sheath model is

$$\bar{S}_{\text{stoc}} = \frac{1}{4} m n \bar{v}_e |u_0|^2 \frac{\omega_{ce}}{\pi(\nu_m^2 + \omega^2)} \left(\nu_m + \frac{\omega_{ce}}{\pi}\right). \tag{3.23}$$

Okuno et al (1994) reported measurements of such an effect of electron acceleration resonant with the sheath motion in a cylindrical, magnetized rf-driven discharge. However, the cross-field resistivity of the bulk plasma also increases due to the magnetic field, leading to an increased bulk ohmic heating. Hutchinson et al (1995) studied the competition between sheath and bulk heating experimentally and with PIC simulations, and Turner et al (1996) compared these results to a fluid (pressure heating) model. The PIC simulations did not show an enhanced heating due to resonant electrons, although an increase in average electron energy was observed within the sheaths. Kang et al (1997) showed a reasonable agreement between measurements and a Child law sheath model incorporating stochastic heating as in (3.23).

Another kind of non-stochastic but collisionless electron heating associated with rf sheath oscillations in capacitive rf discharges has been discussed by Surendra and Dalvie (1993) and by Turner (1995). They showed that there is a powerful heating mechanism due to pressure effects that arises during the expansion and contraction of the sheath in a non-homogeneous plasma model. The pressure effect is caused by the difference in plasma density and electron energy between the bulk plasma and the near-sheath plasma. When the sheath expands, electrons flow into the adjacent bulk plasma and are compressed. At the same time, electrons are rarefied as they flow into the opposite, collapsing sheath. Turner showed that due to finite electron thermal conductivity, these simultaneous rarefactions and compressions of the electron gas produce nonequilibrium thermal disturbances, and the net work done is not zero. Solving the fluid equations with the

electron energy balance equation, Turner was able to demonstrate the pressure heating effect, which agreed well with a PIC simulation. Turner et al (1996) showed experimentally and using kinetic simulations that a weak transverse dc magnetic field can induce a transition between pressure heating and ohmic heating.

Collisionless, as well as collisional electron heating can be effectively treated on the kinetic level in the framework of the *nonlocal approach* to the solution of the Boltzmann equation (Bernstein and Holstein, 1954; Tsendin, 1974, 1995; Kolobov and Godyak, 1995; Kortshagen et al, 1996). In this approach a complicated time-space variable and multi-dimensional problem is reduced to a zero-dimensional Boltzmann equation for the symmetric part of the EEDF:

$$\frac{1}{\sqrt{\mathcal{E}}}\frac{d}{d\mathcal{E}}\frac{\sqrt{\mathcal{E}}}{2}D(\mathcal{E})\frac{df(\mathcal{E})}{d\mathcal{E}} + C^* f(\mathcal{E}) = 0, \tag{3.24}$$

where $\mathcal{E}$ is the total electron energy (kinetic plus potential), $D(\mathcal{E})$ is the time-space averaged energy diffusion coefficient, and $C^* f(\mathcal{E})$ is the inelastic collision integral. The space variation of $f(\mathcal{E})$ and its integrals are defined by the space variation of $\mathcal{E}(\mathrm{r})$; i.e., by the ambipolar potential distribution, and the electron heating and the shape of the EEDF are defined by $D(\mathcal{E})$. The electron heating power density is:

$$p_{\mathrm{eheat}} = \frac{2\sqrt{2}\,\pi}{m^{3/2}}\int_0^\infty f(\mathcal{E})\frac{d}{d\mathcal{E}}[\sqrt{\mathcal{E}}D(\mathcal{E})]\,d\mathcal{E}. \tag{3.25}$$

Thus, $D(\mathcal{E})$ contains all information about the electron heating process. The particular shape of the EEDF $f(\mathcal{E})$ and the power deposition depend on the specific mechanism of electron interaction with the rf field and with the electron phase randomization mechanism (Goedde et al, 1988; Kaganovich et al, 1996). For stochastically heated electrons, $D(\mathcal{E})$ is the product of the square of the random walk step in energy space and the frequency ν_r of such an event:

$$D(\mathcal{E}) = \frac{1}{2}\overline{(\Delta\mathcal{E})^2}\,\nu_r. \tag{3.26}$$

This approach has been used for low pressure capacitively coupled rf discharges in the stochastically heated regime by Kaganovich and Tsendin (1992).

Recently Aliev et al (1996) presented an analysis of collisionless electron heating in rf discharges based on the quasilinear theory of waves in warm plasma given for example, in Ichimaru (1973) and Alexandrov et al (1984). A similar approach was described by Eldridge (1972) for energy deposition in electron cyclotron resonance (ECR) discharges. In application to rf discharges excited by an external rf power source with frequency much lower than the cutoff frequency, the interaction of the electromagnetic field with a bounded plasma is considered as a superposition of decaying (evanescent) waves having a wide spectrum of wavenumbers $k = \omega/v_{\mathrm{ph}}$, where v_{ph} is the wave phase velocity. When the scale of the electromagnetic field (sheath width or skin depth) becomes smaller than the electron mean free path λ_e, then collisionless electron heating occurs as a result of the resonant interaction (acceleration or deceleration) of electrons with waves having their phase velocity close to the electron velocity. This process is very similar to Landau damping but occurs at frequencies much lower than the plasma frequency ($\omega \ll \omega_{pe}$). Separating the space and time scales of the

electromagnetic fields and linearizing the kinetic equation, one can divide the EEDF into a large part $f_0(\mathcal{E})$, averaged over the length scale λ_e, and a small part $f_1(\mathcal{E}) \ll f_0(\mathcal{E})$, accounting for small deviations from $f_0(\mathcal{E})$ on a length scale smaller than λ_e. Using Fourier methods, the structure of the electromagnetic fields and the diffusion coefficient $D(\mathcal{E})$ are found for different kinds of rf discharges (capacitive, inductive, and surface wave). It was shown (Aliev et al, 1996) that the diffusion coefficient that governs the EEDF shape and the electron heating power density is mainly defined by resonance electrons with velocities $v_n = \omega/k = \pi\omega l/n$, with $n = 1, 2, 3, \ldots$

Let us note that this approach is essentially linear; i.e., it involves integration over the unperturbed motions of the electrons. Hence, successive kicks are assumed to be independent with random phases. Therefore, purely nonlinear aspects, such as the existence of phase correlations between successive interactions of electrons with the localized fields, or the existence of an adiabatic barrier to heating, are absent in this model.

Wang et al (1997), Lichtenberg (1997), and Kaganovich (1997) have recently considered the nonlinear effects of the dynamics on the determination of the energy diffusion coefficient $D(\mathcal{E})$ and the resultant discharge equilibrium. Depending on the pressure, driving frequency, discharge length, and other discharge parameters, the existence of strong phase correlations and adiabatic limitations to the chaotic dynamics can play important roles in the theoretical description of the heating. Unfortunately, for many capacitive discharges of commercial interest, interparticle collisions play an equally important role, making the overall analysis difficult. The general approach is to obtain and solve a space- and time-averaged kinetic equation (Wang et al, 1997). The various regimes describing the interplay between collisional and dynamical effects have been classified by Kaganovich et al (1996).

IV. INDUCTIVE RF DISCHARGES

Plasma in an inductive discharge is maintained by application of rf power to an inductive coil, resulting in electron energy absorption due to the induced rf electric field near the coil. The driving frequency is usually 13.56 MHz, although lower (and higher) frequencies are sometimes used. As shown in Fig. 15ab, planar or cylindrical coils in a low aspect ratio (length/diameter) discharge are generally used for low pressure materials processing. The planar coil is a flat helix wound from near the axis to near the outer radius at one end of the discharge chamber ("electric stovetop" coil shape). For a typical 30 cm chamber diameter, the rf power is typically 100-1000 W.

Another kind of inductive discharge is an rf lamp with an internal coil, as shown in Fig. 15c. The internal coil, usually with a ferrite core, is inserted into a re-entrant cavity inside a glass bulb coated inside with fluorescent powder (phosphor). The bulb is filled with a mixture of inert gases such as argon or krypton at a pressure of hundreds of millitorr, and mercury vapor at a few millitorr. The inductive plasma excited inside the bulb has a very high rf power conversion to the mercury resonance uv radiation (60–70%, mainly at

253 nm), and the uv radiation excites the phosphor to emit visible light. The absence of electrodes provides a highly efficient (4–5 times more than an incandescent bulb) and durable (up to 100,000 hours) light source.

Because the voltage across the exciting coil of an inductive discharge can be as large as several kilovolts, a discharge can also be capacitively driven by the coil. There is generally a capacitively driven discharge at low plasma densities, with a transition to an inductive discharge at high densities. An electrostatic shield placed between the coil and the plasma can reduce the capacitive coupling if desired, while allowing the inductive field to couple unhindered to the plasma. Inductive discharges for materials processing are sometimes referred to as ICP's (inductively coupled plasmas), TCP's (transformer coupled plasmas), or RFI's (rf inductive plasmas).

The inductive electric field is non-propagating ($\omega \ll \omega_{pe}$) and typically penetrates into the discharge a distance on the order of a plasma skin depth, which is typically 1–3 cm. Hence plasma heating occurs near the dielectric window surface. The dc plasma potential in these discharges is typically of order 30–40 volts with respect to the walls, and the plasma density is typically in the range 10^{11}–10^{12} cm^{-3}. Hence the sheath thickness is of order 0.1–1 mm (a few Debye lengths).

A. Classical and Anomalous Skin Effect

In an inductively coupled plasma, power is transferred from the electric fields to the plasma electrons within a skin depth layer of thickness δ near the plasma surface by collisional (ohmic) dissipation and by a collisionless heating process in which bulk plasma electrons "collide" with the oscillating inductive electric fields within the skin layer. In the latter situation, electrons are accelerated and subsequently thermalized much like stochastic heating in capacitive rf sheaths, which we treated in Sec. III.

We first consider the so-called *classical* or *normal skin effect* accompanied by ohmic (collisional) electron heating in a semi-infinite spatially uniform plasma. The normal skin effect occurs when the electron thermal motion is negligible and there is a local coupling between the rf current density $\mathbf{J}$ and the rf electric field $\mathbf{E}$ within the skin layer given by $\mathbf{J} = \sigma_p \mathbf{E}$, where

$$\sigma_p = \frac{e^2 n}{m(\nu_m + j\omega)} \tag{4.1}$$

is the complex conductivity of a cold plasma. We consider the case when $\omega \ll \omega_{pe}$, which is always true for inductively coupled plasmas. We also assume a Maxwellian EEDF and an energy-independent electron-atom collision frequency $\nu_m(\mathcal{E}) = \text{const}$. Otherwise, ν_m and ω in (4.1) must be replaced by some effective $\nu_{m\text{eff}}$ and ω_{eff}, both being integrals over the energy $\mathcal{E}$ of the particular EEDF and the ω and $\nu_m(\mathcal{E})$ dependence (Lister et al, 1996).

According to Maxwell's equations, the penetration of the transverse electric field into the plasma is described by the complex wave equation

$$\frac{d^2 E_y}{dx^2} = j\omega\mu_0\sigma_p E_y, \tag{4.2}$$

having solution

$$E_y = E_{y0}\, e^{-x/\delta} \cos(\omega t - \beta x), \tag{4.3}$$

where

$$\delta^{-1} = \mathrm{Re}(j\omega\mu_0\sigma_p)^{1/2} \tag{4.4}$$

is the inverse skin depth and

$$\beta = \mathrm{Im}(j\omega\mu_0\sigma_p)^{1/2} \tag{4.5}$$

is the propagation constant. Substituting (4.1) into (4.4), one obtains the general expression for the classical (normal) skin depth (see for example Weibel, 1967),

$$\delta = \frac{\delta_0}{\cos(\epsilon/2)}, \tag{4.6}$$

where

$$\delta_0 = \frac{c}{\omega_{pe}} \left(1 + \frac{\nu_m^2}{\omega^2}\right)^{1/4} \qquad \text{and} \qquad \epsilon = \tan^{-1}(\nu_m/\omega). \tag{4.7}$$

In the collisional limit ($\nu_m \gg \omega$), typical for non-superconducting metals and high pressure plasmas, $\epsilon = \pi/2$ and

$$\delta = \delta_c = \frac{c}{\omega_{pe}} \left(\frac{2\nu_m}{\omega}\right)^{1/2} = \delta_p \left(\frac{2\nu_m}{\omega}\right)^{1/2} \tag{4.8}$$

and the rf energy collisionally dissipates within the skin layer.

In the high frequency limit ($\nu_m \ll \omega$), called the non-dissipative or high frequency skin effect, $\epsilon = 0$ and

$$\delta = \delta_p = \frac{c}{\omega_{pe}}. \tag{4.9}$$

In this case the electrons collisionlessly oscillate within the skin layer with no net energy gain. For an electromagnetic wave incident on the plasma boundary this case corresponds to the total reflection of the wave from the plasma. For discharge maintenance in this case, the wave reflection is not perfect, and a small fraction of the incident wave power is locally deposited within the skin layer.

There is a third situation for which electrons incident on a skin layer of thickness δ_a satisfy the condition $\bar{v}_e/\delta_a \gg \omega, \nu_m$, where δ_a is determined below. In this case the interaction time of the electrons with the skin layer is short compared to the rf period or the collision time. The rf field penetration in this regime was first estimated by Pippard (1949) with application to the high frequency skin effect in metals at low temperatures, and was determined self-consistently by Reuter and Sondheimer (1949) for metals and by Weibel (1967) for a homogeneous plasma half-space with a Maxwellian EEDF. To see the essential scalings, following Pippard, we consider the ordering $\nu_m \gg \omega$ and divide the electrons into two groups, those moving at small angles to the surface which spend most of their time between collisions within the skin layer, and the rest, whose chance of collision is small. We ignore the latter group of ineffective electrons. The velocities of the effective electrons form angles less than δ_a/λ_e and their relative number is of order δ_a/λ_e,

where λ_e is the electron-neutral mean free path for momentum transfer. This results in an effective plasma density $n_{\rm eff} = K_{\rm eff} n\delta_a/\lambda_e$ and an effective plasma frequency $\omega_{pe\rm eff} = \omega_{pe}(K_{\rm eff}\delta_a/\lambda_e)^{1/2}$ within the skin layer, where $K_{\rm eff}$ is a constant of order unity. Substituting these effective quantities into (4.1) and (4.8) yields an expression for the effective collision frequency $\nu_{\rm eff}$, analogous to that introduced in (3.13) for capacitive rf discharges, and for the anomalous skin depth δ_a:

$$\nu_{\rm eff} = \frac{\bar{v}_e}{K_{\rm eff}\delta_a} \qquad \text{and} \qquad \delta_a = \left(\frac{2\bar{v}_e c^2}{K_{\rm eff}\omega\omega_{pe}}\right)^{1/3}.$$

A more careful averaging based on the kinetic theory of the anomalous skin effect (Weibel, 1967; Ichimaru, 1973; Alexandrov et al, 1984) gives $K_{\rm eff} = 4$ and

$$\nu_{\rm eff} = \frac{\bar{v}_e}{4\delta_a} \qquad \text{and} \qquad \delta_a = \left(\frac{\bar{v}_e c^2}{2\omega\omega_{pe}^2}\right)^{1/3} = \delta_p \left(\frac{\bar{v}_e\omega_{pe}}{2c\omega}\right)^{1/3}. \tag{4.10}$$

According to (4.10), for a strong anomalous skin effect where $\bar{v}_e\omega_{pe} \gg c\omega$ and $\omega \gg \nu_m$, the penetration of the rf electric field into the plasma is deeper than for the non-dissipative skin effect in the high frequency limit: $\delta_a > \delta_p$.

A general *nonlocality parameter* for the non-local interaction of electrons with the electromagnetic field has been given by Fried and Conte (1961) and used in the analysis of the anomalous skin effect by Weibel (1967) and Sayasov (1979):

$$\Lambda = \left(\frac{\bar{v}_e\omega_{pe}}{c}\right)^2 \frac{\omega}{(\omega^2+\nu_m^2)^{3/2}}. \tag{4.11}$$

Formulae for the classical skin effect are applicable when $\Lambda \ll 1$; for $\Lambda \gtrsim 1$, the anomalous skin effect takes place. Note that Λ is small for both very low and very high frequency and reaches it maximum at $\omega = \nu_m/\sqrt{2}$ where $\Lambda_{\rm max} \approx (\omega_{pe}\bar{v}_e/\omega c)^2$, which is close to its high frequency ($\omega \gg \nu_m$) limit. In the opposite case ($\nu_m \gg \omega$), $\Lambda \approx (\omega_{pe}\bar{v}_e/\omega c)^2(\omega/\nu_m)^3 \ll 1$, and the normal (collisional) skin effect occurs. Figure 16 shows the boundary dividing the classical and the anomalous skin effect ($\Lambda = 1$) in the space of λ_e/δ_0 and ω/ν_m, and thus the boundary between collisional and collisionless electron heating.

Let us describe some essential features of the anomalous skin effect which are the result of the nonlocal interaction of electrons with the electromagnetic field due to their thermal motion:

(1) The spatial decay of the electromagnetic field into a plasma for the anomalous skin effect is not exponential, as it is in the classical skin effect. Moreover, the decay may be nonmonotonic and may exhibit local maxima and minima in the plasma, as shown by Weibel (1967) in his kinetic analysis (see Fig. 17), and in the experiments of Demirkhanov et al (1964) and Joye and Schneider (1979) (see Fig. 18).

(2) As has been shown by Kondratenko (1979), for a strong anomalous skin effect ($\Lambda \gg 1$) the penetration length of the rf electric field δ_E and that of the rf magnetic field δ_B are essentially different, $\delta_E < \delta_B$, while for the normal skin effect $\delta_E = \delta_B$. The less rapid spatial decay of the rf magnetic field (and accompanying rf current density) is due to the ballistic transport of rf current caused by the electron thermal

motion. Different formulae for δ can be seen in the literature (which differ by factors of order unity) due to different definitions of the electron thermal velocity [$(\kappa T_e/m)^{1/2}$, $(2\kappa T_e/m)^{1/2}$, or $(8\kappa T_e/\pi m)^{1/2}$], and, more importantly, due to different definitions of δ_a by different authors. The δ_a value can be defined as $\delta_a = |d \ln E_y/dx|^{-1}_{x=0}$, or as $\delta_a = E_{y0}^{-1} \int_0^\infty E_y\, dx$, or as a distance where the rf electric or magnetic field (or rf power) decays by one (or two) e-foldings. Different values can be obtained for δ_E or δ_B using these definitions, while for the normal skin effect all these definitions give the same formula (4.6).

(3) In the regime of the strong anomalous skin effect neither the skin depth δ_a nor the energy dissipation in the skin layer depend on the collision frequency ν_m. In this case the rf energy dissipation process occurs even in the limit $\nu_m \to 0$. The non-collisional dissipation has a simple explanation. For a relatively thin skin layer when $\delta < \bar{v}_e/\omega$ and $\delta < \lambda_e$, the electrons reflecting from the space charge sheath at the plasma-wall boundary cross the skin layer in a time less than the rf field period. Hence the electrons gain energy within the skin layer as in a dc field. This differs from collisionless electron motion in a homogeneous rf field when $\delta \gg \bar{v}_e/\omega$, corresponding to the high frequency limit of the normal skin effect in which electrons gain energy from the field during one quarter cycle and return the energy back to the field during the next quarter cycle.

For both the normal and the anomalous skin effect, there is no electron heating unless some phase mixing (randomization) mechanism breaks the regularity of the electron motion. For collisional heating corresponding to the normal skin effect, randomization occurs locally within the skin layer due to electron-atom (and/or electron-ion) collisions. For the anomalous skin effect the randomization is provided by the electron thermal motion which moves electrons out of the skin layer into the neighboring plasma having no rf field, thus preventing the electrons from returning the energy acquired in the skin layer back to the rf field. For a bounded plasma such as an inductive discharge where electrons can repeatedly interact with the rf field in the skin layer, some randomization mechanism must be present in the bulk plasma to provide an effective electron heating in the skin layer.

Let us note that the kinetic treatment of the anomalous skin effect (e.g., Weibel, 1967) is a linear theory in which the dissipation is determined by integration over the *unperturbed* motion (orbits) of the electrons. Low velocity electrons can have strongly perturbed orbits, leading to wave trapping and ponderomotive force effects. But if the average energy gain is much less than the thermal energy, then this class of electrons contribute little to the overall energy absorption. The repeated interaction of high energy electrons with the skin layer in a bounded system can lead to strong phase correlations and adiabatic interactions of electrons with the skin layer in the absence of external stochastic forces such as electron-neutral collisions. These mechanisms are similar for inductive and capacitive discharges (see Sec. III) and have recently been analyzed by Kaganovich et al (1996).

B. Fermi Acceleration Model of Collisionless Heating

To determine the heating at low pressures using a Fermi acceleration model, we consider an electron from the bulk plasma incident on the rf electric field within a skin depth layer in slab geometry. We assume

a simple model in which the transverse electric field within the slab decays exponentially with distance x from the edge into the slab,

$$E_y(x,t) = E_0 e^{-|x|/\delta} \cos(\omega t + \phi). \tag{4.12}$$

We also assume that the force due to the rf magnetic field is negligible and that the collisionality is weak, $\nu_m \ll \bar{v}_e/2\delta$; hence there are no electron collisions within the skin layer. A similar model was first introduced by Holstein (1952) to describe the low temperature optical and infrared reflectivity of metals. Because there are no x-directed forces, we can write

$$\begin{aligned} x(t) &= -v_x t, \qquad t < 0, \\ &= v_x t, \qquad t > 0, \end{aligned} \tag{4.13}$$

where the electron reflects from the surface at $t = 0$. Substituting (4.13) into (4.12) yields the transverse electric field seen by the electron,

$$\begin{aligned} E_y(t) &= \mathrm{Re}\, E_0 e^{(j\omega + v_x/\delta)t + j\phi}, \qquad t < 0, \\ &= \mathrm{Re}\, E_0 e^{(j\omega - v_x/\delta)t + j\phi}, \qquad t > 0. \end{aligned} \tag{4.14}$$

The transverse velocity impulse,

$$\Delta v_y = -\int_{-\infty}^{\infty} dt \frac{eE_y(t)}{m}, \tag{4.15}$$

is calculated by substituting (4.14) into (4.15) and integrating to obtain

$$\Delta v_y = \frac{2eE_0\delta}{m} \frac{v_x}{v_x^2 + \omega^2\delta^2} \cos\phi. \tag{4.16}$$

The energy change $\Delta\mathcal{E}$, averaged over a uniform distribution of initial electron phases ϕ, is then

$$\begin{aligned} \Delta\mathcal{E} &= \frac{1}{2} m \langle (\Delta v_y)^2 \rangle_\phi \\ &= \frac{1}{4} m \left(\frac{2eE_0\delta}{m} \right)^2 \frac{v_x^2}{(v_x^2 + \omega^2\delta^2)^2}, \end{aligned} \tag{4.17}$$

which can be integrated over the particle flux to obtain the stochastic heating power

$$S_{\mathrm{stoc}} = \int_{-\infty}^{\infty} dv_y \int_{-\infty}^{\infty} dv_z \int_0^{\infty} dv_x\, f_e v_x \Delta\mathcal{E}(v_x). \tag{4.18}$$

For a Maxwellian electron distribution f_e, the integrals over v_y and v_z are easily done, and the v_x integral can be evaluated in terms of the exponential integral E_1. For the regime of large stochastic heating,

$$\zeta = \frac{4\omega^2\delta^2}{\pi\bar{v}_e^2} \ll 1, \tag{4.19}$$

we obtain (Lieberman and Lichtenberg, 1994, Appendix C)

$$S_{\mathrm{stoc}} \approx \frac{mn_s}{\bar{v}_e} \left(\frac{eE_0\delta}{m} \right)^2 \frac{1}{\pi} \left[\ln\left(\frac{1}{\zeta} \right) - 1.58 \right]. \tag{4.20}$$

We can introduce an effective collision frequency $\nu_{\rm eff}$ by equating the stochastic heating (4.20) to an effective collisional heating power flux,

$$S_{\rm ohm} = \frac{1}{2}\int_0^\infty dx \left(E_0 e^{-x/\delta}\right)^2 \frac{e^2 n_s}{m}\frac{\nu_{\rm eff}}{\nu_{\rm eff}^2+\omega^2}$$
$$= \frac{1}{4}\frac{e^2 n_s \delta}{m}\frac{\nu_{\rm eff}}{\nu_{\rm eff}^2+\omega^2}E_0^2. \tag{4.21}$$

For $\omega \ll \nu_{\rm eff}$, we have

$$S_{\rm ohm} = \frac{1}{4}\frac{e^2 n_s \delta}{m\nu_{\rm eff}}E_0^2,$$

and equating this to (4.20), we determine

$$\nu_{\rm eff} = \frac{\bar{v}_e}{\delta}\frac{4}{\pi}\left[\ln\left(\frac{1}{\zeta}\right) - 1.58\right], \tag{4.22}$$

With $\zeta \ll 1$, we find $\nu_{\rm eff} \sim \bar{v}_e/\delta$, in agreement with the simple estimate (4.10).

Although Fermi acceleration models of the velocity impulse lead to simple estimates of the effective collision frequency due to stochastic heating, they are not self-consistent because the form of the spatial variation of the electric field has been assumed. The heating power and effective collision frequency have been determined over the entire range of collisionality from a Fermi acceleration model with an exponentially decaying electric field profile by Vahedi et al (1995). We summarize their results and compare them to a self-consistent model in the next subsection.

C. Self-Consistent Collisionless Heating

The self-consistent analysis of Reuter and Sondheimer (1949), using a Fermi-Dirac electron distribution to determine the anomalous skin resistance of a low temperature metal, was first applied by Weibel (1967) to a classical plasma having a Maxwellian electron distribution. The rf power absorption due to the skin effect can be characterized by a complex surface impedance

$$Z_s = Z_{s\rm R} + jZ_{s\rm I} = E_y(0)/H_z(0). \tag{4.23}$$

The time-average power absorbed by the plasma per unit area can be written in terms of Z_s as:

$$S_{\rm abs} = {\rm Re}\left(\frac{1}{2}E_y(0)H_z^*(0)\right) = {\rm Re}\left(\frac{1}{2}Z_s|H_z^*(0)|^2\right). \tag{4.24}$$

For the classical (normal) skin effect, we find

$$Z_s = j\omega\mu_0\delta_p\left[\sqrt{b(1+b)/2} + j\sqrt{b(1-b)/2}\right]^{-1}, \tag{4.25}$$

where $b = (1+\nu_m^2/\omega^2)^{-1/2}$. For $\nu_m \gg \omega$, corresponding to the normal skin effect dominated by collisional heating, we find

$$Z_s = \frac{\omega\mu_0\delta_c}{2}(1+j), \tag{4.26}$$

with δ_c given by (4.8). For the anomalous skin effect (see Weibel, 1967; Turner, 1993; and Shaing, 1996), we obtain

$$Z_s = \frac{2\omega\mu_0\delta_a}{3}\left(\frac{1}{\sqrt{3}} + j\right), \tag{4.27}$$

with δ_a given by (4.10).

The self-consistent analysis of the anomalous skin effect of Weibel (1967) and Blevin et al (1970) was applied to heating in inductive discharges of finite extent by Turner (1993), who also compared the results to a kinetic simulation. Following the Blevin et al (1970) analysis, Kolobov and Economou (1997) calculated analytically the surface impedance for a plasma slab model over a wide range of collisionality, $10^{-2} < \nu_m/\omega < 10^2$. The results, which closely coincide to the simulations of Turner (1993), are shown in Fig. 19. In the collisional regime where $\nu_m/\omega \geq 3$, the results of kinetic (warm plasma) theory practically coincide with hydrodynamic (cold plasma) theory, corresponding to the classical skin effect. In the collisionless limit when $\nu_m/\omega \to 0$, the real part of the surface impedance disappears in the classical (cold plasma) skin effect theory (there is no heating in the high frequency limit), but remains a constant, independent of the collision frequency, in the kinetic theory of the skin effect acounting for the electron thermal motion.

Typical behaviors for the anomalous skin depth, the surface impedance, the effective stochastic collision frequency and the normalized rf power dissipation in the skin layer are shown in Figs. 20, 21, 22, and 23 respectively, as calculated by Vahedi et al (1995). In these figures the calculated parameters are given as functions of the normalized rf frequency $w = c\omega/\bar{v}_e\omega_{pe}$ for $\lambda_e > \delta$, where $w = \Lambda^{-1/2}$ (Λ is the nonlocality parameter for $\omega^2 \gg \nu_m^2$). The comparisons with self-consistent results for the normalized rf power absorption (Fig. 23) and with the formula for the anomalous skin depth (Fig. 22 for $w < 1$ show good agreement and justify the simplifications assumed by Vahedi et al (1995) for calculating the absorbed power.

Both collisional and collisionless results are modified when the system length l becomes comparable to the skin depth δ. This was first noted by Kondratenko (1979) and confirmed by Turner (1993), who obtained from his finite length simulation a reduced collisionless heating, as compared to the semi-infinite slab result (4.27). This effect has been treated analytically by Kondratenko (1979), Shaing and Aydemir (1996), and Kolobov and Economou (1997). With rare electron collisions in the plasma slab, the surface impedance and electron heating can be affected by the bounce resonance electrons for which $\omega \approx \Omega_b$, where $\Omega_b \approx v_x/2L$ and v_x is the electron velocity component along x.

One might think that the stochastically heated electrons absorb energy along the direction of the wave electric field; i.e., along the y-direction in the slab model. That this is not the case can be seen by considering the canonical angular momentum $P_y = mv_y - eA_y(x,t)$, where $E_y(x,t)$ is obtained from the vector potential as $E_y = -\partial A_y/\partial t$. Because the Hamiltonian for the motion is independent of y, P_y is conserved. Since A_y vanishes a few skin depths into the plasma, it follows that v_y within the plasma is a constant of the motion. Hence, the transverse acceleration of the electron along y within the skin layer is converted by the wave magnetic field into a longitudinal acceleration along x as the electron exits the layer (Cohen and Rognlien,

1996). Therefore the stochastic heating is along the direction of motion, a classical Fermi acceleration model. Because the magnetic field does no work on the electron, the kick in energy is the same; only the direction of the kick is altered.

The wave magnetic field can have other important effects, especially at low frequency and pressure when the electron gyration frequency ω_{ce} can exceed the driving and collision frequencies. In this case one observes enhanced penetration of the wave into the plasma (Tuszewski, 1996). This effect has been modeled in terms of an effective conductivity in the presence of the rf magnetic field that is time-averaged over an rf period. This leads to an effective collision frequency $\nu_{\rm eff} \approx |\omega_{ce}|$ which, when inserted into (4.8), yields an effective magnetic skin depth

$$\delta_m \approx \frac{c}{\omega_{pe}} \left(\frac{2|\omega_{ce}|}{\omega} \right)^{1/2} . \tag{4.28}$$

Other works that treat modifications of the skin depth and the field profiles in terms of ponderomotive forces have been given by Helmer and Feinstein (1994), DiPeso et al (1995), and Cohen and Rognlien (1996). The role of this effect becomes important for low frequency inductive discharges where maintaining the discharge rf field E_θ requires a large value of $B_{\rm rf}$ because $E_\theta \sim \omega \delta B_{\rm rf} \sim$ const.

Recently, extensive modeling of low pressure inductive discharges (Gibbons and Hewett, 1995; Turner, 1996; Yoon et al, 1996; Kolobov and Economou, 1997; Kolobov et al, 1997) has demonstrated the importance of non-local electron heating effects. Turner (1996) has showed that the introduction of an appropriate viscosity into fluid equations can adequately account for some kinetic effects including the anomalous skin effect and electron stochastic heating. An analytical solution for a one-dimensional planar coil inductive rf discharge with finite length and at arbitrary collisionality has been obtained by Shaing and Aydemir (1996) and by Yoon et al (1996). As shown in Fig. 24, the real part of the surface impedance exhibits a slight maximum at a certain chamber length. This maximum is a result of the finite size coupled with the resonance condition for bouncing electrons within the plasma slab ($2L\omega/v_x \approx 1, 2, 3, \ldots$). As is shown by Kolobov (1997), these resonance conditions do not result in a pronounced resonance behavior for the discharge characteristics due to the wide ranges of electron velocity angles and magnitudes that are present in a warm (Maxwellian) distribution. The finite plasma dimension is also important for electron heating when $\lambda_e > L$ (Kaganovich et al, 1996). In the absence of collisions there is no heating if the rf magnetic field influence on the electron motion is neglected. This situation corresponds to a constant bounce frequency, for which there is no intrinsically dynamical phase randomization during the motion. Thus there is no randomization without electron-atom collisions. On the other hand, resonance electrons can effectively gain energy due to rare collisions during multiple bouncing, since the average electron lifetime is much greater than the bounce time: $\tau \approx L/u_B \gg \Omega_b^{-1} = 2L/v_x$. However, the effective collision frequency in this limit scales with the electron-atom collision frequency, corresponding to phase randomization only on the timescale of the rare collisions; i.e., the electron power deposition is proportional to the pressure.

Kolobov et al (1997) have modeled a one-dimensional rf discharge excited by an azimuthal induction electric field produced by an infinitely long cylindrical coil. The electron heating was treated in terms of the energy diffusion coefficient $D(\mathcal{E})$, as in (3.25). Sharp peaks of $D(\mathcal{E})$ were found for resonance electrons in a weakly collisional regime, but averaging $D(\mathcal{E})$ over angles in velocity space diminishes the resonance behavior. A similar effect may be expected for an inductive discharge excited by a planar coil. The EEDF in this work was found from the linearized Boltzmann equation and from a Monte Carlo simulation taking into account the rf magnetic field and finite size effects over a large range of gas pressure and rf frequency. Yoon et al (1997) have recently developed a two-dimensional nonlocal heating theory for planar inductively coupled discharges and obtained the effective plasma resistance and the ponderomotive force potential.

D. Experiments

Demirkhanov et al (1964) were the first to observe the anomalous skin effect in a plasma. Measuring the rf magnetic field distribution in a toroidal inductive rf discharge with a magnetic probe, they found an anomalous penetration of the rf field into the plasma at some combination of the external discharge parameters (rf power, gas pressure, and frequency), typical for the anomalous skin effect. They also found a minimum in the rf magnetic field between the discharge axis and the wall, similar to that shown in Fig. 18, which they explained as resulting from rf current dispersion due to electron thermal motion. According to the classical skin effect, the minimum should be at the discharge axis. This experimental work inspired extensive theoretical studies of the anomalous skin effect using kinetic models during the following decade. Although the anomalous rf field penetration and non-collisional electron heating are coupled, early experimental works focused on the field penetration rather than power absorption.

Recently, the wide application of inductively coupled plasmas (ICP's, TCP's) in plasma processing and in lighting technology have revitalized interest in ICP physics and, particularly, in the anomalous skin effect and non-collisional electron heating. Non-collisional heating is now recognized as being essential to ICP operation in the milliTorr pressure range, but quantitative experimental evidence that this process exists has not been easy to obtain. The main problem is to distinguish (separate) the collisional and collisionless parts of the measured rf power absorbed by the plasma, which are parametrized by the corresponding collision frequencies ν_m and ν_{stoc}. To identify collisionless effects by comparing skin depths measured in experiments with those calculated for the classical collisional or high frequency skin effect, or the anomalous skin effect, is practically impossible since all these skin depths are nearly the same for the usual experimental regimes. Also, plasma and rf field inhomogeneities, together with a non-Maxwellian EEDF, make it difficult to compare the experimental observations with the theories, which assume a homogeneous plasma having a Maxwellian EEDF and a non-variable ν_m. Moreover, all theories describe a one-dimensional (flat) skin effect, whereas in experiments the plasma and the configuration of the rf fields are at least two-dimensional.

In a typical ICP experiment in a short metal cylindrical chamber with a dielectric window and a planar coil, the axial distribution of the rf field even without plasma is very inhomogeneous. Therefore, the rf field decay during its propagation into the plasma is a combined effect of the chamber geometry and the plasma

screening due to the skin effect. As was mentioned in Godyak et al (1994), collisionless heating in ICP's might occur even without the skin effect originated by the plasma conductivity, due to the vacuum rf field inhomogeneity alone, which always exists in an inductive discharge. This situation corresponds to an ICP with a low plasma density (power) where the skin depth δ_p is greater than the characteristic length δ_v of the vacuum field inhomogeneity.

For the classical skin effect in a uniform plasma excited by a planar coil in a metallic cylindrical chamber of radius R, for the lowest-order radial mode, the electric field profile next to the window has the form $E_\theta(r,z) = E_{\theta 0}\mathrm{J}_1(3.83r/R)\exp(-z/\delta)$, where J_1 is the first-order Bessel function and the plasma skin depth is (see, for example, Vahedi et al, 1995):

$$\delta = \delta_p \left(\frac{2(1+\nu_m^2/\omega^2)}{a[1+(1+\nu_m^2/\omega^2 a^2)^{1/2}]} \right)^{1/2}, \tag{4.29}$$

where

$$a = 1 + \frac{\delta_p^2}{\delta_v^2}\left(1 + \frac{\nu_m^2}{\omega^2}\right) \tag{4.30}$$

and $\delta_v \approx R/3.83$. For the anomalous skin effect, ν_m can approximately be replaced by an effective collision frequency ν_{eff} as in (4.10). It follows from (4.29) that for $\delta_p \gg \delta_v$ (low plasma density), $\delta = \delta_v$; and for $\delta_p \ll \delta_v$ (high plasma density), δ is the classical skin depth given by (4.6).

A method has been developed to evaluate experimentally the effective electron collision frequency ν_{eff}, accounting for both collisional and stochastic heating, by considering the primary induction coil as a transformer with the plasma being the secondary winding (Piejak et al, 1992). This method is based on calculation of the plasma Q-factor $Q_p = \omega/\nu_{\text{eff}}$ from the measured changes in the primary induction coil impedance induced by the plasma load (Godyak et al, 1994):

$$\frac{\omega}{\nu_{\text{eff}}} = \frac{\xi}{\rho} - \frac{\xi^2+\rho^2}{K_p^2 X_0 \rho}, \tag{4.31}$$

where ξ and ρ are respectively the change in the coil reactance and resistance, $X_0 = \omega L_0$ is the unloaded coil reactance, and $K_p < 1$ is the coupling coefficient between the coil and the plasma. There are a number of ways to measure K_p. However, in experiments the second term in (4.30) is usually small compared to the first. In this way, Godyak et al (1994) obtained $\nu_{\text{eff}} = 4 \times 10^7\ \text{s}^{-1}$ in an argon rf discharge operating at 10 mTorr and 13.56 MHz in the rf power range between 20–150 W. This value of ν_{eff} was found to be much larger than ν_m calculated as $\nu_m = n_g \sigma_m(\bar{v}_e)\bar{v}_e$. Consequently, Godyak et al (1994) stated that in their experiment a collisionless mechanism was dominating the electron heating. Later, a more accurate calculation of ν_m for conditions close to this experiment based on integration of the measured EEDF showed that the measured ν_{eff} was actually very close to ν_m (Godyak, 1997). Also, Kortshagen (1996) modeled this experiment accounting only for collisional heating, and his results were in reasonable agreement with the experiment.

An experimental study of a low pressure inductive discharge over a wide range of argon gas pressure, rf power and frequency has been recently performed at OSRAM SYLVANIA and reported by Godyak (1997). The EEDF and rf field and current density distribution were measured in a near-collisionless regime in a metal chamber with a planar ICP excitation coil using Langmuir and magnetic probes. The chamber diameter was 20 cm and the length was 10.5 cm. From the magnitudes and phases of the measured components of rf magnetic field B_r and B_z within the skin layer and the plasma, the rf electric field E_θ and current density J_θ were determined from Maxwell's equations. The absolute values of the power density absorbed and the effective electron collision frequency were then directly found according to the relations

$$p_{\rm abs} = J_\theta E_\theta \cos\psi \qquad \text{and} \qquad \nu_{\rm eff} = \frac{e^2 n_1 E_\theta \cos\psi}{m J_\theta},$$

where ψ is the measured phase shift between J_θ and E_θ, and n_1 is the local plasma density measured with a Langmuir probe. In Table 1 are shown results of calculations for 6.78 MHz based on measurements within the skin layer at the maximum of the rf current density distribution (approximately 1 cm from the glass window) at a radial position of 4 cm, corresponding to maximum of the rf electric field radial distribution. As is seen in Table 1, at $p = 1$ mTorr, $\nu_{\rm eff} \gg \nu_m$, such that collisionless electron heating dominates. At $p = 10$ mTorr, $\nu_{\rm eff} \approx \nu_m$, and power absorption in the skin layer is predominantly collisional. It is interesting to compare values of $\nu_{\rm eff}$ found experimentally at 1 mTorr where $\nu_{\rm eff} \gg \nu_m$ with a theoretical expression for the collisionless (stochastic) frequency $\nu_{\rm stoc} = \bar{v}_e/4\delta$ given by Vahedi et al (1995) for a one-dimensional model with an exponential rf profile. The values δ were determined as the distance from the glass window where the measured rf electric field decays by one e-folding. The calculated values of $\nu_{\rm stoc}$ given in Table 1 appear to be close to the measured values of $\nu_{\rm eff} - \nu_m$.

The rf power absorption density integrated along the direction of electromagnetic field propagation, $S(z) = \int_0^z E_\theta J_\theta \cos\psi \, dz'$, is shown in Fig. 25 as a function of the distance from the window. Here the measured total absorbed power flux S is compared with that calculated from the measured E_θ and J_θ distributions assuming collisional power absorption:

$$S_{\nu E} = \int_0^z E_\theta^2 \,{\rm Re}(\sigma_p) dz' \qquad \text{and} \qquad S_{\nu J} = \int_0^z J_\theta^2 \,{\rm Re}(\sigma_p^{-1}) dz',$$

with σ_p given in (4.1). The comparison shows that the collisionless process dominates the rf power absorption in these particular cases.

The spatial distribution of the absorbed rf power density is shown in Fig. 26. The power density was calculated as $E_\theta J_\theta \cos\psi$. As expected, practically all power is dissipated within the skin layer near the window. However, far from the window the power absorption for $p = 1$ mTorr oscillates with distance and becomes negative in certain regions. The negative power absorption occurs where the phase of the electron current (transfered from the skin layer due to electron thermal motion) differs from the local rf field phase

by more than 90°. Here, the electrons arriving from the skin layer transfer the energy they acquired from within the skin layer back to the rf field.

For the normal skin effect, the rf current is defined by the product of the rf electric field and the local value of the cold plasma conductivity, such that $J_\theta E_\theta \cos\psi$ is always positive. For the anomalous skin effect the current far away from the skin layer is that which is translated from the skin layer by the electron thermal motion, and its phase is defined by the transit time $\tau_J \approx z/\bar{v}_e$, while the electric field phase is defined by a delay due to the phase velocity, which depends on frequency and plasma density, $\tau_E \approx z/v_{\rm ph}$. The different mechanisms of phase delay for current and electric field can result in various phase combinations including those corresponding to a negative power absorption. Apparently, the negative power absorption can exist only in the collisionless regime ($\lambda_e \lesssim L$); otherwise, electron-atom collisions destroy the translational motion of the current, yielding a local coupling between rf current and electric field, as shown in the high pressure cases in Fig. 26b. The rf power absorption along the plasma is shown in Fig. 27 at various frequencies for $p = 10$ mTorr (where $\lambda_e \approx L$), and a discharge power of 100 W. A transit time effect is clearly seen for the appearance of the first negative power absorption region. The distance d between the middle of the skin layer and the first zero crossing of the power correspond well with the relation $d = \bar{v}_e/2f$, where $f = \omega/2\pi$ is the rf frequency. Note that apparently there is no negative power absorption at the lowest frequency of 3.39 MHz, where the anomalous skin effect (large Λ) and the electron ballistic phenomena are expected to be greatest. This has a simple explanation: for 3.39 MHz, the electron transit time $L/\bar{v}_e$ is smaller than half of an rf period $(2f)^{-1}$.

An analytical calculation of rf power absorption for parameters of the Godyak (1997) experiment has been performed by Kolobov (1997) within the framework of the existing theory of the anomalous skin effect for a homogeneous plasma (Kondratenko, 1979), modified to account for the inhomogeneity of the vacuum rf field, as in (4.29). The result shown in Fig. 27b demonstrates a good agreement with the experiment in Fig. 27a.

V. ELECTRON CYCLOTRON RESONANCE DISCHARGES

Waves generated near a plasma surface can propagate into the plasma or along the surface where they can be subsequently absorbed, leading to heating of plasma electrons and excitation of a discharge (Lieberman and Lichtenberg, 1994, Chapter 13). The classical example is an electron cyclotron resonance (ECR) discharge, in which a right circularly polarized electromagnetic wave propagates along dc magnetic field lines to a resonance zone, where the wave energy is absorbed by collisionless heating. This is a type of stochastic heating in which electrons receive "kicks" in energy at each passage through the resonance zone; i.e., it is a type of Fermi acceleration.

ECR discharges are generally excited at microwave frequencies (e.g., 2450 MHz), and the wave absorption requires application of a strong dc magnetic field (875 G at resonance). The power is usually coupled through a dielectric end-window into a cylindrical metal source chamber. One or several concentric magnetic field

coils are used to generate a nonuniform, axial magnetic field $B(z)$ within the chamber to achieve the ECR condition, $\omega_{ce}(z_{\rm res}) \approx \omega$, where $z_{\rm res}$ is the axial resonance position. When a low pressure gas is introduced, the gas breaks down and the discharge forms inside the chamber. For materials processing applications, the plasma diffuses along the magnetic field lines into a process chamber toward a wafer holder. The source diameter is 15–30 cm, and the microwave power is 1–5 kW.

Two separated magnet coils generate a so-called *magnetic mirror* field configuration having a high field underneath the two coils and a weaker field in the midplane between the coils. Electrons can be axially trapped between the high field regions by the axial magnetic field gradients and repeatedly bounce between the mirror coils (e.g., see Lieberman and Lichtenberg, 1994, Sec. 4.3). By proper choice of the field strength and profile, there can be two resonance zones symmetrically located with respect to the midplane. This configuration can yield high ionization efficiencies, due to enhanced confinement of hot (superthermal) electrons that are magnetically trapped between the two mirror (high-field) positions.

Because the gas pressure in these discharges can be as low as 0.1–0.01 mTorr and the field strengths can be large (large kicks), phase randomization due to nonlinear dynamical effects can be very important. Dynamical effects such as the influence of phase correlations in slowing the quasilinear heating rate, and the existance of adiabatic barriers to heating, have been observed experimentally in these discharges.

To determine the collisionless heating power from a Fermi acceleration model, the nonuniformity in the magnetic field profile $B(z)$ must be considered. For $\omega_{ce} \neq \omega$, an electron does not continuously gain energy, but rather its energy oscillates at the difference frequency $\omega_{ce} - \omega$. As an electron moving along z passes through resonance, its energy oscillates as shown in Fig. 28, leading to a transverse energy gained (or lost) in one pass. For low power absorption, where the electric field at the resonance zone is known, the heating can be determined as follows. We expand the magnetic field near resonance as

$$\omega_{ce}(z') = \omega(1 + \alpha z'), \tag{5.1}$$

where $z' = z - z_{\rm res}$ is the distance from exact resonance, $\alpha = \partial\omega_{ce}/\partial z'$ is proportional to the gradient in $B(z)$ near the resonant zone, and we approximate $z'(t) \approx v_{\rm res}t$, where $v_{\rm res}$ is the parallel speed at resonance.

The complex force equation for the right hand component of the transverse velocity, $v_r = v_x + jv_y$, can be written in the form

$$\frac{dv_r}{dt} - j\omega_{ce}(z)v_r = -\frac{e}{m}E_r e^{j\omega t}, \tag{5.2}$$

where E_r is the amplitude of the RHP wave with

$$\mathbf{E} = \text{Re}\left[(\hat{x} - j\hat{y})E_r e^{j\omega t}\right] \tag{5.3}$$

and $\hat{x}$ and $\hat{y}$ unit vectors along the x and y directions. Using (5.1) and substituting $v_r = \tilde{v}_r \exp(j\omega t)$ into (5.2), we obtain

$$\frac{d\tilde{v}_r}{dt} - j\omega\alpha v_{\rm res}t\tilde{v}_r = -\frac{e}{m}E_r. \tag{5.4}$$

Multiplying by the integrating factor $e^{-j\theta(t)}$ and integrating (5.4) from $t = -T$ to $t = T$, we obtain

$$\tilde{v}_r(T)e^{-j\theta(T)} = \tilde{v}_r(-T)e^{-j\theta(-T)} - \frac{eE_r}{m}\int_{-T}^{T} dt' e^{-j\theta(t')}, \tag{5.5}$$

where

$$\theta(t) = \omega\alpha v_{res}t^2/2. \tag{5.6}$$

In the limit $T \gg (2\pi/\omega|\alpha|v_{res})^{1/2}$, the integral in (5.5) is the integral of a Gaussian of complex argument, which has the standard form

$$\int_{-T}^{T} dt' e^{-j\theta(t')} = (1-j)\left(\frac{\pi}{\omega|\alpha|v_{res}}\right)^{1/2}. \tag{5.7}$$

Substituting (5.7) into (5.5), multiplying (5.5) by its complex conjugate, and averaging over the initial "random" phase $\theta(-T)$, we obtain

$$|\tilde{v}_r(T)|^2 = |\tilde{v}_r(-T)|^2 + \left(\frac{eE_r}{m}\right)^2\left(\frac{2\pi}{\omega|\alpha|v_{res}}\right). \tag{5.8}$$

The average energy gain per pass is thus

$$W_{ecr} = \frac{\pi e^2 E_r^2}{m\omega|\alpha|v_{res}}. \tag{5.9}$$

This can also be written as

$$W_{ecr} = \frac{1}{2}m(\Delta v)^2, \tag{5.10}$$

where $\Delta v = (eE_r/m)\Delta t_{res}$, and

$$\Delta t_{res} = \left(\frac{2\pi}{\omega|\alpha|v_{res}}\right)^{1/2} \tag{5.11}$$

is the effective time in resonance. The effective resonance zone width (see Fig. 28) is

$$\Delta z_{res} \equiv v_{res}\Delta t_{res} = \left(\frac{2\pi v_{res}}{\omega|\alpha|}\right)^{1/2}, \tag{5.12}$$

which, for typical ECR parameters, gives $\Delta z_{res} \sim 0.5$ cm.

The absorbed power per unit area is found by integrating (5.9) over the flux nv_{res} of electrons incident on the zone, yielding

$$S_{ecr} = \frac{\pi n e^2 E_r^2}{m\omega|\alpha|}. \tag{5.13}$$

We can understand the form of Δt_{res} as follows: an electron passing through the zone coherently gains energy for a time Δt_{res} such that

$$[\omega - \omega_{ce}(v_{res}\Delta t_{res})]\,\Delta t_{res} \approx 2\pi. \tag{5.14}$$

Inserting (5.1) into (5.14) and solving for Δt_{res}, we obtain (5.11). A more careful derivation of the absorbed power, including the effect of non-constant v_{res} during passage through resonance, is presented by Jaeger et al (1972), giving similar results.

At high power absorption, the electric field is not known but must be determined self-consistently with the energy absorption, in the same manner as for inductive discharges. The propagation and absorption of microwave power in ECR sources is an active area of research and is not fully understood. However, the essence of the wave coupling, and transformation and absorption at the resonance zone, can be seen by considering the one dimensional problem of a righ-hand polarized wave propagating strictly along the magnetic field in a plasma that varies only along the axial direction z. This problem was originally studied in connection with wave propagation in the ionosphere, and the solution was obtained analytically by Budden (1966) for the approximation of constant density and linear magnetic field variation. For a wave travelling into a decreasing magnetic field, he obtained the solution

$$S_{\rm abs}/S_{\rm inc} = 1 - {\rm e}^{-\pi\eta}, \tag{5.15}$$

$$S_{\rm trans}/S_{\rm inc} = {\rm e}^{-\pi\eta}, \tag{5.16}$$

$$S_{\rm refl}/S_{\rm inc} = 0, \tag{5.17}$$

where $\eta = \omega_{pe}^2/(\omega c|\alpha|)$. Hence some of the incident wave power is absorbed at the resonance while some tunnels through to the other side, but no power is reflected. Taking a typical case for which $\alpha = 0.1$ cm^{-1} and $k_0 = 0.5$ cm^{-1}, we find that $\eta > 1$ corresponds to $\omega_{pe}^2/\omega^2 > 0.2$. Thus at 2450 MHz we expect most of the incident power will be absorbed for a density $n_0 \gtrsim 1.5 \times 10^{10}$ cm^{-3}.

For high electric field strengths and low pressures, the energy gain per passage through resonance is large, and the nonlinear dynamical aspects of the problem come into play. For electrons heated to high energies by repeated interaction with the resonance zones, strong phase correlations can reduce the heating rate below that obtained from a random phase interaction, and an adiabatic barrier to heating can exist. Such phenomena were observed experimentally in a high field (50 kG) magnetic mirror compression experiment (Wyeth et al, 1975), in which a short pulse (0.25 μs) of high power (maximum 250 kW) microwaves was used to heat plasma electrons early during the compression, which were subsequently further heated by the increasing magnetic field. With increasing microwave power (field strength), a transition from a high to a lower heating rate was found that agreed well with analytical and numerical mapping estimates of the expected transition from a regime of random phase interaction to a regime of high phase correlations.

Another experiment was performed by Shoyama et al (1996) in a magnetic mirror field configuration, ECR discharge at low pressures (3–8 $\times 10^{-5}$ Torr) using up to 4 kW of 2.45 GHz continuous wave power. A steady state plasma having a typical electron temperature of 6 V and density of 7×10^{11} cm^{-3} was formed, having a high energy electron tail of order 10 kV as determined by x-ray bremsstrahlung measurements. From the theory of Fermi acceleration and as confirmed by numerical iteration of the appropriate Fermi mapping for this system, the maximum possible energy $\mathcal{E}_{\rm max}$ of the heated electrons was found to scale with the input microwave power $P_{\rm in}$ as $\mathcal{E}_{\rm max} \propto P_{\rm in}^{0.5-0.6}$, due to the existance of an adiabatic barrier to heating. The experimental data confirmed this scaling.

VI. CONCLUDING DISCUSSION

Collisionless (stochastic) heating of electrons by time-varying fields has been shown to be fundamental to the operation of radio frequency (rf) and microwave discharges. Such heating is due to spatial variation of the fields, which lead to randomization of the electron phase during its thermal motion, even in the absence of collisions. Generally, electrons are heated collisionlessly by repeated interaction with fields that are localized within a sheath or skin depth layer inside the discharge. Consequently, the Fermi acceleration model of a ball bouncing elastically back and forth between a fixed and an oscillating wall is a paradigm to describe collisionless heating and phase randomization in capacitive, inductive, and ECR discharges. We introduced several mapping models for Fermi acceleration and showed how to use the Fokker-Planck formalism to determine the heating rate and the effects of phase correlations. We reviewed the role of collisionless heating in capacitive and inductive discharges, using simple Fermi models to determine the heating rates and comparing these with self-consistent (kinetic) calculations where available. We reviewed experimental measurements and computer simulations and compared these to theoretical calculations of the heating. We described recent measurements and calculations of nonlocal heating effects, such as negative electron power absorption. The effects of partial phase randomization in reducing the heating rates were most clearly seen in low pressure ECR discharges. We described the use of Fermi acceleration models to determine the collisionless heating rates for these discharges, and showed that incomplete phase randomization could reduce the heating rate and lead to the existence of adiabatic barriers to heating.

A number of outstanding issues remain that either are not well understood theoretically or lack experimental validation. Let us first mention that there is little understanding of the role of the rf (or microwave) magnetic field in collisionless heating phenomena. The magnetic field can alter the skin depth for the field decay and also the electron dynamics that leads to phase randomization. In a cylindrical inductive discharge excited by a planar coil at one end, for example, the kick in velocity within the skin layer is in the θ direction, but this is converted by the rf magnetic field into a kick along the z direction within the bulk plasma. This suggests the existence of r and z components of the electron current density $\mathbf{J}$ within the bulk plasma, and these may in turn induce electric fields with these same components. Hence the usual assumption that only azimuthal rf electric fields and currents exist in cylindrical inductive discharges may not be valid. Both theoretical models and experimental results obtained using rf magnetic probes may need to be modified to account for these effects.

In rf capacitive discharges, PIC simulations suggest the existence of a small negative electron power absorption in the bulk of the discharge. There is no definitive experimental confirmation of this effect. On the other hand, both theory and experimental observations of rf inductive discharges show that such negative power absorption regions exist within the discharge bulk, but there are no PIC simulations demonstrating this effect.

There is scanty experimental or PIC simulation evidence that incomplete randomization of the electron phase plays a significant role in determining the collisionless heating rates in capacitive or inductive rf

discharges. There is considerable evidence that these effects can be important in very low pressure ECR discharges.

The Fermi acceleration model has been shown to be an effective tool for describing collisionless heating in gas discharge plasmas having strong rf fields on the boundary, for which the traditional quasilinear approach in plasma electrodynamics may some times be questionable. Amazingly, collisionless electron heating, which is usually associated with high temperature space and fusion plasmas, appears to be a fundamental process in the warm plasmas of low pressure discharges that are used in today's technology.

ACKNOWLEDGEMENT

The authors gratefully acknowledge helpful discussions with V.I. Kolobov. The work of one of the authors (MAL) was partially supported by NSF Grants ECS-9529658 and INT-9602544, by the Lam Research Corporation, and by the Space Plasma and Plasma Processing Group at The Australian National University, Canberra.

REFERENCES

Alexandrov, A.F., L.S. Bogdankevich, and A.A. Rukhadze (1984), *Principles of Plasma Electrodynamics*, Springer, New York.

Aliev, Yu. M., I.D. Kaganovich, and H. Schlüter (1996), "Quasilinear theory of collisionless electron heating in rf gas discharge," Arbeitsgemeinschaft Plasmaphysik (APP), SFB Niedertemperatur-Plasmen.

Akhiezer, A.I. and A.S. Bakai (1976), *Fiz. Plasmy* **2**, 654 [*Sov. J. Plasma Phys.* **2** 359, (1976)].

Bernstein, I.B. and T. Holstein (1954), *Phys. Rev.* **94**, 1475.

Blevin, H.A., J.A. Reynolds, and P.C. Thonemann (1970), *Phys. Fluids* **13**, 1259.

Brahic, A. (1971), *Astron. Astrophys.* **12**, 98.

Buddemeier, U., U. Kortshagen, and I. Pukropski (1995), *Appl. Phys. Lett.* **67**, 191.

Budden, K.G. (1966), *Radio Waves in the Ionosphere*, Cambridge University Press, Cambridge, UK.

Cohen, R.H. and T.D. Rognlien (1996), *Plasma Sources Sci. Technol.* **5**, 442.

Demirkhanov, R.A., I.Ya. Kadysh and Yu.S. Khodyrev (1964), *Sov. Phys. JETP* **19**, 791.

DiPeso, G., T.D. Rognlien, V. Vahedi, and D.W. Hewett (1995), *IEEE Trans. Plasma Sci.* **23**, 550.

Eldridge, O. (1972), *Phys. Fluids* **15**, 676.

Fermi, E. (1949), *Phys. Rev.* **75**, 1169.

Fried, B.D. and S.D. Conte (1961), *The Plasma Dispersion Function*, Academic Press, New York.

Friedlander, M.W. (1989), *Cosmic Rays*, Harvard University Press, Cambridge.

Gabor, D., E.A. Ash, and D. Dracott (1955), *Nature* **176**, 916.

Gibbons, M.R. and D.W. Hewett (1995), *J. Comp. Phys.* **120**, 231.

Godyak, V.A. (1971), *Zhurnal Teknicheskoi Fiziki* **41**, 1364 [*Sov. Phys.—Tech. Phys.* **16** 1073, (1972)].

Godyak, V.A. (1976a), *Fiz. Plasmy* **2**, 141 [*Sov. J. Plasma Phys.* **2** 78, (1976)].

Godyak, V.A., O.A. Popov, and A.H. Khanna (1976b), *Fiz. Plasmy* **2**, 1010 [*Sov. J. Plasma Phys.* **2** 560, (1976)].

Godyak, V.A. and O.A. Popov (1979), *Fiz. Plasmy* **5**, 400 [*Sov. J. Plasma Phys.* **5** 227, (1979)].

Godyak, V.A. (1986), *Soviet Radio Frequency Discharge Research*, Delphic Associates, Inc., Falls Church, Virginia.

Godyak, V.A. (1990), Private communication (result reproduced in Lieberman and Lichtenberg, 1994, Fig. 11.10).

Godyak, V.A. (1997), presented at the NATO Workshop on Electron Kinetics in Glow Discharges, St. Petersburg, 19–23 May; to be published by Plenum Press.

Godyak, V.A. and R.B. Piejak (1990), *Phys. Rev. Lett.* **65**, 996.

Godyak, V.A., R.B. Piejak, and B.M. Alexandrovich (1991), *IEEE Trans. Plasma Sci.* **19**, 660.

Godyak, V.A., R.B. Piejak, and B.M. Alexandrovich (1992), *Plasma Sources Sci. Technol.* **1**, 36.

Godyak, V.A., R.B. Piejak, and B.M. Alexandrovich (1994), *Plasma Sources Sci. Technol.* **3**, 169.

Goedde, C.G., A.J. Lichtenberg, and M.A. Lieberman (1988), *J. Appl. Phys.* **64**, 4375.

Gould, R.W. (1964), *Phys. Lett.* **11**, 236.

Harwit, M. (1984), *Cosmic Discovery—The Search, Scope, and Heritage of Astronomy*, MIT Press, Cambridge.

Helmer, J.C. and J. Feinstein (1994), *J. Vac. Sci. Technol. B* **12**, 507.

Holstein, T. (1952), *Phys. Rev.* **88**, 1427.

Hutchinson, D.A.W., M.M. Turner, R.A. Doyle, and M.B. Hopkins (1995), *IEEE Trans. Plasma Sci.* **23**, 636.

Ichimaru, I. (1973), *Basic Principles of Plasma Physics: A Statistical Approach*, Benjamin, Reading MA.

Jaeger, F., A.J. Lichtenberg, and M.A. Lieberman (1972), *Plasma Phys.* **14**, 1073.

Joye, B. and H. Schneider (1978), *Helvetica Physica Acta* **51**, 804.

Kaganovich, I.D. (1997), presented at the NATO Workshop on Electron Kinetics in Glow Discharges, St. Petersburg, 19–23 May; to be published by Plenum Press.

Kaganovich, I.D., V.I. Kolobov, and L.D. Tsendin (1996), *Appl. Phys. Lett.* **69**, 3818.

Kaganovich, I.D. and L.D. Tsendin (1992), *IEEE Trans. Plasma Sci.* **20**, 86.

Kolobov, V.I. (1997), presented at the NATO Workshop on Electron Kinetics in Glow Discharges, St. Petersburg, 19–23 May; to be published by Plenum Press.

Kolobov, V.I. and D.J. Economou (1997), *Plasma Sources Sci. Technol.* **6**, 1.

Kolobov, V.I. and V.A. Godyak (1995), *IEEE Trans. Plasma Sci.* **23**, 503.

Kolobov, V.I., D.P. Lymberopoulos and D.J. Economou (1997), *Phys. Rev. E* **55**, 3408.

Kondratenko, A.N. (1979), *RF Field Penetration into Plasma* [in Russian], Atomizdat, Moscow, p. 51.

Kortshagen, U. (1996), Private communication.

Kortshagen, U., C. Busch, and L.D. Tsendin (1995), *Plasma Sources Sci. Technol.* **5**, 1.

Landau, L.D. (1937), *Zh. Eksper. Theor. Fiz.* **7**, 203.

Landau, L.D. (1946), *J. Phys. (USSR)* **10**, 25.

Landau, L.D. and E.M. Lifshitz (1960), *Electrodynamics of Continuous Media*, Pergamon Press, Oxford, p. 253.

Lichtenberg, A.J. (1997), presented at the NATO Workshop on Electron Kinetics in Glow Discharges, St. Petersburg, 19–23 May; to be published by Plenum Press.

Lichtenberg, A.J. and M.A. Lieberman (1992), *Regular and Chaotic Dynamics*, Springer-Verlag, New York.

Lichtenberg, A.J., M.A. Lieberman and R.H. Cohen (1980), *Physica* **1D**, 291.

Lichtenberg, A.J., M.A. Lieberman and N.W. Murray (1987), *Physica* **28D**, 371.

Lieberman, M.A. and A.J. Lichtenberg (1972), *Phys. Rev. A* **5**, 1852.

Lieberman, M.A. (1988), *IEEE Trans. Plasma Sci.* **16**, 638.

Lieberman, M.A. (1989), *IEEE Trans. Plasma Sci.* **17**, 338.

Lieberman, M.A., A.J. Lichtenberg, and S.E. Savas (1991), *IEEE Trans. Plasma Sci.* **19**, 189.

Lieberman, M.A. and A.J. Lichtenberg (1994), *Principles of Plasma Discharges and Materials Processing*, J. Wiley, New York.

Lister, G.G., Y.-M. Li and V.A. Godyak (1996), *J. Appl. Phys.* **79**, 8993.

Murray, N.W., M.A. Lieberman and A.J. Lichtenberg (1985), *Phys. Rev. A* **32**, 2413.

Nitschke, T.E. and D.B. Graves (1994), *J. Appl. Phys.* **76**, 5646.

Okuno, Y., Y. Ohtsu, and H. Fujita (1994), *Appl. Phys. Lett.* **64**, 1623.

Park, J.-C. and B. Kang (1997), *IEEE Trans. Plasma Sci.* **25**, 499.

Pavkovich, J. and G.S. Kino (1963), *Proc. VIth Conf. on Ionisation Phenomena in Gases* **3**, 129.

Piejak, R.B. V.A. Godyak, and B.M. Alexandrovich (1992), *Plasma Sources Sci. Technol.* **1**, 179.

Pippard, A.B. (1949), *Physica* **15**, 45.

Popov, O.A. and V.A. Godyak (1985), *J. Appl. Phys.* **57**, 53.

Popov, O.A. and V.A. Godyak (1986), *J. Appl. Phys.* **59**, 1759.

Rechester, A.B. and R.B. White (1980), *Phys. Rev. Lett.* **44**, 1586.

Rechester, A.B., M.N. Rosenbluth and R.B. White (1981), *Phys. Rev. A* **23**, 2664.

Reuter, G.E.H. and E.H. Sondheimer (1949), *Proc. Roy. Soc.* **A195**, 336.

Sato, A.H. and M.A. Lieberman (1996), *J. Appl. Phys.* **68**, 6117.

Sayasov, Yu.S. (1979), *Helvetica Physica Acta* **52**, 288.

Shaing, K.C. (1996), *Phys. Plasmas* **3**, 3300.

Shaing, K.C. and A.Y. Aydemir (1996), "Collisionless Electron Heating in Inductively Coupled Discharges," Institute for Fusion Studies Report IFS-754.

Shoyama, H., M. Tanaka, S. Higashi, Y. Kawai, and M. Kono (1996), *J. Phys. Soc. Japan* **65**, 2860.

Surendra, M. and M. Dalvie (1993), *Phys. Rev. E* **48**, 3914.

Surendra, M., D.B. Graves, and I.J. Morey (1990), *Appl. Phys. Lett.* **56**, 1022.

Surendra, M. and D.B. Graves (1991), *IEEE Trans. Plasma Sci.* **19**, 144.

Surendra, M. and D.B. Graves (1991), *Phys. Rev. Lett.* **66**, 1469.

Surendra, M. and D. Vender (1994), *Appl. Phys. Lett.* **65**, 153.

Tsendin, L.D. (1974), *Sov. Phys. JETP* **39**, 805.

Tsendin, L.D. (1995), *Plasma Sources Sci. Technol.* **4**, 200.

Turner, M.M. (1993), *Phys. Rev. Lett.* **71**, 1844.

Turner, M.M. (1995), *Phys. Rev. Lett.* **75**, 1312.

Turner, M.M. (1996), *Plasma Sources Sci. Technol.* **5**, 159.

Turner, M.M., D.A.W. Hutchinson, R.A. Doyle, and M.B. Hopkins (1996), *Phys. Rev. Lett.* **76**, 2069.

Tuszewski, M. (1996), *Phys. Rev. Lett.* **77**, 1966.

Ulam, S.M. (1961), *Proceedings of the 4th Berkeley Symposium on Mathematical Statistics and Probability,* Vol. 3, p. 315 (University of California Press, Berkeley).

Vahedi, V., C.K. Birdsall, M.A. Lieberman, G. DiPeso, and T.D. Rognlien (1994), *Plasma Sources Sci. Technol.* **2**, 273.

Vahedi, V., M.A. Lieberman, G. DiPeso, T.D. Rognlien, and D. Hewett (1995), *J. Appl. Phys.* **78**, 1446.

Vender, D., and R.W. Boswell (1990), *IEEE Trans. Plasma Sci.* **18**, 725.

Vender, D. (1990), *Numerical Studies of the Low Pressure RF Plasma*, Thesis, The Australian National University, Canberra.

Vender, D., and R.W. Boswell (1992), *J. Vac. Sci. Technol. A* **10**, 1331.

Wang, M.C. and G.E. Uhlenbeck (1945), *Phys. Rev.* **188**, 416.

Wang, Z.D., A.J. Lichtenberg, and R.H. Cohen (1997), to appear in *IEEE Trans. Plasma Sci.*

Weibel, E.S. (1967), *Phys. Fluids* **10**, 741.

Wendt, A.E. and W.N.G. Hitchon (1992), *J. Appl. Phys.* **71**, 4718.

Wood, B.P. (1991), *Sheath Heating in Low Pressure Capacitive Radio Frequency Discharges*, Thesis, University of California, Berkeley.

Wood, B.P., M.A. Lieberman and A.J. Lichtenberg (1995), *IEEE Trans. Plasma Sci.* **23**, 89.

Yoon, N.S., S.M. Hwang, and D.-I. Choi (1997), *Phys. Rev. E* **55**, 7536.

Yoon, N.S., S.S. Kim, C.S. Chang, and D.-I. Choi (1996), *Phys. Rev. E* **54**, 757.

Zaslavskii, G.M. and B.V. Chirikov (1965), *Soviet Phys. Dokl.* **9**, 989.

p (mTorr)	P_{plasma} (W)	n_1 (10^{10} cm^{-3})	ν_m (10^7 s^{-1})	ν_{eff} (10^7 s^{-1})	ν_{stoc} (10^7 s^{-1})	$\nu_{\text{eff}} - \nu_m$ (10^7 s^{-1})
1	25	1.1	0.71	3.0	1.8	2.3
1	100	4.1	0.55	3.9	2.4	3.3
10	50	4.8	4.5	5.3	1.8	0.8
10	150	16	3.0	5.7	2.3	2.7

Table 1. Comparison of collisional and collisionless heating frequencies

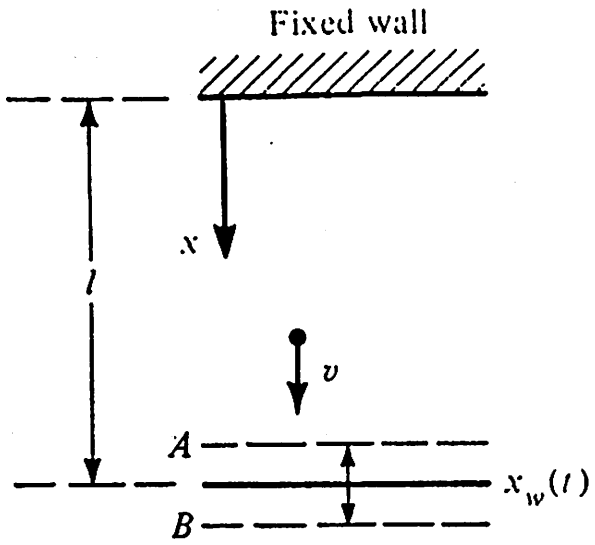

Figure 1. Fermi acceleration in which a particle bounces between a fixed and an oscillating wall.

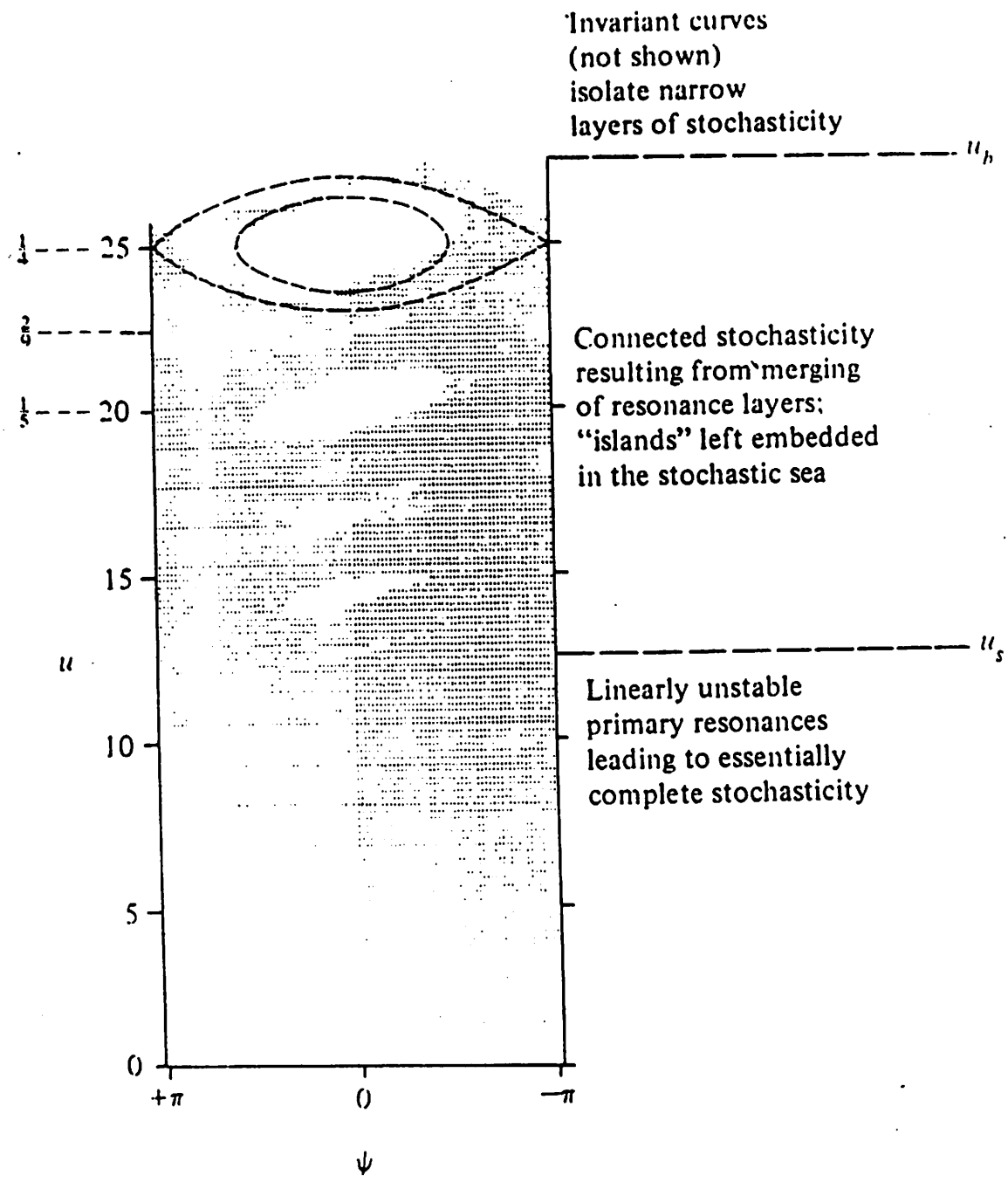

Figure 2. Surface of section for the Fermi problem, showing occupation of phase space cells for 623,000 iterations of a single initial condition. Dashed curves are calculated from secular perturbation theory (after Lieberman and Lichtenberg, 1972).

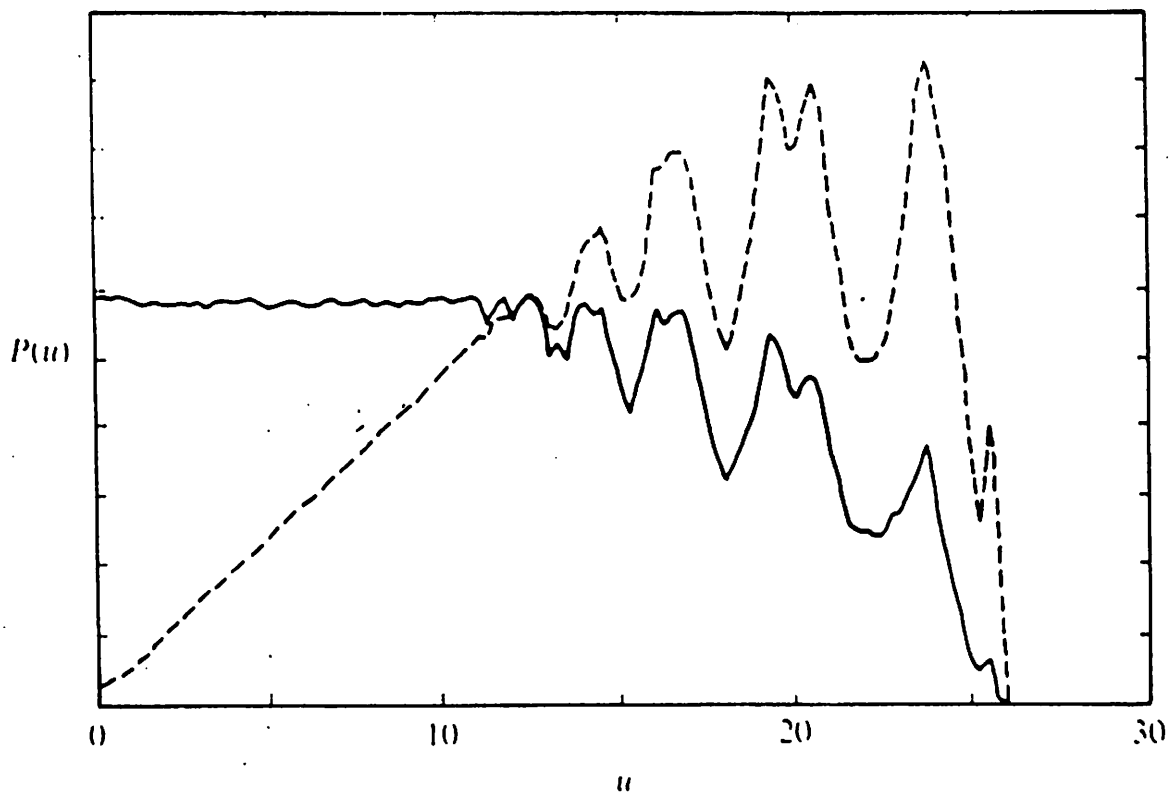

Figure 3. Comparison of velocity distribution $f(u)$ [here $P(u)$] for the simplified Fermi map (2.3) [solid line] and the exact Fermi map (2.1) [dashed line] (after Lichtenberg and Lieberman, 1992).

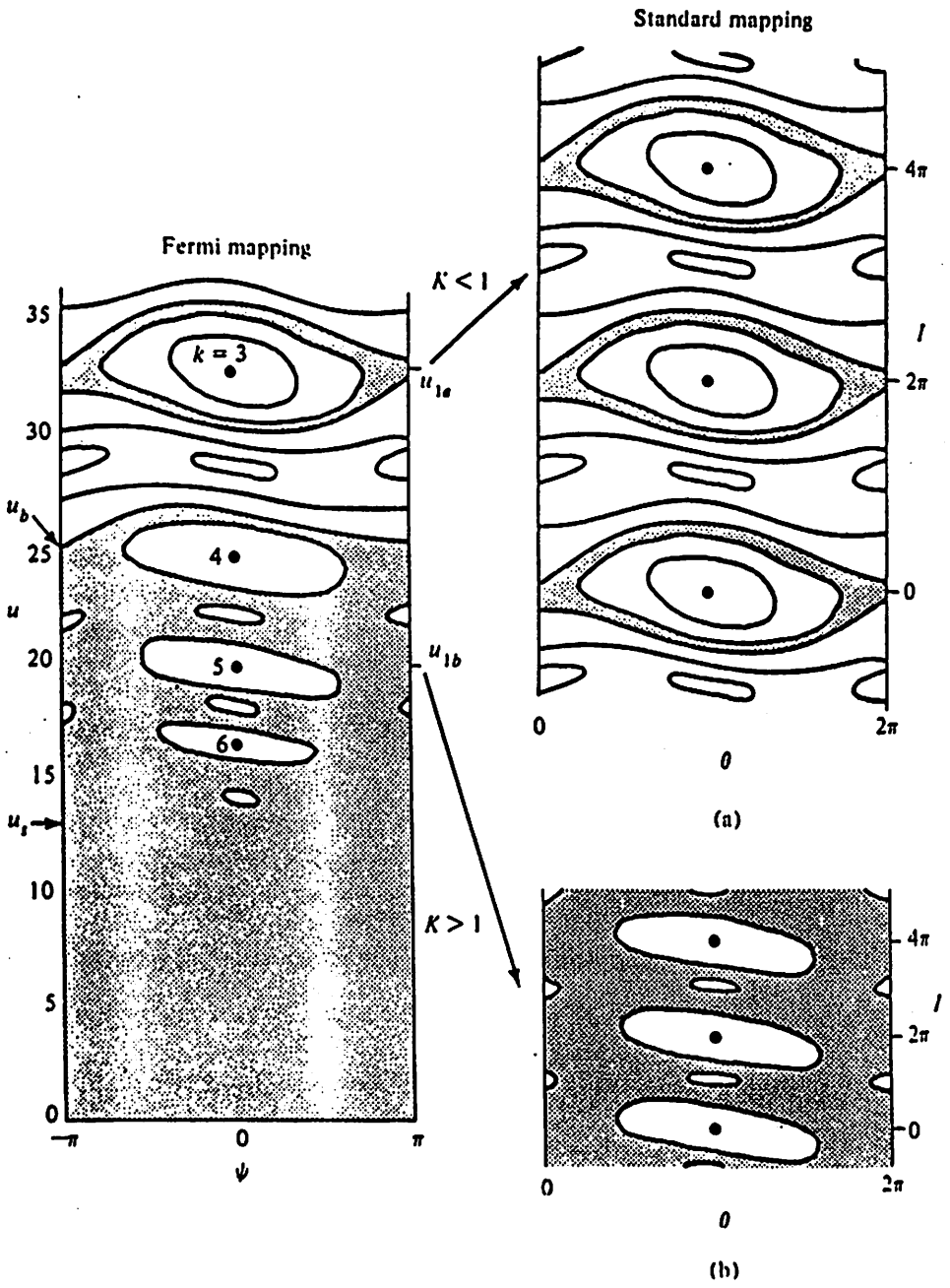

Figure 4. Local approximation of the Fermi mapping by the standard mapping. (a) Linearization about u_{1a} leading to K small and local stochasticity; (b) linearization about u_{1b} leading to K large and global stochasticity (after Lichtenberg and Lieberman, 1992).

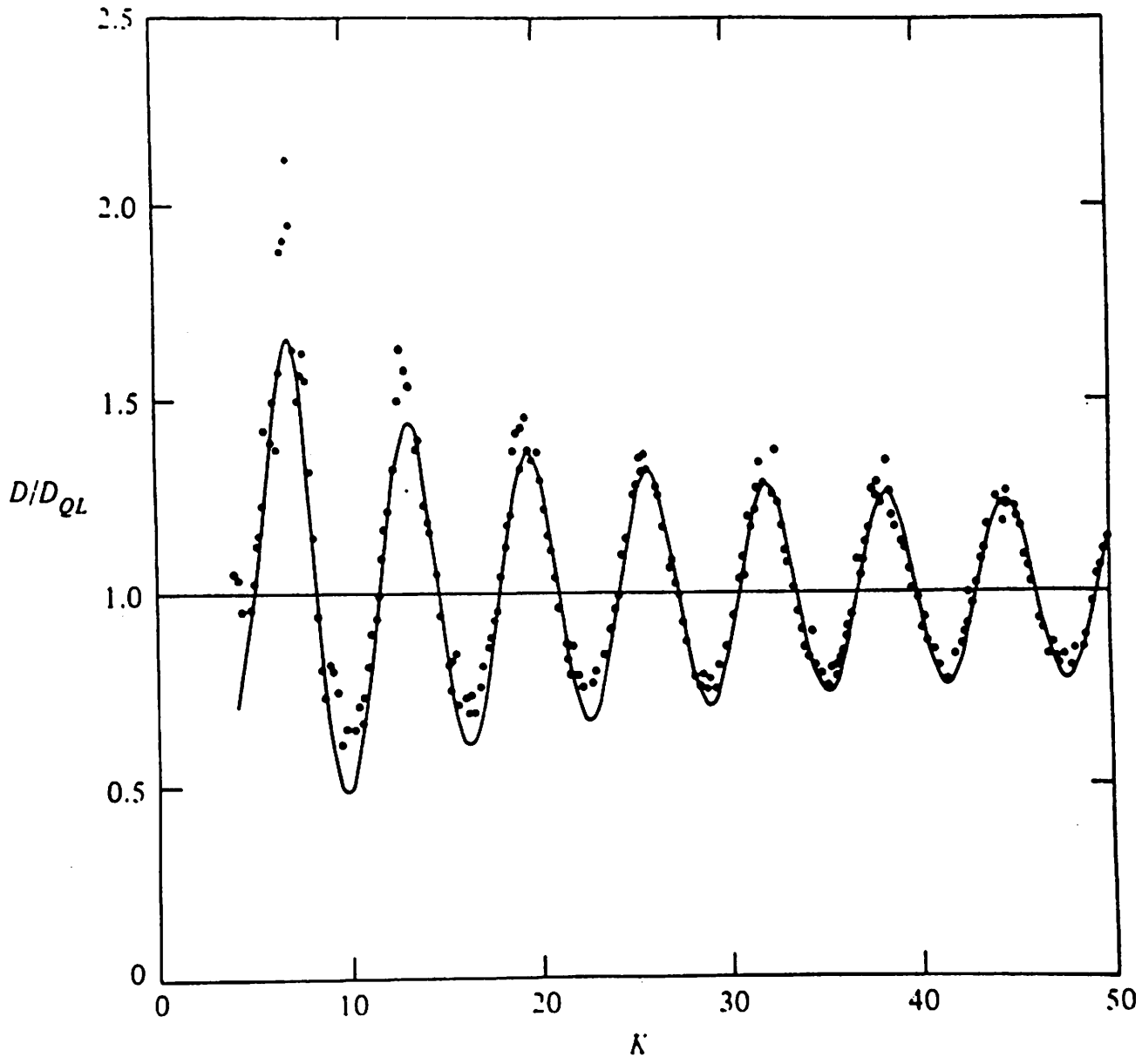

Figure 5. Plot of D/D_{QL} versus stochasticity parameter K. The dots are the numerically computed values and the solid line is the theoretical result in the large K limit (after Rechester and White, 1980).

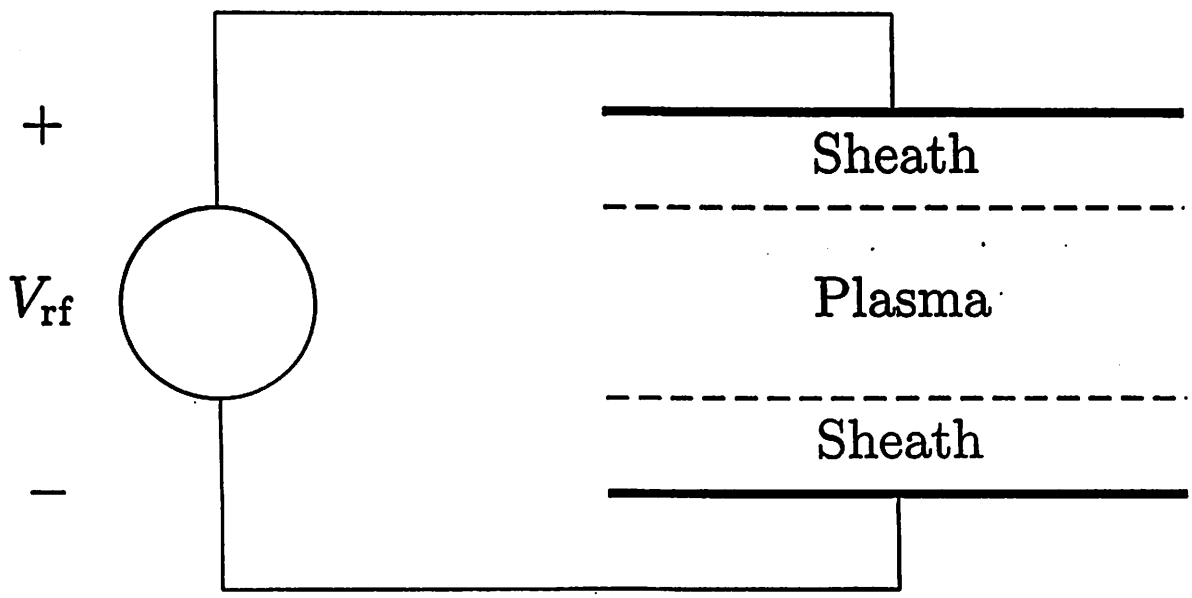

Figure 6. Sheath-plasma-sheath sandwich structure of a capacitive rf discharge.

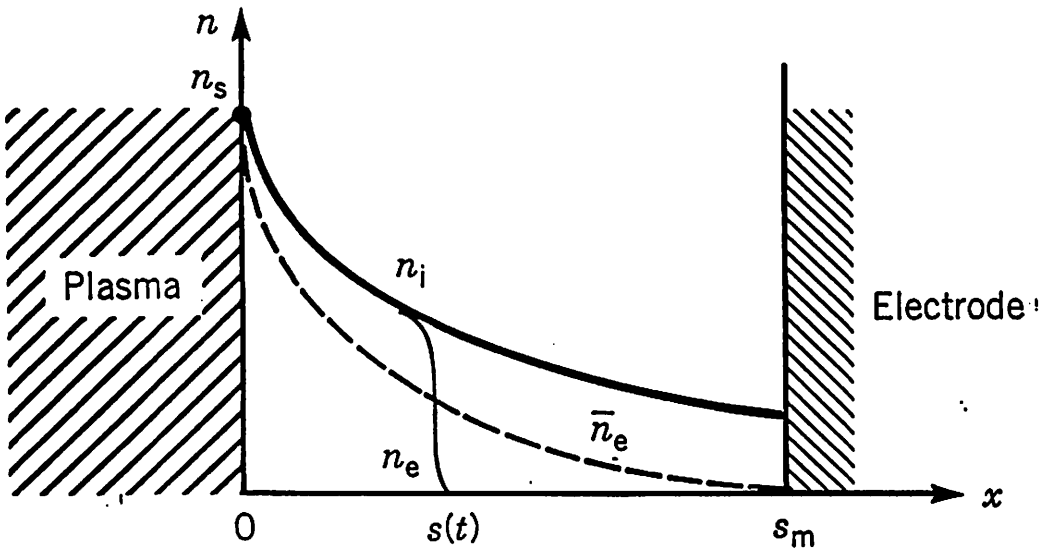

Figure 7. Schematic plot of the densities in a high voltage capacitive rf sheath.

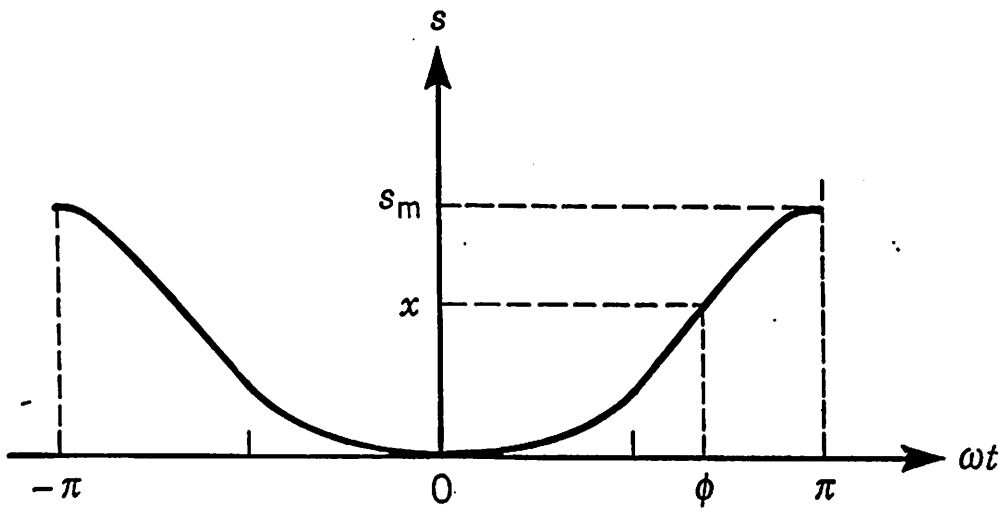

Figure 8. Sketch of the electron sheath thickness s versus ωt.

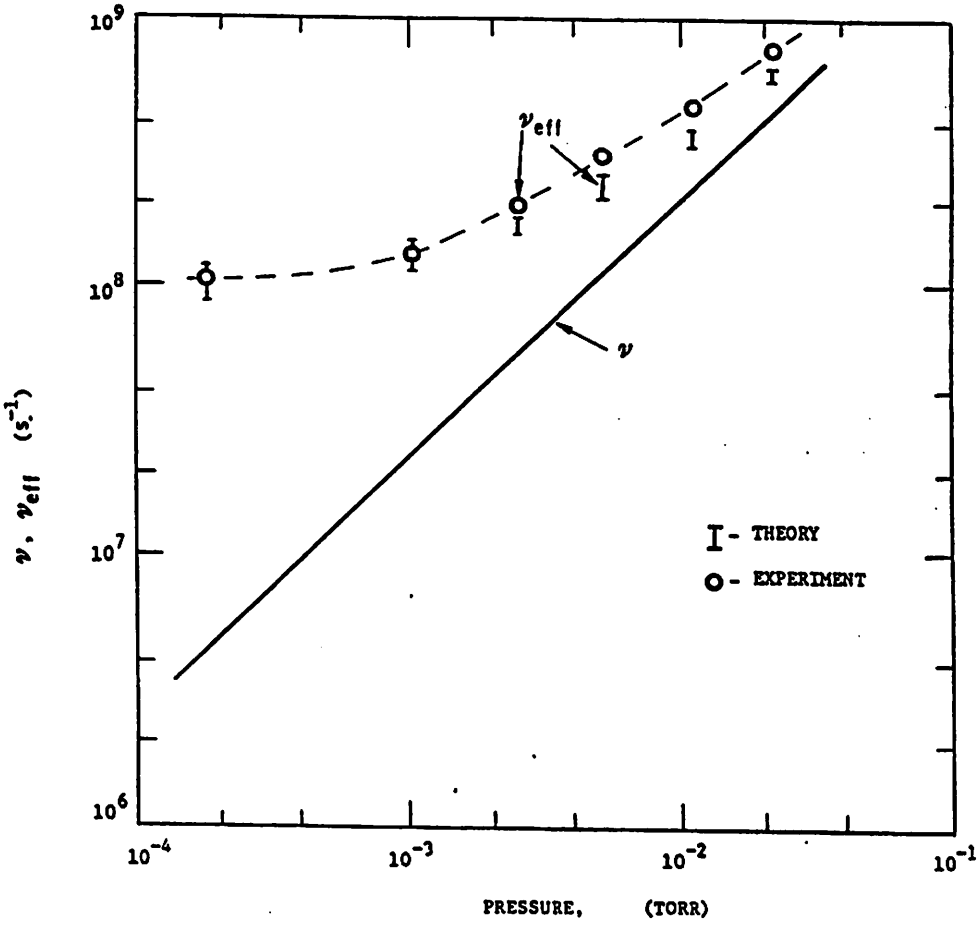

Figure 9. Effective collision frequency ν_{eff} versus pressure p for a mercury discharge driven at 40.8 MHz. The solid line shows the collision frequency due to ohmic dissipation alone (after Godyak et al, 1976b).

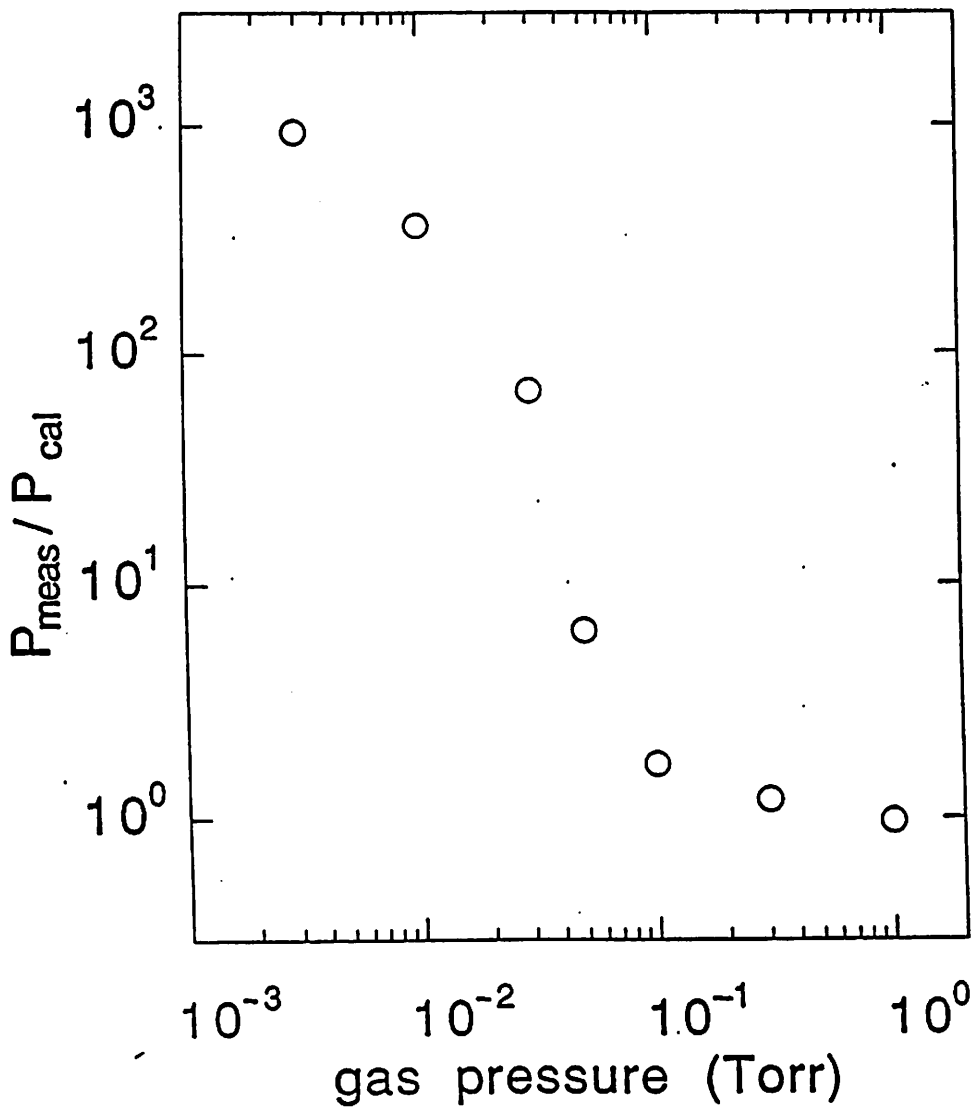

Figure 10. The ratio between total and collisional rf power transferred to the plasma electrons versus argon pressure; $l = 6.7$ cm and $J = 1$ mA/cm^2 (after Godyak et al, 1992).

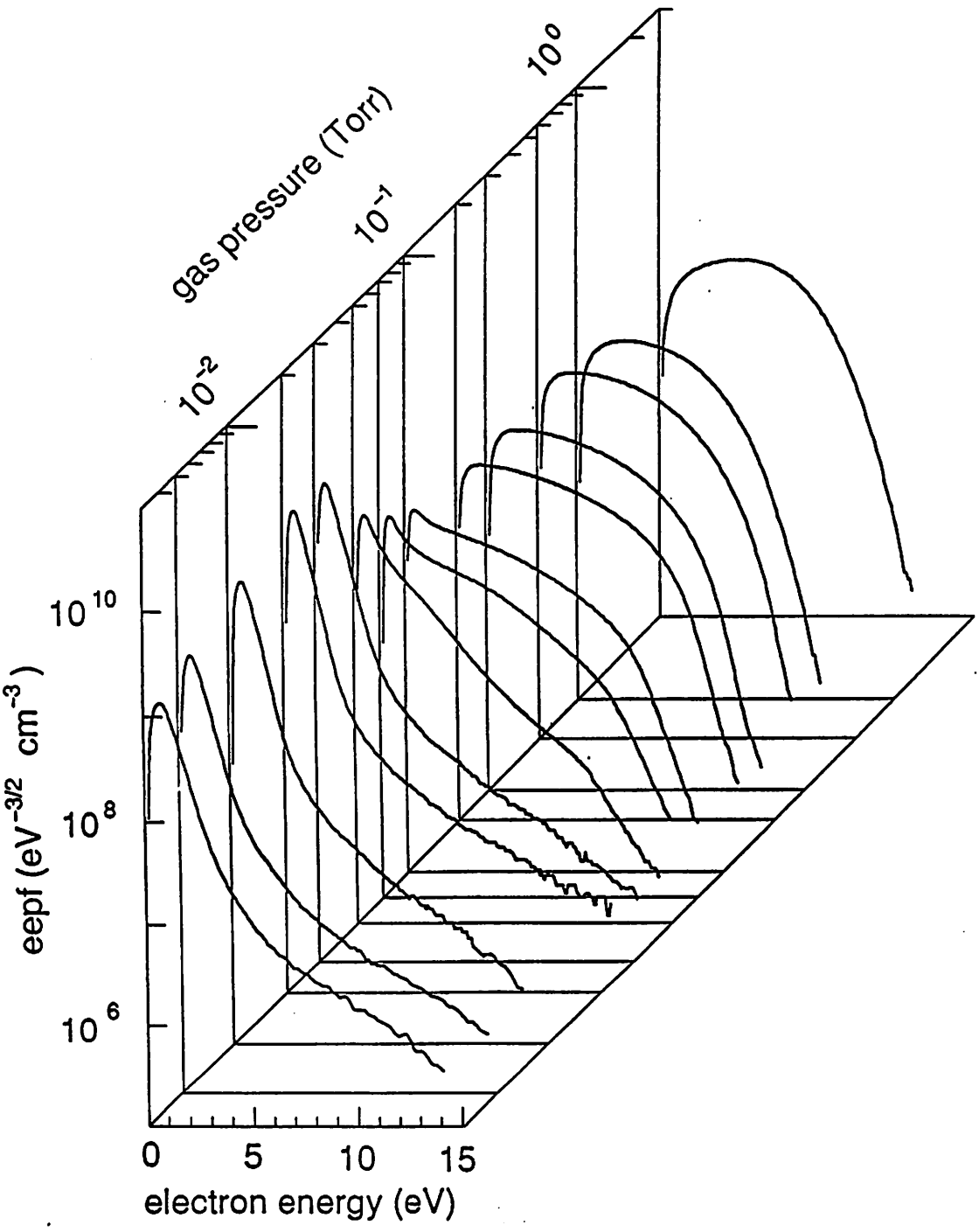

Figure 11. Evolution of the electron energy probability function (EEPF) $g_p(\mathcal{E})$ with pressure in argon; $l = 6.7$ cm and $J = 1$ mA/cm^2 (after Godyak et al, 1992).

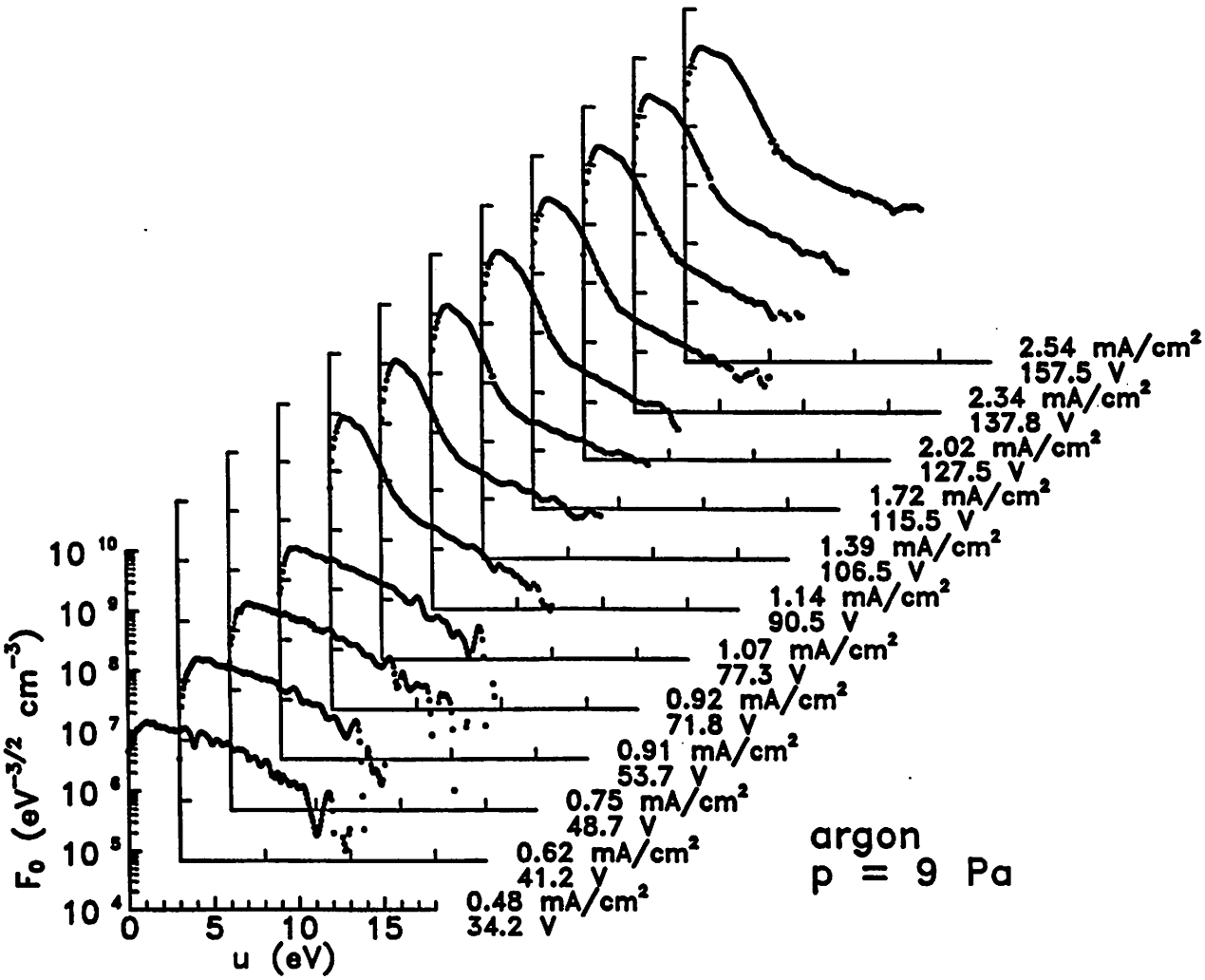

Figure 12. Electron energy distribution functions in the midplane of a capacitive rf discharge (6 cm gap, 15 cm electrode diameter) in argon for constant pressure and varying rf current densities given in mA/cm^2 (rf discharge voltages in volts); (after Buddemeier et al, 1995).

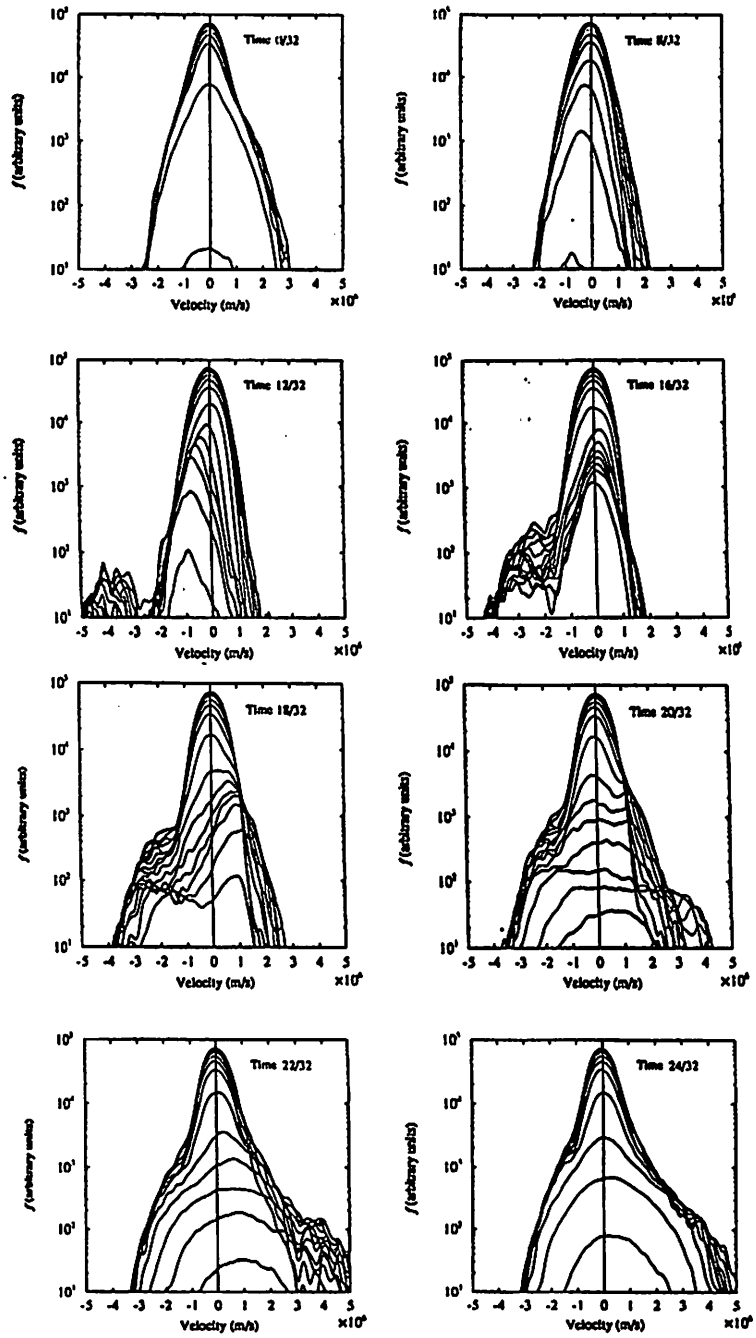

Figure 13. One-dimensional electron velocity distribution function $f_e(x, v_x, t)$ for a 10 cm electrode spacing in a 3 mTorr argon discharge; each plot covers a time window of 1/32 of an rf cycle. Each line on a plot represents a spatial window of 2 mm (after Wood, 1991).

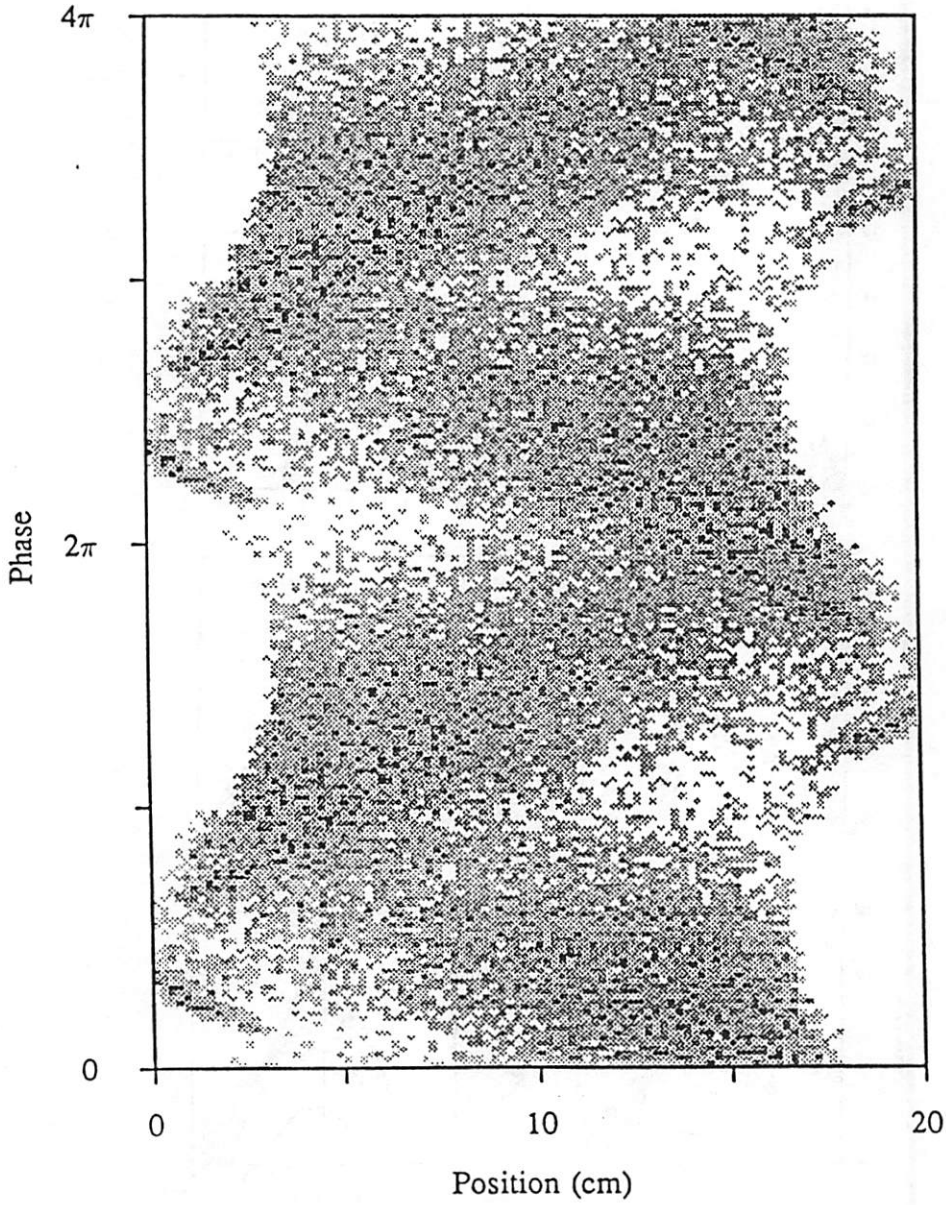

Figure 14. Spatiotemporal distribution of ionizing collisions collected over 20 rf cycles, for a 10 MHz, 20 mTorr hydrogen discharge (Vender and Boswell, 1990).

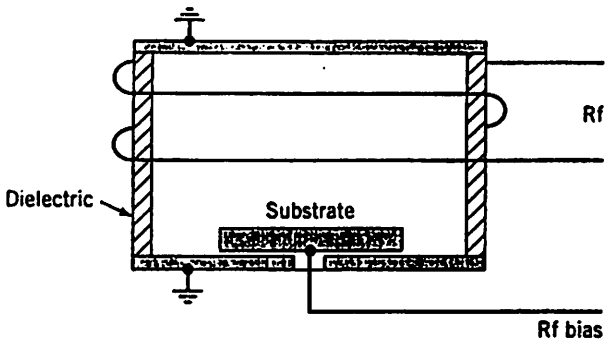

(a)

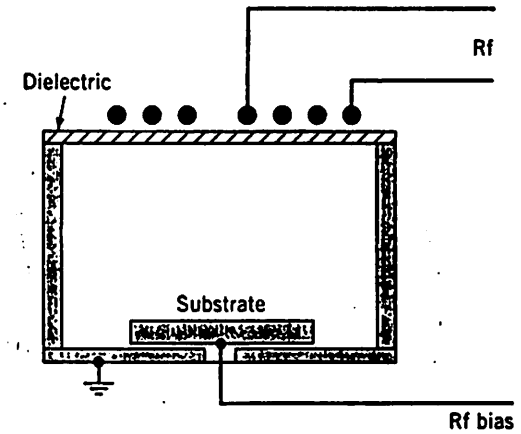

(b)

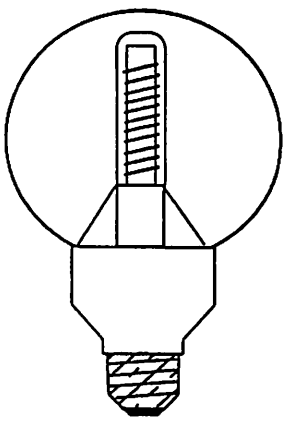

(c)

Figure 15. Schematic of inductively driven discharge in (a) cylindrical, (b) planar, and (c) re-entrant geometries; (a) and (b) are used for materials processing and (c) is used for lighting.

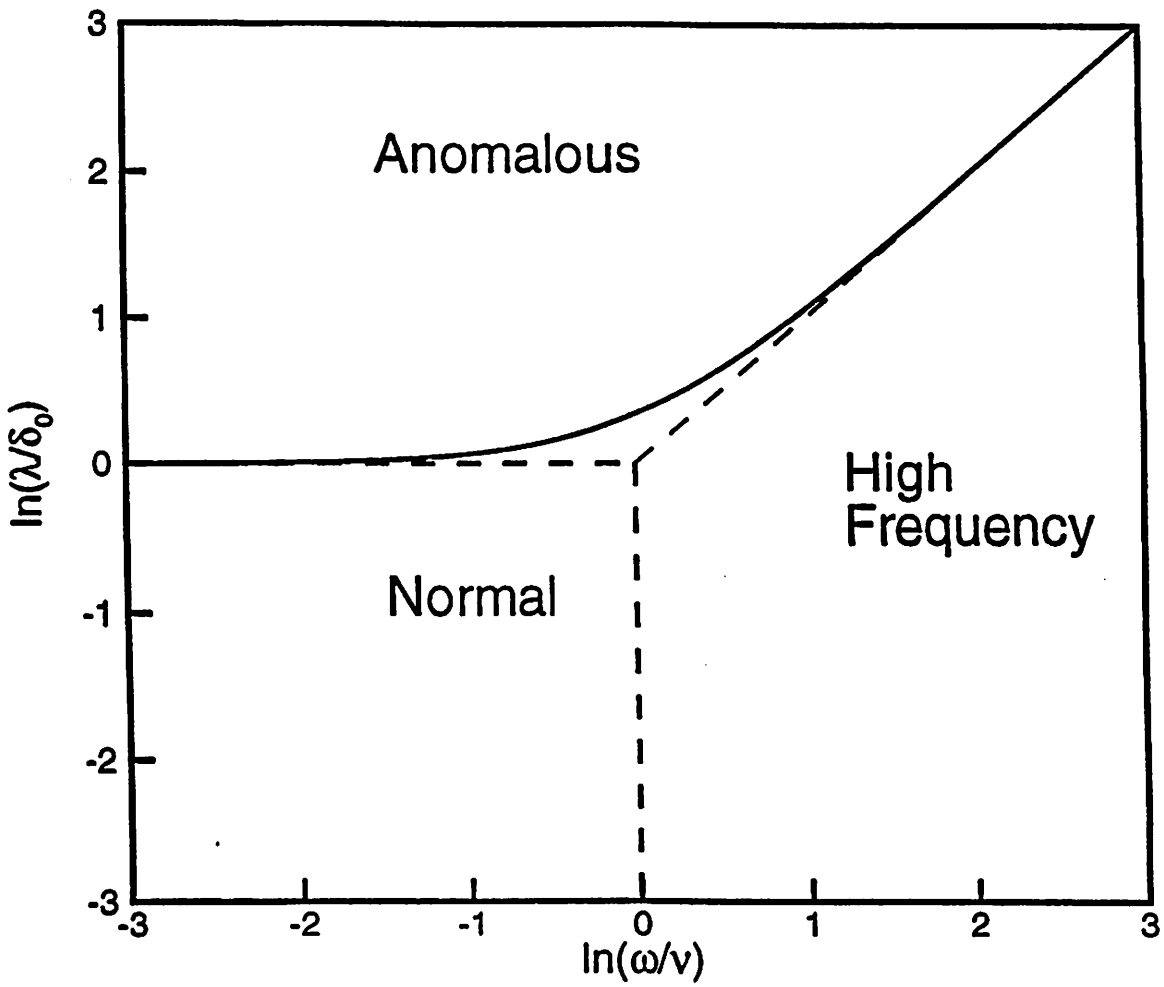

Figure 16. Plot of $\ln(\lambda_e/\delta_0)$ versus $\ln(\omega/\nu_m)$, showing the regimes of collisional, high frequency, and anomalous skin effect in a semi-infinite plasma; the solid line, corresponding to nonlocality parameter $\Lambda = 1$, is the boundary of the anomalous skin effect (after Kolobov and Economou, 1997).

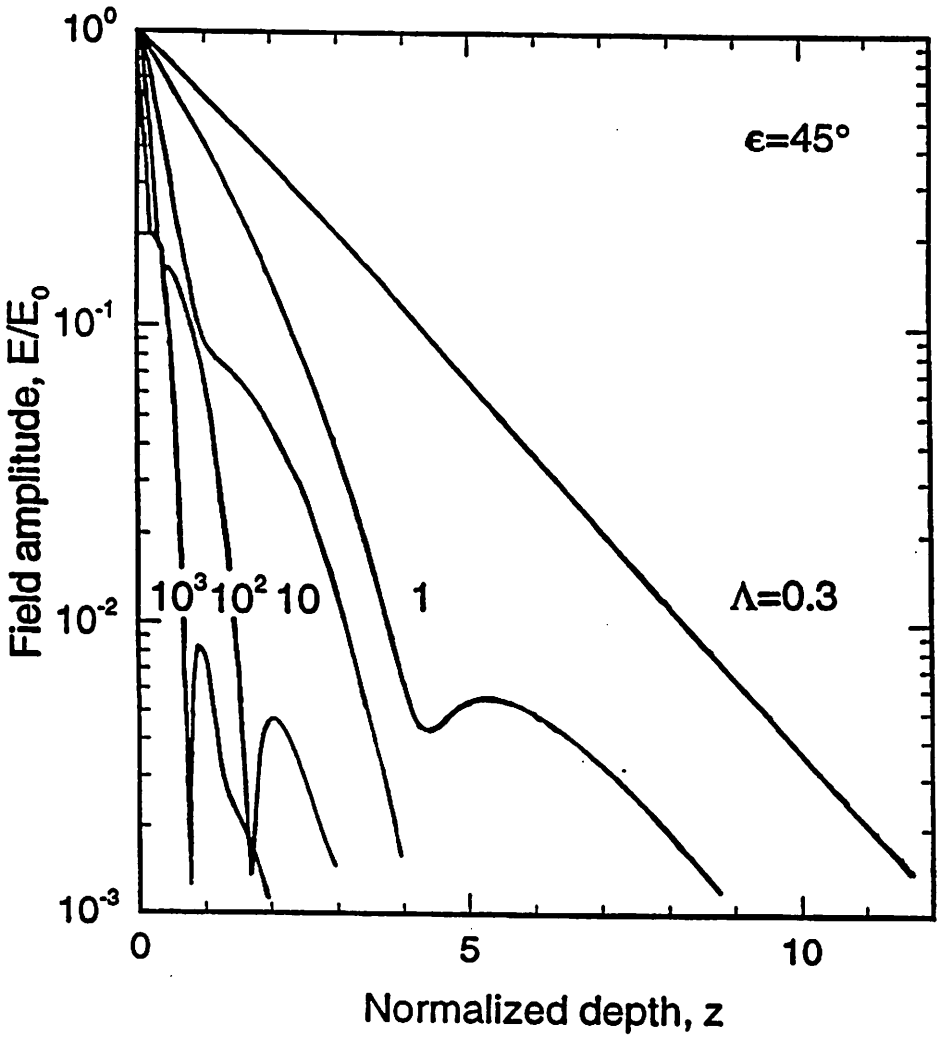

Figure 17. Normalized electric field amplitude versus normalized distance along the propagation direction for $\nu_m/\omega = 1$ and for various nonlocality parameters Λ (after Weibel, 1967).

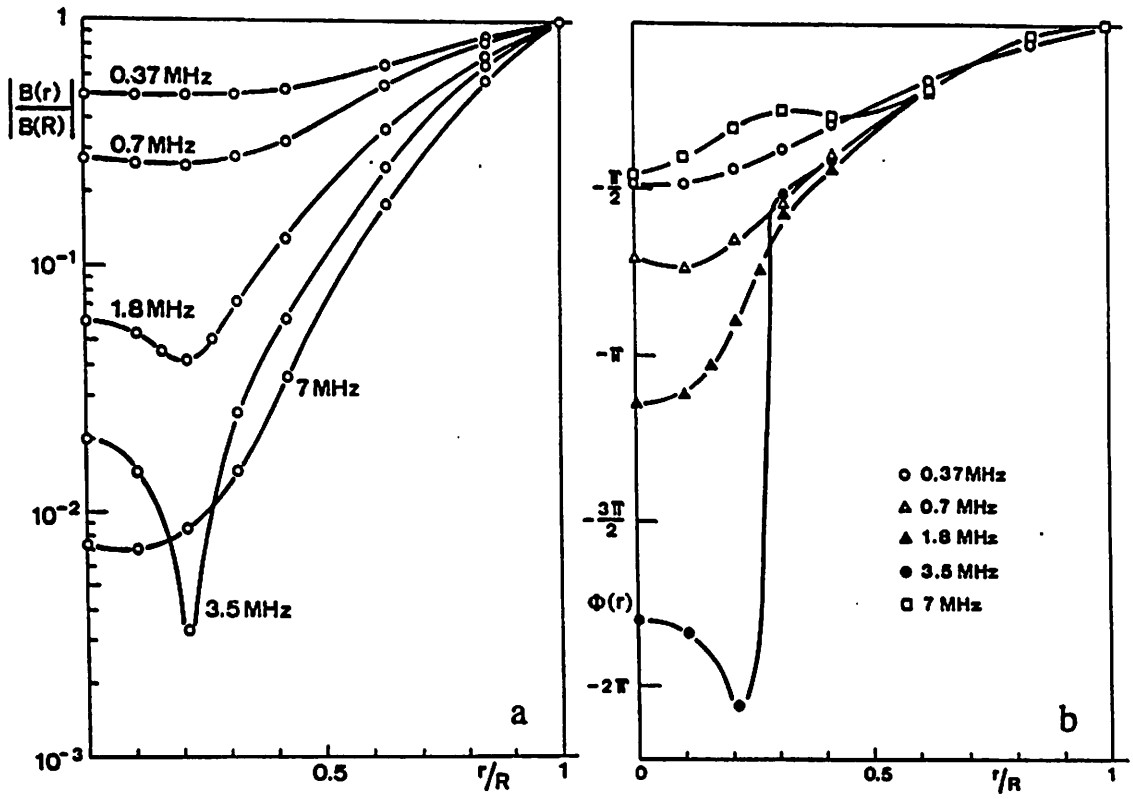

Figure 18. The radial distributions of the amplitude and phase of the rf magnetic field in a cylindrical argon plasma. Dotted lines show experimental data for $p = 10$ mTorr, average plasma density $n = 4.2 \times 10^{12}$ cm^{-3}, and $T_e = 2.1$ V. Solid lines are calculations according to the theory of Sayasov (1979) for $n = 3 \times 10^{12}$ cm^{-3} and $\nu_m = 4 \times 10^7$ s^{-1} (after Joye and Schneider, 1978).

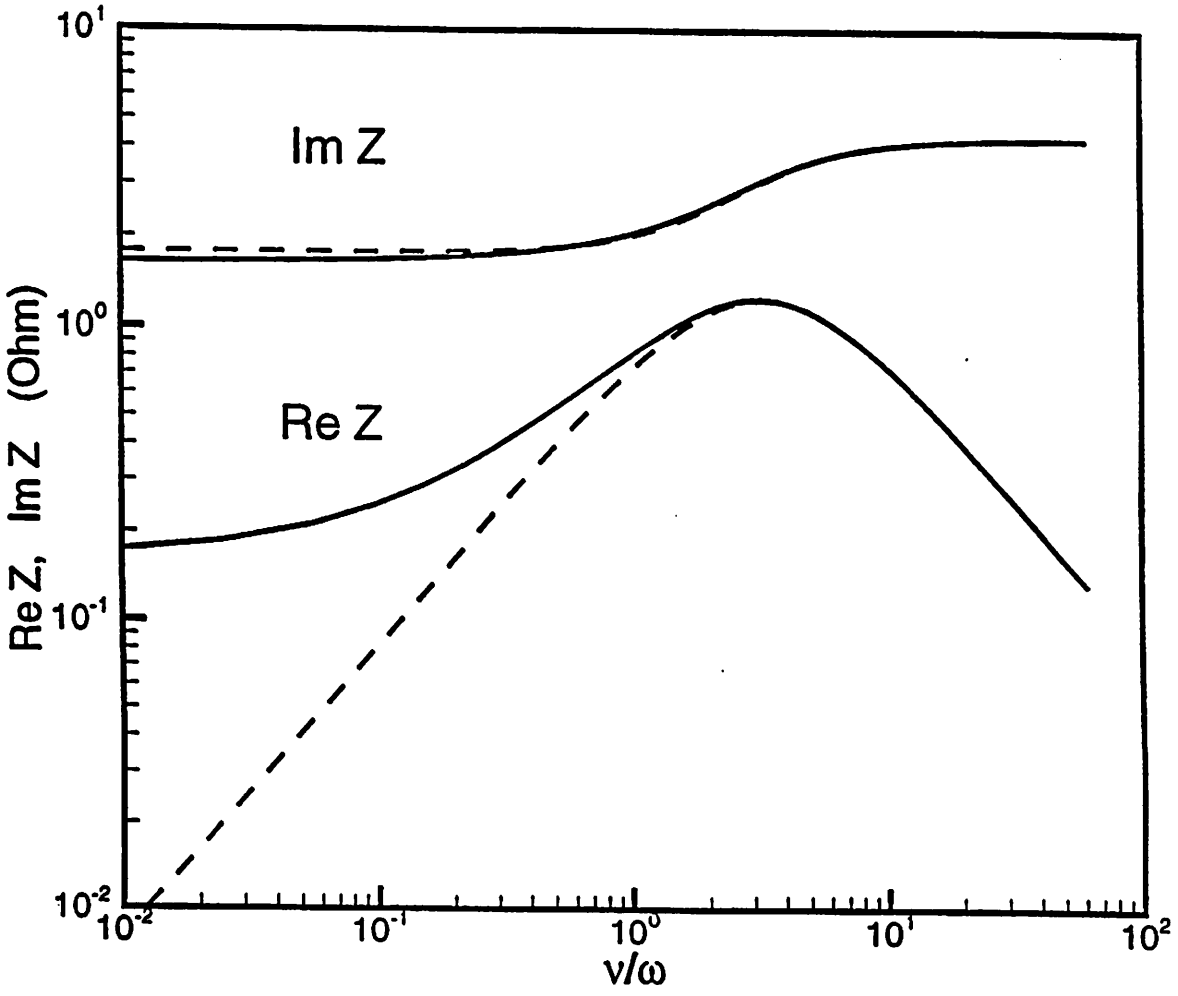

Figure 19. The real and imaginary parts of the surface impedance Z_s for a plasma slab, shown as functions of ν_m/ω. The plasma parameters are $n_e = 10^{11}$ cm^{-3}, $T_e = 5$ V, and $L = 4$ cm. The dashed lines are the cold plasma results (after Kolobov and Economou, 1997).

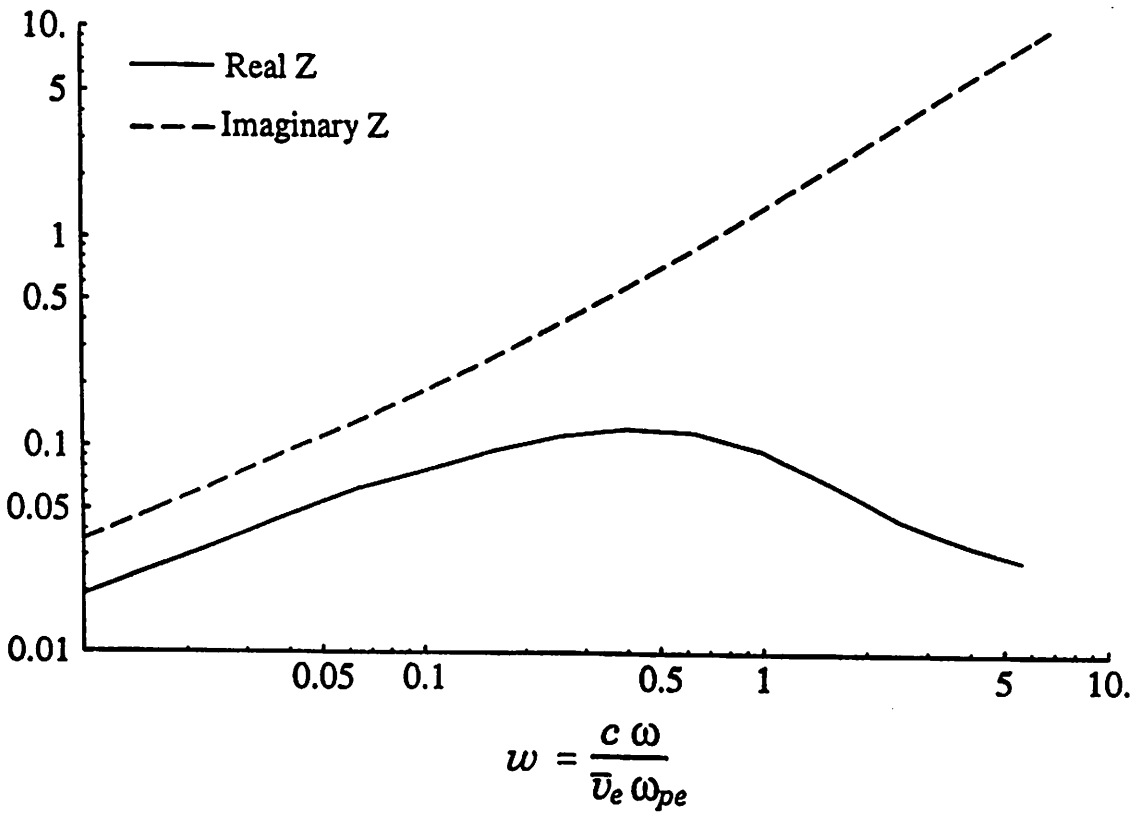

Figure 20. The real (solid line) and imaginary (dashed line) parts of the normalized surface impedance Z_s/Z_0 versus the normalized frequency $w = (\omega c)/(\bar{v}_e\omega_{pe}) \approx \Lambda^{-1/2}$ for a near-collisionless case of $\nu_m/\omega = 0.008$; $Z_0 = (\bar{v}_e/\pi c)(\mu_0/\epsilon_0)^{1/2}$ (after Vahedi et al, 1995).

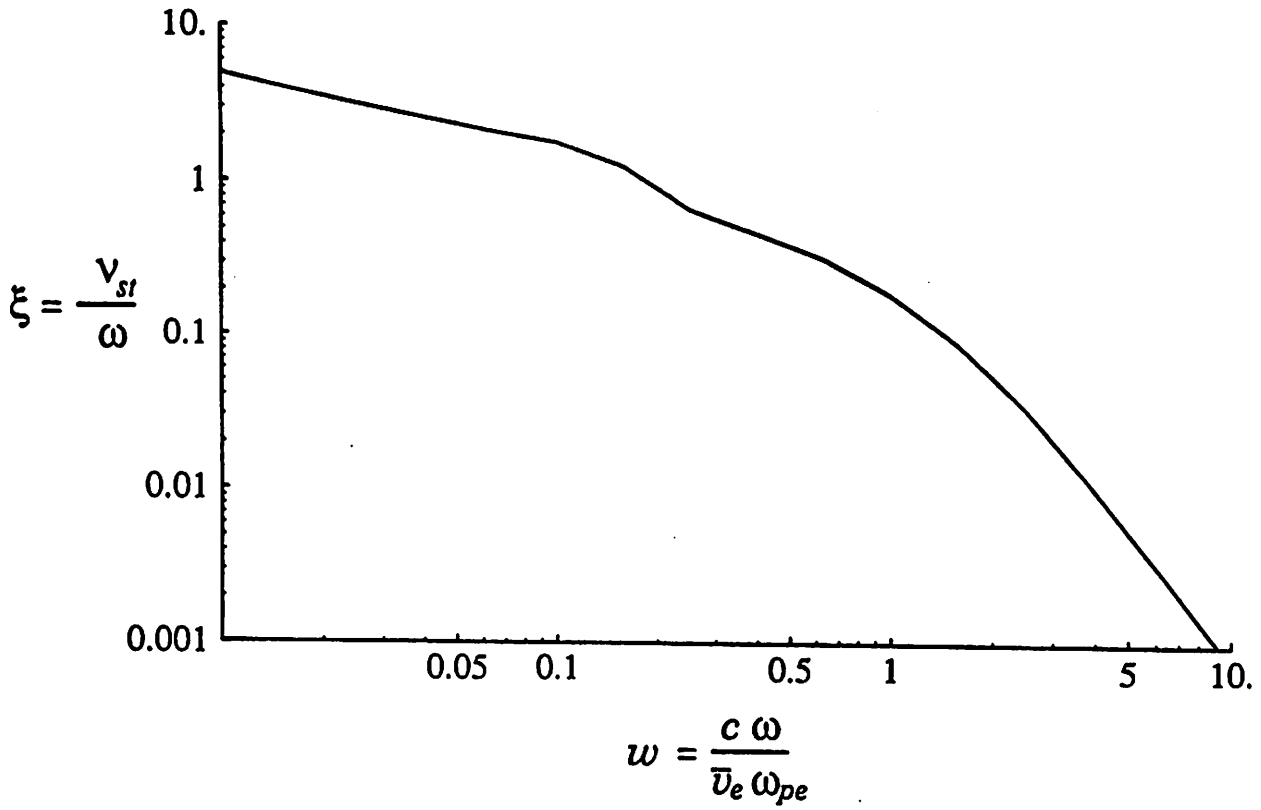

Figure 21. The normalized stochastic frequency ν_{stoc}/ω versus the normalized frequency $w = (\omega c)/(\bar{v}_e\omega_{pe})$ for a near-collisionless case of $\nu_m/\omega = 0.008$ (after Vahedi et al, 1995).

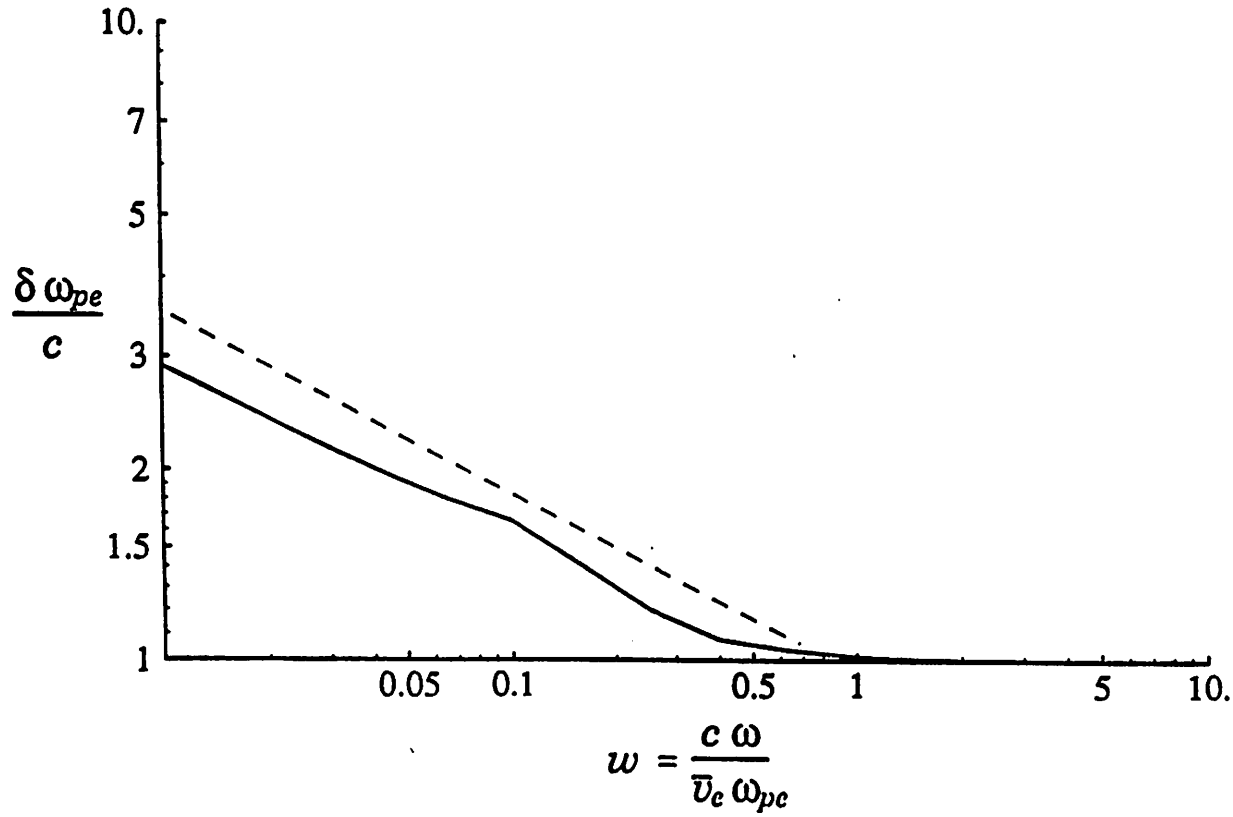

Figure 22. The normalized effective skin depth δ/δ_p versus the normalized frequency $w = (\omega c)/(\bar{v}_e\omega_{pe})$ for a near-collisionless case of $\nu_m/\omega = 0.008$. The dashed line shows δ_a/δ_p obtained from kinetic theory for comparison (after Vahedi et al, 1995).

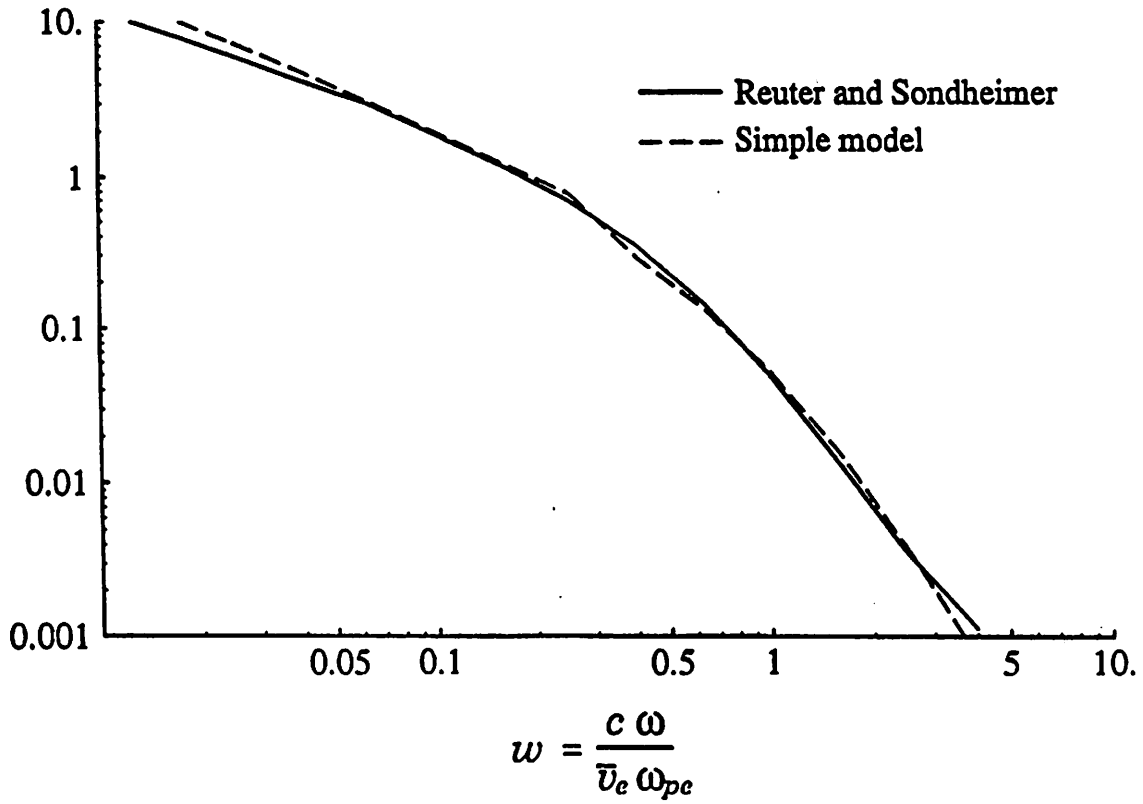

Figure 23. Normalized input power versus normalized frequency $w = (\omega c)/(\bar{v}_e \omega_{pe})$. The dashed line shows the result obtained from the (non self-consistent) Fermi model for a near-collisionless case of $\nu_m/\omega = 0.008$, and the solid line shows the result of the nonlocal theory of Weibel (1967) [Reuther and Sondheimer (1949) theory using a Maxwellian electron distribution] (after Vahedi et al, 1995).

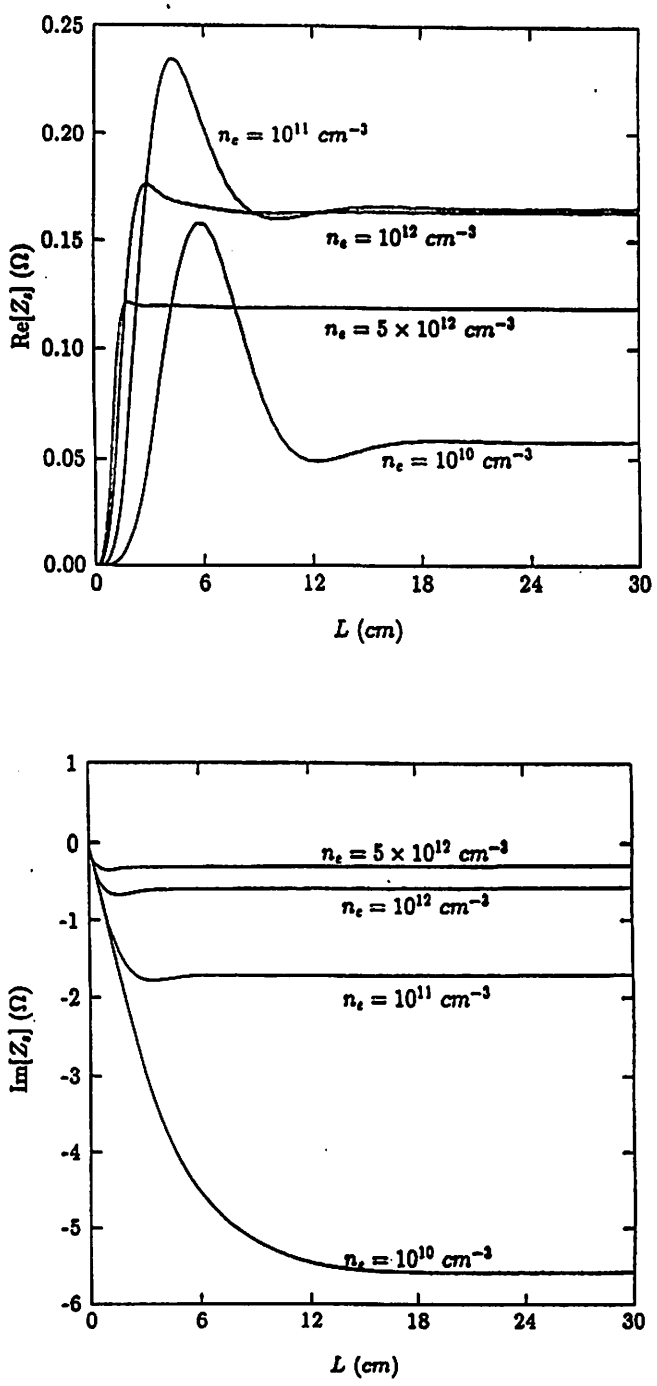

Figure 24. Real (a) and imaginary (b) parts of the surface impedance Z_s versus gap size L for various electron densities, for a collisionless plasma ($\nu_m = 0$) with $T_e = 5$ V (after Yoon et al, 1996).

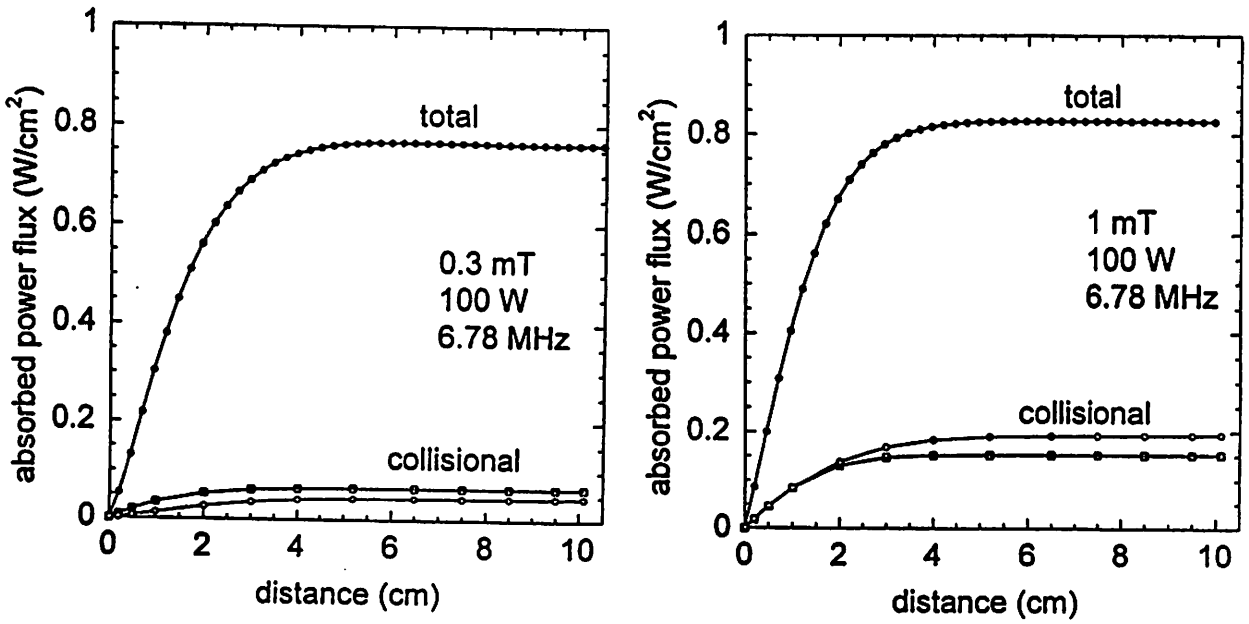

Figure 25. Absorbed rf power flux versus distance for (a) $p = 0.3$ mTorr and (b) $p = 1$ mTorr (after Godyak, 1997).

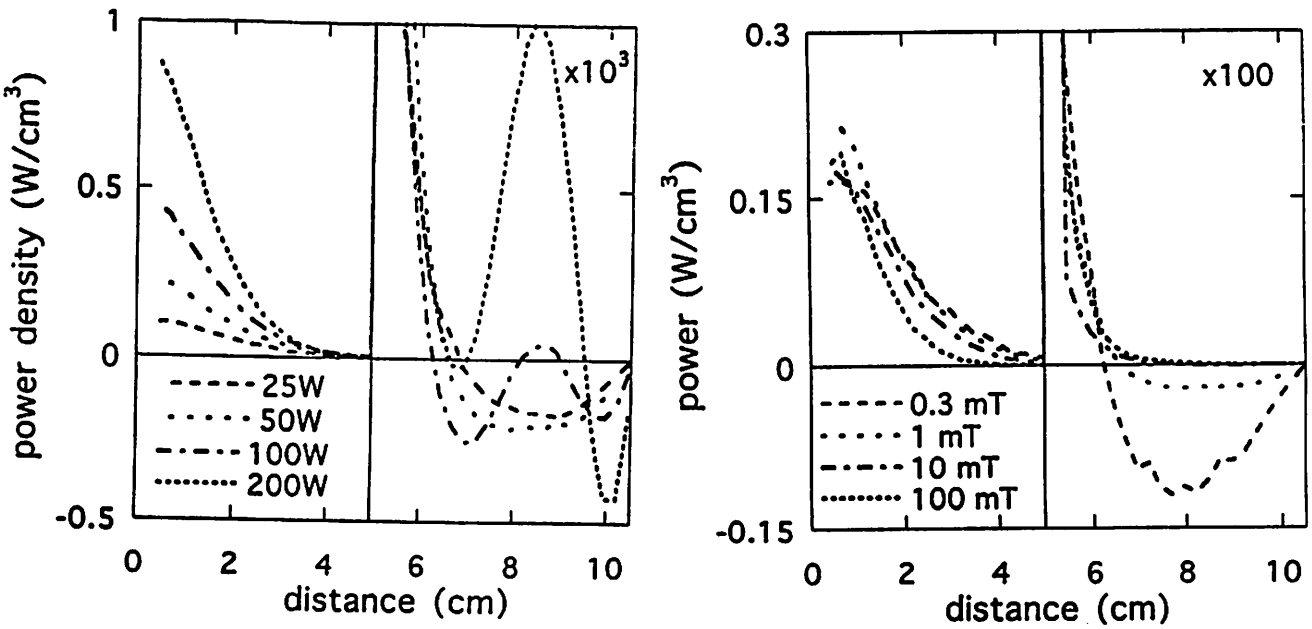

Figure 26. Spatial distribution of absorbed rf power density for an argon discharge driven at 6.78 MHz; (a) 1 mTorr pressure, with absorbed plasma power varying from 25–200 W, and (b) 50 W absorbed plasma power, with pressure varying from 0.3–100 mTorr (after Godyak, 1997).

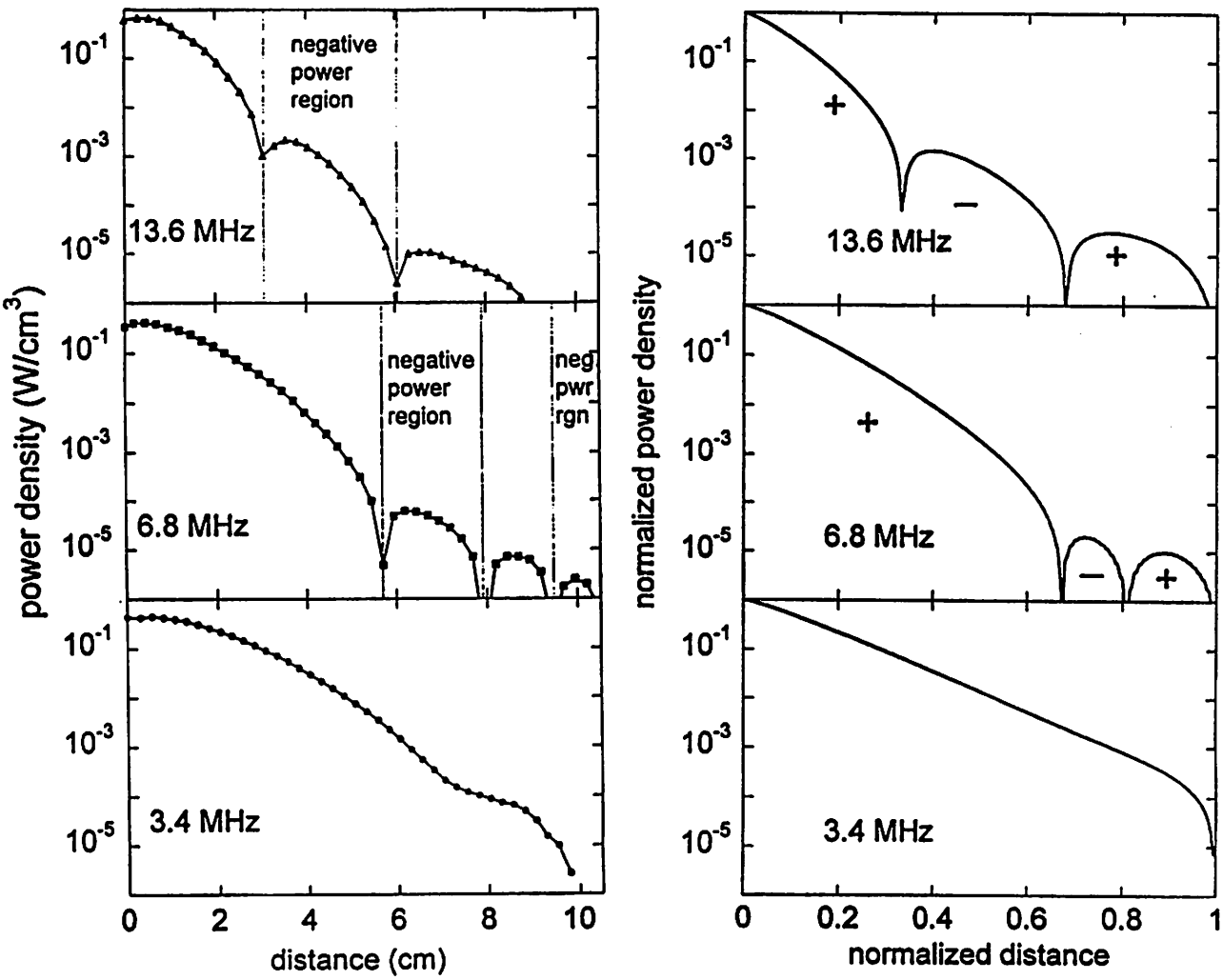

Figure 27. Effect of frequency variation on the spatial distribution of the rf power density absorbed by the plasma; (a) measured distribution for 10 mTorr and 100 W absorbed plasma power, and (b) distribution calculated from a one-dimensional model by Kolobov (after Godyak, 1997).

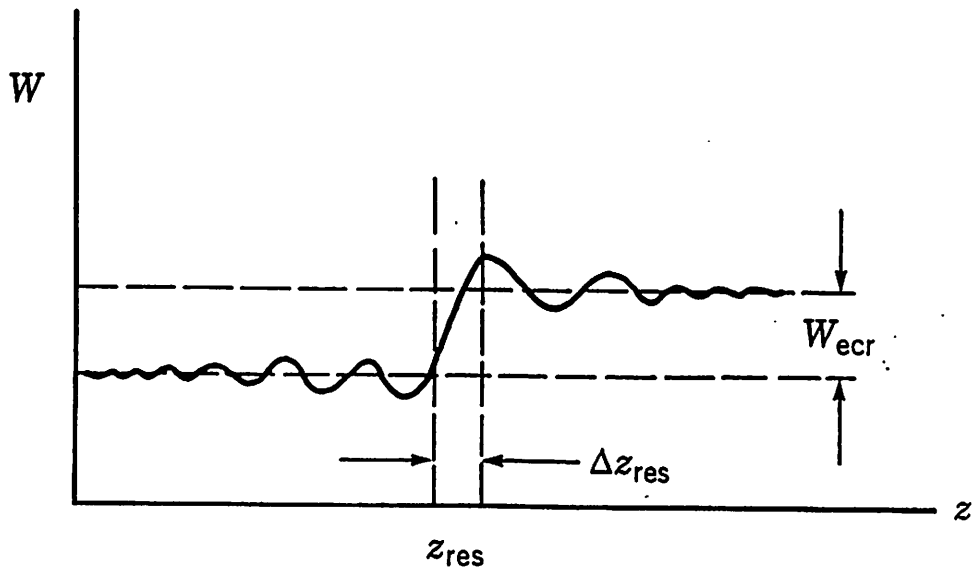

Figure 28. Energy change in one pass through an ECR resonance zone (after Lieberman and Lichtenberg, 1994).